POLITECNICO DI TORINO

Corso di Laurea Magistrale in Ingegneria Energetica e Nucleare

Tesi di Laurea Magistrale

CFD model for tubular SOFC cell fed directly by biomass – Complete biomass gasification system integrated with SOFCs stack

Relatori
prof. Massimo Santarelli
prof. Davide Papurello
prof. Domenico Ferrero

Candidato
Gioacchino Coppola

Marzo 2020

CFD model for tubular SOFC cell fed directly by biomass – Complete biomass gasification system integrated with SOFCs stack

Gioacchino Coppola

Marzo 2020

Abstract

Nowadays, with the advancing climatic emergency and the urgent need to reduce more and more the use of fossil fuels, we are constantly looking for new sources of renewable energy and devices capable of converting various forms of energy with high efficiency. In this context, the DB-SOFC project was launched, which is based on the use of biomass as a primary energy source for the production of syngas and SOFCs as energy conversion devices. The biomass chosen for this project is the olive kernel which is widely available in the area of interest of the project, that is the Euro-Mediterranean area. The biomass is initially gasified in a special reactor with CO_2 as a gasifying agent, and the syngas produced is used as a fuel in SOFCs. Solid oxide fuel cells were chosen specifically thanks to their ability to electrochemically oxidize both pure hydrogen and carbonaceous fuel. This thesis follows the simulation work done on a single SOFC which had extracted from it the polarization curve and the efficiency of a single cell. The aim of the thesis is to simulate, through the COMSOL Multiphysics® software, the entire process of gasification and use of the fuel by all the fuel cells, thus extracting the velocity, temperature and pressure profiles of the syngas produced and the relative molar fractions of the gases at the outlet of the integrated system, using 3D geometry in the simulation. First, we tried to give a background on the state of the art of biomass and fuel cell technologies, explaining, when necessary, the theory behind these technologies. After that, I tried to explain the main chemical-physical characteristics of biomass, trying to characterize it as much as possible. At this point the physical equations the software must solve have been defined and the physical assumptions and hypothesis have been made to fully characterize the computational analysis of the problem. Starting from the constant parameters of the system, the geometry of the system, the mass flow rate of the biomass and CO_2 were varied, trying to construct curves which, depending on the CO_2/Biomass ratio, give relevant information on which geometry optimizes the process. The geometries taken into account in the xy plane have a square and circular geometry, while the height of the reactor along the z axis remains constant. The main variable, used to decide the most suitable geometry, is the total efficiency of the system. Finally, I graphed, in a 2D cross section of the system, the molar fractions of the various chemical species involved in the device, the temperature and all the most relevant results. Finally, a grid independence was performed to validate the model and calculate the uncertainty of the results. Some final observations and conclusions were also made regarding the project in its entirety.

Contents

Acronyms

SOFC	Solid Oxide Fuel Cell
DB-SOFC	Direct conversion of biomass to electricity in MED area via internal catalytic gasification in solid oxide fuel cell
MED	Mediterranean
OECD	Organization for Economic Co-operation and Development
IEO	International Energy Outlook
IEA	International Energy Agency
GSE	Gestore dei Servizi Energetici
RES	Renewables Energy Sources
PAN	Paino d'Azione Nazionale
MSW	Municipal Solid Wastes
CFD	Computational Fluid Dynamics
GHG	Green House Gases
FC	Fixed Carbon
VM	Volatile Matter
TG	Thermogravimetry
DTG	Differential Thermogravimetry
WT	weight
HF	Heat of Formation
HR	Heat of Reaction
HHV	Higher Heating Value
LHV	Lower Heating Value
OFMSW	Organic Fraction of Municipal Solid Wastes
OK	Olive Kernel
GV	Grapes Vine
WG	Water-Gas reaction
WGS	Water-Gas Shift reaction
OCV	Open Circuit Voltage
YSZ	Yttria-Stabilized Zirconia

List of Figures

List of Tables

Chapter 1

Introduction

1.1 Current energy landscape

The fulfilment of the energy demand associated with an appropriate use of the resources available is an extremely current and global topic, it is interconnected with aspects such as demographic and economic development and the environmental protection, especially in terms of containing gas emissions greenhouse. Estimates on world population growth and on domestic product growth, global gross rate address towards an increase in global demand of primary energy, as shown in figure 1.1

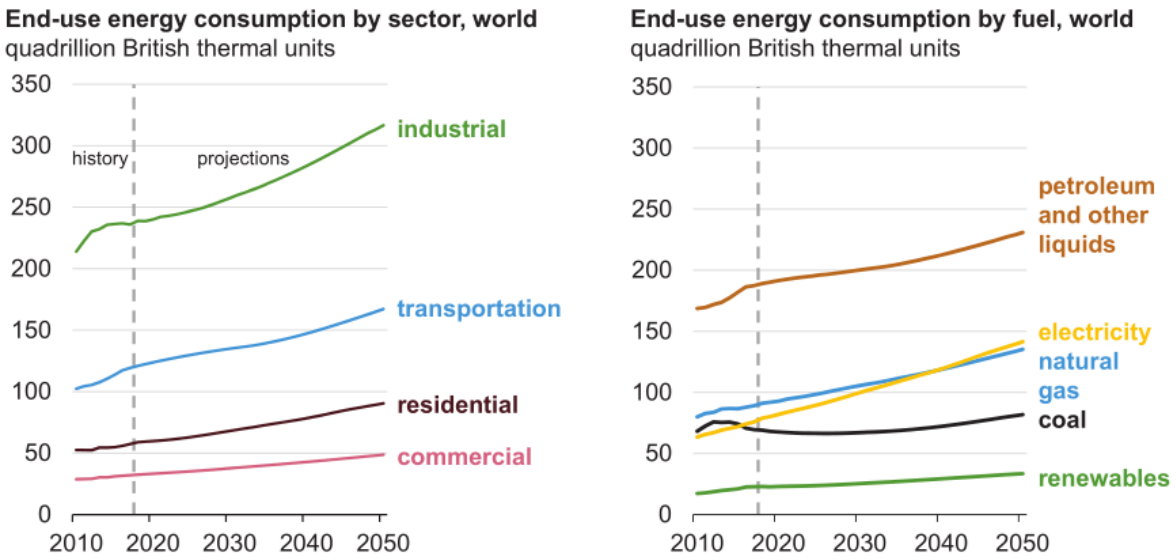

Figure 1.1: End-use energy consumption

End-use fuels include those fuels consumed in the industrial, transportation, and building sectors and exclude fuels used for electric power generation. Liquid fuels, because of energy density, cost, and chemical properties, continue to be the predominant transportation fuel and an important industrial feedstock. Electricity use in the residential and commercial building sectors increases rapidly because of growing income, a growing population, and increased access to electricity in non-OECD (Organization of Economic Cooperation and Development) regions; furthermore electricity use in the industrial sector and transportation sector also grows, respectively, as a result of increasing product demand and increasing use of electric vehicles. Coal continues to be an important end-use fuel in industrial processes, including the production of cement and steel[1]. The period 2018-2050 will see a considerable increase in terms of secondary energy, electricity (+ 79%); this is associated with a consequent growth of renewables in terms of primary energy, to demonstrate once again how the progressive shift of the global energy system towards electricity, is fundamental for the decarbonization process. In particular, the IEO19 provides for renewables - including solar photovoltaic, wind, hydroelectric, geothermal, biomass, biofuels, etc. - an average increase between 2018 and 2050 of 3.1% per year. To better understand the importance of this figure, it is good to compare it with the average annual growth over the same period of the use of oil (+ 0.6%), coal (+ 0.4%) and natural gas (+ 1.1%). Following these rhythms, renewable sources will become the most widely used primary energy, exceeding natural gas and coal by 2030, and oil by 2050. According to EIA, the use of natural gas will grow by about 40% between 2018 and 2050, while the use of oil and similar only around 20%[1]. The whole concept is summarized into figure 1.2. At the European level, medium-term objectives are binding and defined in the Climate-Energy Package also assigned Package 20-20-20 which impose by 2020: the reduction of greenhouse gas emissions by 20% compared to those of 1990, with the possibility of rising to 30% if within a global agreement; the increase in production from renewable sources for a share equal to 20% on gross final energy consumption and reduction of energy consumption by 20% compared at the trend value in 2020, through actions aimed on energy efficiency. At national level, the latest report by the "Gestore dei Servizi Energetici" (GSE) concerning the national energy situation highlights that in the last 12 years the total value of energy from RES has more than doubled passing from 10.7 Mtoe in 2005 to 22.0 Mtoe of 2017. At the same time, there was a progressive decrease in overall consumption (CFL), mainly due to the economic crisis, energy efficiency and climate factors. The combined effect of the three phenomena has caused a marked increase in the RES share over the 2011-2013 period (considerable RES growth and a strong decrease in consumption) and a more

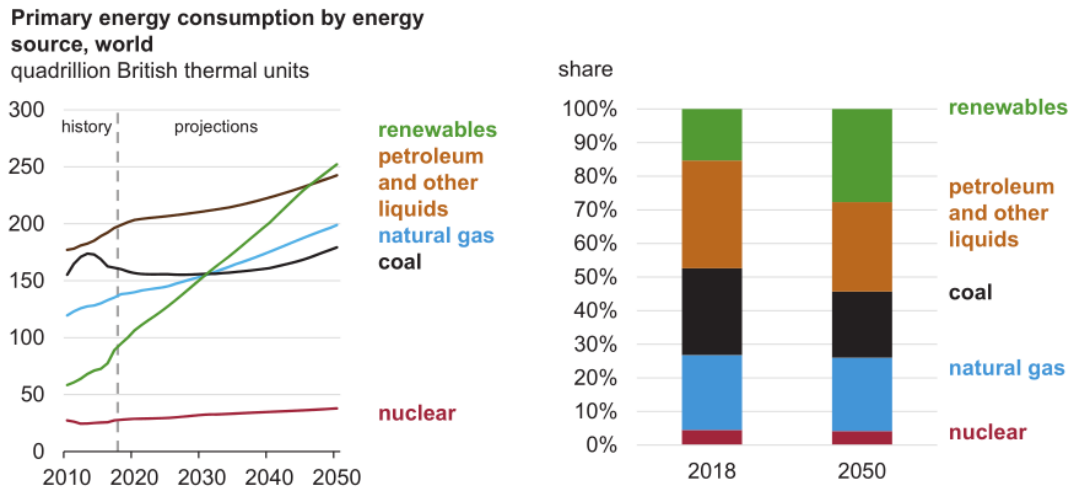

Figure 1.2: Primary energy cunsumption by energy suorce

modest growth in the 2014-2017 period (slight recovery in consumption). In 2017, the target set by the PAN (Piano d'Azione Nazionale per le energie rinnovabili) to 2020 of energy from renewable sources in the electricity sector has been largely overcome. This result is due to multiple factors; among these, a widespread use of photovoltaics far superior to what was assumed in the PAN[2]. As shown in figure1.3, nowadays RES plays a key role in the national energy landscape, especially

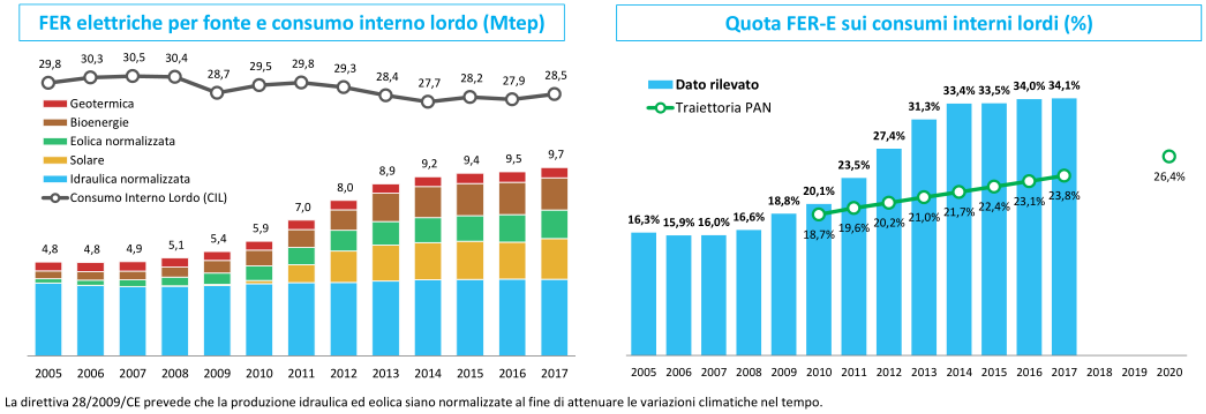

Figure 1.3: RES in national energy coverage of consumption

this thesis will focus on the impact of the biomass as primary energy source to create energy and in particular in the form of electricity through a relatively new high energy conversion efficiency systems which are the fuel cells.

1.2 Potential of biomass and fuel cells

As seen so far, the RES represent an increasingly sought-after source of energy, especially if the energy conversion takes place at high efficiencies. Among all the renewable energy sources, biomass and fuel cells represent those with the highest potential. At present, biomass is mainly used for heating in both domestic and industrial sectors, with the majority coming from traditional biomass sources, for example fuel wood. It is also used in the transport sector in the form of biofuels (0.8% of total global energy consumption, 2.8% of all transport). Lipid and protein rich agricultural crops can be employed to produce biofuels, such as biodiesel from rapeseed and palm oil, which is a versatile substitute/blender for fossil diesel. Biodiesel production increased internationally from 2.4 billion litres annually in 2004 to 30.1 billion litres in 2015, a factor of 12.5. However, care has to be taken that no conflicts arise between crop use for food or fuel production, causing a potential reallocation of crops from food to energy markets. Biomass can extend to include waste streams, such as municipal solid wastes (MSW), animal wastes and food processing wastes. Using biomass conversion pathways that yield hydrogen-rich and light hydrocarbons gases like biogas and syngas can provide alternatives for fossil natural gas and can produce higher usable gas yields[3]. In this study the favourite pathway in which the biomass will be converted in fuel is the thermochemical way. The more interesting thermochemical process is the gasification, in which the pure biomass is

Tabel 1.1: Typical Syngas and Biogas composition

Molar composition of syngas				**Molar composition of biogas**			
Hydrogen	H_2	$\longrightarrow$	~50-52%	Methane	CH_4	$\longrightarrow$	~60%
Carbon Monoxide	CO	$\longrightarrow$	~25-28%	Carbon Dioxide	CO_2	$\longrightarrow$	~39%
Carbon Dioxide	CO_2	$\longrightarrow$	~16-19%	Nitrogen	N_2	$\longrightarrow$	<1%
Methane	CH_4	$\longrightarrow$	~4-6%	Hydrogen Sulphide	H_2S	$\longrightarrow$	Trace amounts
Sulphur Dioxide	SO_2	$\longrightarrow$	Trace amounts	Silicon Dioxide	SiO_2	$\longrightarrow$	Trace amounts

directly converted in syngas. The produced syngas will be rich in hydrogen and carbon monoxide that are the most suitable fuels for the SOFCs (Solid Oxide Fuel Cells), that are one of the few fuel cells that can be worked even with carbonaceous fuels. In figure 1.4 are shown all the existing fuel cell technologies. SOFC has a solid ceramic electrolyte, non-platinum catalyst, and operates on inputs of, amongst others: syngas, natural gas, biogas, methane, or hydrogen at ~650-800°C. Logically, if the fuel gas contains carbon, the fuel cell will emit carbon dioxide. This emission is carbon-neutral if the fuel gas has been sourced from biomass. Therefore, net carbon emissions only result from using fossil resources such as town gas or natural gas, both in the fuel stream itself

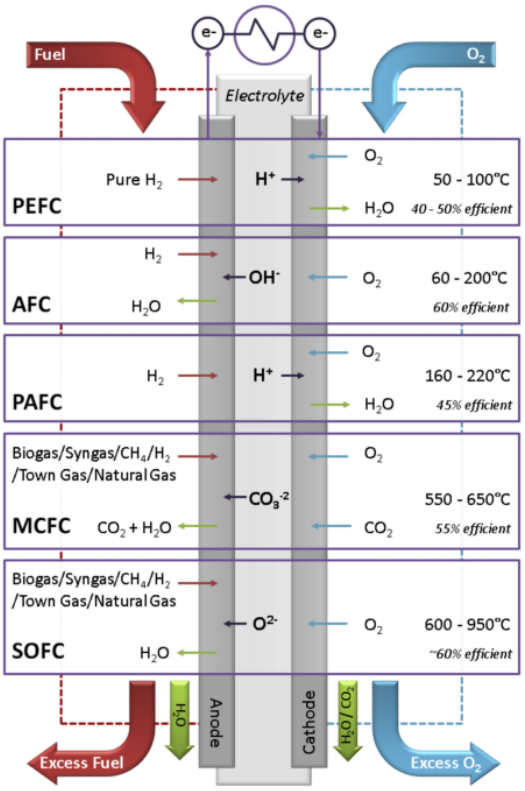

Figure 1.4: Overview of fuel cell technologies

and any auxiliary energy consuming steps involved in processing the fuel gas, which are driven by fossil sources. Low temperature variations of SOFCs run at 500-600°C. They lose the potential of internal reforming and will need to be operated on hydrogen or syngas. SOFCs are currently predominately used for CHP in domestic and industrial applications, as well as auxiliary power units on vehicles.

1.3 The DB-SOFC project

Nowadays many countries want to exploit the biomass as a primary source of energy to create new devices that convert the intrinsic chemical energy of the biomass in clean energy environmentally friendly. With this purpose, some countries of the Euro-Mediterranean zone as Spain, Italy, Greece, Turkey, Morocco, German, Cyprus created a consortium to take advantage of the abundant biomass present in this area. The countries mentioned before hold more than 85% of the world's olive production, cultivating at the same time large areas with grape vines. Given this, there is enormous potential regarding olive kernel and pruning from olive oil and grape vine cultures. Furthermore, these EURO-MED countries are still behind current progress towards energy use of municipal

solid waste (MSW). In light of the above aspects, the DB-SOFC project aims to develop an ecological and highly efficient process for the direct upgrading of solid carbon materials with low added value (for example biomass) and of a particular type importance for the EURO-MED area, namely: agricultural residues of olive and grape vines and the organic fraction of urban waste, in a solid oxide fuel cell system (SOFC), aided by an internal catalyst gasification process, towards electricity generation. DB-SOFC is just the acronym of the project, instead the full title is "Direct Conversion of Biomass to Electricity in MED area via an Internal Catalytic Gasification Solid Oxide Fuel Cell"[4]. The novel feature respect the consolidated SOFC plants is that the conversion of biomass to syngas directly takes place in the same system where are the fuel cells. The feasibility of this process has recently been successfully demonstrated after employing different carbon types as solid fuels and CO_2 as a gasifying agent. Nevertheless, several issues related to cell design and fabrication, electro-catalytic materials, gasifying agents, mechanistic considerations and structure-activity relationships remain to be resolved towards the scale-up of the process. The work plan is divided into eight work packages along with the corresponding tasks with clear objectives, deliverables and interactions/synergies to each other ensuring the successful project implementation. The work packages are:

- **Selection & treatment of biomass**
  - Selection and characterization of biomass sources
  - Production and characterization of biochar
  - Suitable preparation of DB-SOFC feedstock
- **Material synthesis & characterization**
  - Synthesis of catalysts/electrodes
  - Physicochemical characterization
- **Catalytic evaluation and mechanistic studies**
  - Activity Tests
  - Stability tests
  - Surface chemistry and mechanistic investigations

- **DB-SOFC construction**
  - Single-cell fabrication
  - DB-SOFC apparatus assembly
- **DB-SOFC operation**
  - Electrochemical characterization of cell materials
  - DB-SOFC performance evaluation
  - Post-test analysis of components/system
- **Simulation & feasibility studies**
  - CFD simulation studies
  - Process simulation and optimization at system level
  - Techno-economic assessment
- **Results dissemination and exploitation**
  - Creation of dissemination material
  - Dissemination events
  - Exploitation of results
- **Project Management & Coordination**
  - Overall project management
  - Communication within the project
  - Liaison with Call Secretariat

This thesis will focus on the CFD simulation studies, by examining the effect of the operation conditions on DB-SOFC performance. After the single cell simulation, now all the SOFC integrated gasification system will be analyzed, to do this, the software COMSOL Multiphysics® have been used. This software solves coupled differential equations of mass, energy and species conservation laws along with the reaction kinetics that will be also inserted into the CFD software employing the appropriate boundary conditions. The simulations will provide full flow-field solutions as well as species and temperature distributions. Potential and current distribution of the fuel cell will

be already available thanks to the previous CFD simulation on the single cell. By combining all the information obtained thanks to CFD analysis, it will be possible to obtain the overall characterization of the system.

1.4 CFD as tool for engineering

CFD is a branch of fluid mechanics that uses numerical methods and algorithms to solve and analyze problems involving fluid flows. Computers are used to perform the calculations required to simulate the interaction of liquids and gases in well-defined volume geometries with surfaces defined by boundary conditions. In CFD, continuity, momentum and energy equations are solved, they are three fundamental physical principles, namely, mass conservation, energy conservation and Newton's second law. A new trend is that engineers use more and more CFD to analyze flow and design performance of new systems and processes. CFD has a wide variety of applications: it is used in the automotive sector, aerospace, chemical, energy industry and so on. It allows a detailed analysis of the combined flow with mass and heat transfer. With CFD it is possible to obtain detailed local information on the simulated system. It also offers the flexibility to change design parameters in very little time. But its solutions depend on the correctness of the model (eg. turbulence, compressibility, chemistry, multiphase flow). Another limitation of the CFD is the fact that numerical errors are introduced by solving equations on a computer. Many commercial CFD programs are available, eg Fluent®, CFX®, Star-CD®, FLOW-3D®, Phoenics® and COMSOL Multiphysics®. First of all there is the pre-processing where the geometry of the model is defined, the grid is generated, the physical laws governing the model are defined, the properties of the fluid are set and initial and boundary conditions. The second stage is the resolution in which the appropriate solver must be selected and convergence requirements must be established, etc. Finally, in the last phase, the results are analyzed in the so-called post-processing, in which the most important results will be extrapolated and exposed.

Chapter 2

Biomass Characterization

2.1 General overview on biomass

The chemical composition and characteristics of the biomass highly influences the performance of the conversion of the latter into useful energy, but the first question to be asked is: What is biomass? The D.L. 30/07/2005 n°128 assumes for biomass the following definition: "Biomass is the non-fossilized and biodegradable organic material originating from plants, animals and micro-organisms. This shall also include products, by-products, residues and waste from agriculture, forestry and related industries as well as the non-fossilized and biodegradable organic fractions of industrial and municipal wastes". It is also possible to include in the definition of biomass gas and liquids recovered from the decomposition of biodegradable and non-fossilized organic materials. The planet continuously generates biomass through the interaction between carbon dioxide, water, earth, sunlight, plants and animals. Unlike what happens with fossil fuels, where generation times are of the same order as the magnitude of the geological ages, the speed at which the biomass formation processes occur is instead comparable to that at which this source is consumed. For this reason, biomass can be considered in all respects a renewable source. Moreover, the carbon dioxide released by its combustion does not affect the total CO_2 level of the planet, since the CO_2 emitted during this process corresponds exactly to that accumulated by the organism in the recent past through the photosynthesis reaction, as observed in the schematic representation 2.1. It is therefore legitimate to consider biomass a fuel with zero GHG emissions (GreenHouse Gas). It is possible to differentiate biomass in two main categories: primary biomass and biomass waste. Primary or virgin biomasses derive directly from animals or plants and include wood, plants,

leaves, crops and other plants. The biomass waste derives from other organic products and includes the biodegradable fraction of solid and liquid waste (MSW), waste water, human and animal dejections, landfill gas and agricultural waste.

2.1.1 Biomass formation

Vegetable biomasses are formed following the conversion of carbon dioxide present in the earth's atmosphere in carbohydrates, this transformation is achieved from plants due to the presence of sunlight, water and chlorophyll. The process by which plants absorb solar energy is called photosynthesis. Green plants are able to take advantage of some wavelengths of the light to break down water molecules so as to obtain the electrons and protons necessary to transform CO_2 into glucose (CHmOn) and at the same time release O_2 as reaction waste. Photosynthesis (R 2.1) can be schematized using the following reaction:

$$CO_2 + H_2O + \text{Solar Radiation} \longrightarrow Cn(H_2O)n + O_2 \qquad \text{(R 2.1)}$$

Through chlorophyll, the green pigment that covers the leaves along with the incident solar radiation activates a chemical conversion mechanism that fundamentally involves the reaction between the CO_2 present in the air and the water absorbed through the roots from the soil to form the compounds organic which will then form the structure of the plant. Considering that the sintered organic compound is glucose ($C_6H_{12}O_6$), the above report schematizes the mechanism of photosynthesis as follows:

$$6\,CO_2 + 6\,H_2O + \text{Solar Radiation} \longrightarrow C_6H_{12}O_6 + 6\,O_2 \qquad \text{(R 2.2)}$$

As mentioned earlier, it can once again be noted that for each mole of CO_2 absorbed, one mole of O_2 is released into the atmosphere, which in turn comes from the water that the plant has absorbed from the atmosphere (water vapour) or by ground.

2.1.2 Biomass classification

The main classification divides biomass into:

- Residuals (i.e. Agricultural, industry and forestry residues)

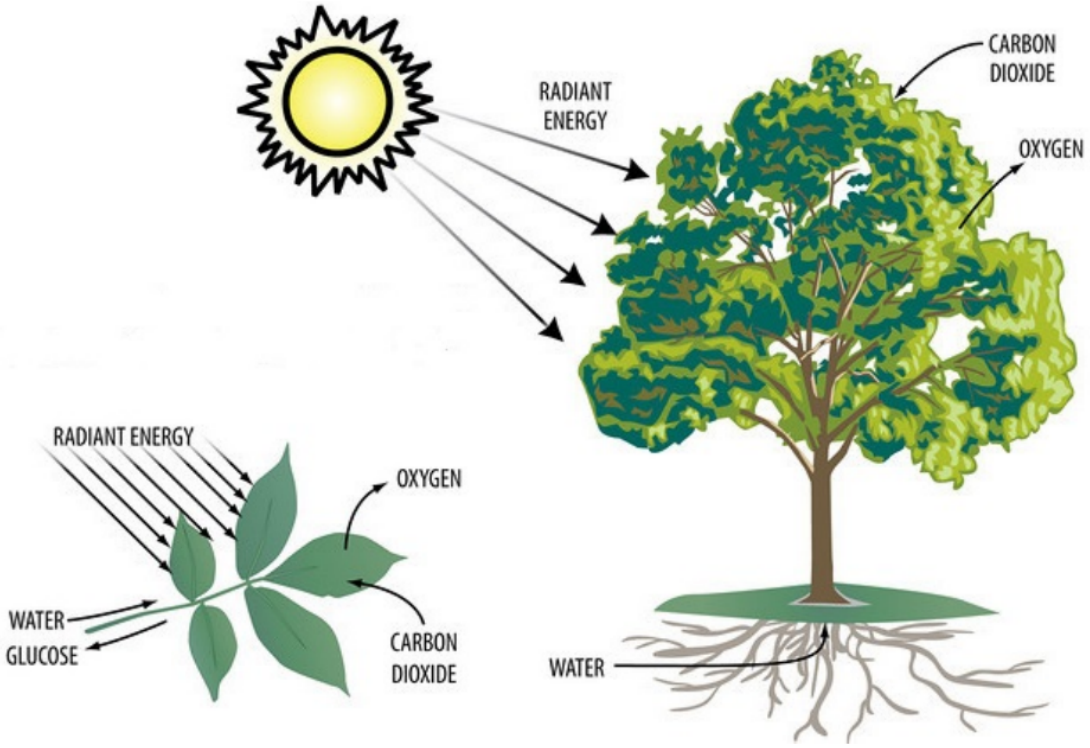

Figure 2.1: Biomass formation through photosynthesis

- Non-residuals (i.e. Energy crops)

Residual biomasses have the double advantage of reducing the dependence on fossil fuels and to lighten the environmental problems linked to the disposal of residues in landfills, preventing the release of methane in the atmosphere resulting from the degradation processes. In turn, residual biomass can be divided according to the origin area: then, those coming from agriculture; oil and alcohol plants for the production of biodiesel and bioethanol, forest residues; the industrial ones that is the waste coming from the industry of the wood and paper or from the food industry; zootechnical waste and urban waste, i.e. the organic part of solid waste and the vegetable part. Non-residual biomasses can be classified into three types: alcoholic cultures characterized by a high sugar content from which ethanol is produced; oil crops with a high vegetable oil content that can be used directly or transformed into biodiesel; lignocellulosic crops, large productions of dry matter intended for different energy purposes. However, appreciable the double advantage deriving from residual biomass, a significant contribution of biomasses in the world energy consumption cannot be separated from the use of energy crops on a large scale.

2.1.3 Constituents of biomass

Biomass is a complex mixture of organic materials such as carbohydrates, proteins, fats, along with small amounts minerals, such as sodium, calcium, iron and phosphorus. The main components of biomass are: extractives, fibre, cell walls components and ashes[5].

- Extractives: substances present in plant tissues that can be isolated through a series of solvent treatments and then recovered by evaporating the solution. Proteins, oils, starch and sugars are included in this category.

- Cell walls: substances that give support to the plant allowing it to rise out of the ground without the need for any external support. They are typically composed of carbohydrates and lignin. The former are substantially present in the cellulose and hemicellulose fibers which give solidity to the structure of the plant, while the lignin holds the fibers together. The distribution of these constituents varies from plant to plant.

- Ashes: composed of the inorganic part of the biomass.

Although extractives and ashes are present, most of the constituents of the biomass are those that form the cell wall of the plant, hence cellulose hemicellulose and lignin. In figure 2.2 is shown how the three components interact with each other. The presence of weight in the three constituents varies from one biomass to another. Typical cellulose, hemicellulose and lignin content were estimated for each feedstock using average values available in literature[6].

Tabel 2.1: Typical cellulose, hemicellulose and lignin content of raw feedstocks (dry basis)

	Cellulose (wt%)	**Hemicellulose (wt%)**	**Lignin (wt%)**
Palm Shell	30	18	53
Sugarcane bagasse	39	26	24
Rice husk	38	18	22
Coconut shell	20	49	30
Wheat straw	35	25	19
Cotton stalk	35	39	21
Olive pomace	34	15	20
Coconut fibre	46	15	33

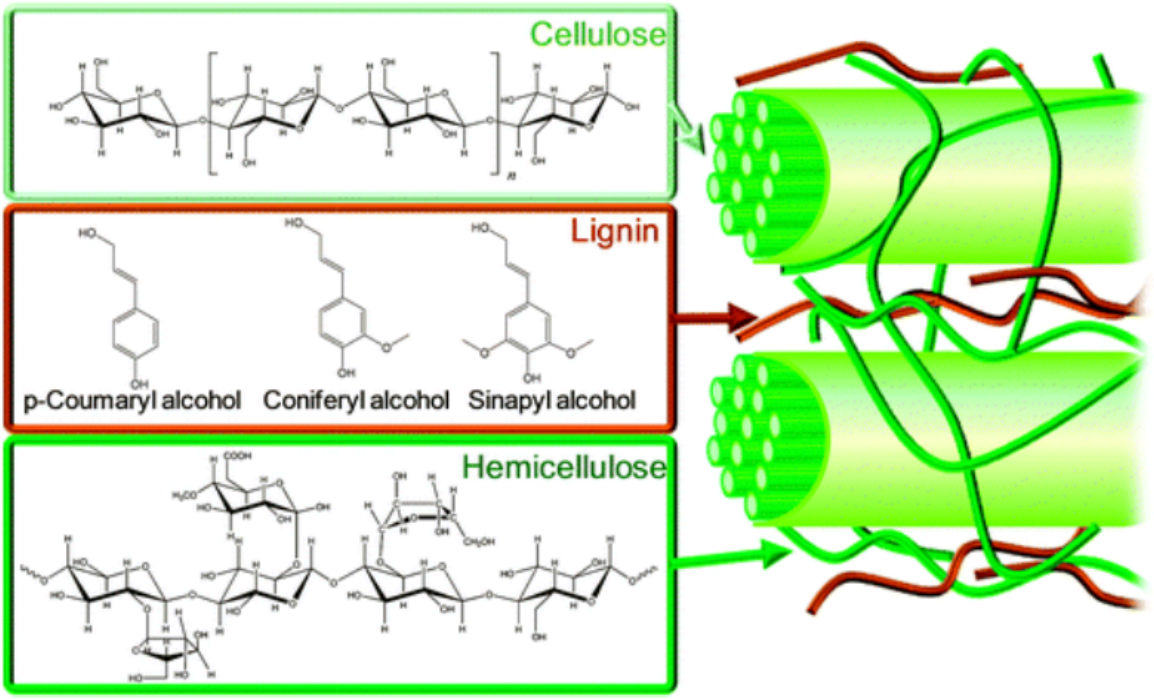

Figure 2.2: Internal structure of biomass

2.2 Biomass Properties

Regarding the elemental composition of biomass, among the main elements of organic compounds there are carbon (C), oxygen (O), hydrogen (H), nitrogen (N) and sulphur (S) while the inorganic part of the biomass constitutes the ashes. The latter represent the inorganic solid residues that are obtained following the complete combustion of biomass, the main components are: silica, aluminium, iron and calcium, as well as possible small amounts of magnesium, titanium, sodium and potassium. Biomass is also characterized by the presence of volatile matter which is given by condensible and non-condensible vapours that are released when the fuel is heated and by a certain fixed carbon content which represents the remaining mass after that, the volatile matter, the ash and the humidity leave the initial biomass . The quantities of the elements present in the biomass and above all their relationship, they are very important in order to verify their value as a fuel; of particular interest are the H/C and O/C ratios which influence the calorific value of the biomass. The problems connected to the release of sulphur-based compounds in atmospheric emissions, following combustion processes, are normally negligible in the case of lignocellulosic biomasses due to the low sulphur content that characterizes them[7]. For most biomasses the H/C

ratio can be expressed as a linear function of the O/C ratio according to the equation 2.1.

$$\left[\frac{H}{C}\right] = 1.4125 \left[\frac{O}{C}\right] + 0.5004 \tag{2.1}$$

The figure 2.3 is called the *Krevelen diagram*, it shows that biomass has a H/C and O/C ratio much higher than fossil fuel. These ratios are as high as the fuel is geologically young, this also affects the lower heating value which is higher in older fuels with low atomic ratios. But on the other side, biomass has a high reactivity; this aspect, together with the wide availability of the biomass in the world, makes the biomass suitable for thermal treatment such as pyrolysis or gasification. As mentioned above, excluding the presence of impurities, the main components of the molecular structure of biomass are carbon, hydrogen, oxygen and nitrogen. To know exactly the chemical composition of the biomass, it is practise to perform analyzes on the samples available such as those listed below:

- Ultimate analysis
- Proximate analysis
- Thermogravimetric analysis

The composition and the physical property of biomass is often expressed on a different basis depending on the situation. They are used using the following conditions:

- **As received (ar):** The conditions of the raw biomass, often with high humidity.
- **Air dry (ad):** The conditions of the biomass after a hot air drying treatment in which the core temperature of the biomass did not reach 100 °C. The total percentage of humidity M (wt%) is given by the sum of two factors: the surface humidity M_s (wt%) and the intrinsic humidity M_i (wt%). In this case, the surface moisture M is removed, on the contrary the intrinsic humidity is retained. To calculate the percentage of generic constituent on a dry air base starting from a receiving base, the amount of constituent is divided by the total mass of the sample minus the mass of surface moisture.
- **Total dry (db):** The conditions of the biomass after a drying treatment with hot air in which the biomass core temperature exceeds 100 °C. In this way, the percentage of total humidity M is removed. To calculate the percentage of the generic constituent in this case, the quantity of constituent is divided by the total mass minus the total moisture mass.

- **Dry ash-free (daf):** This is the non-organic component of biomass. To calculate the percentage of generic constituent in this case, the quantity of constituent is divided by the total mass minus the mass of total humidity and the mass of ash.

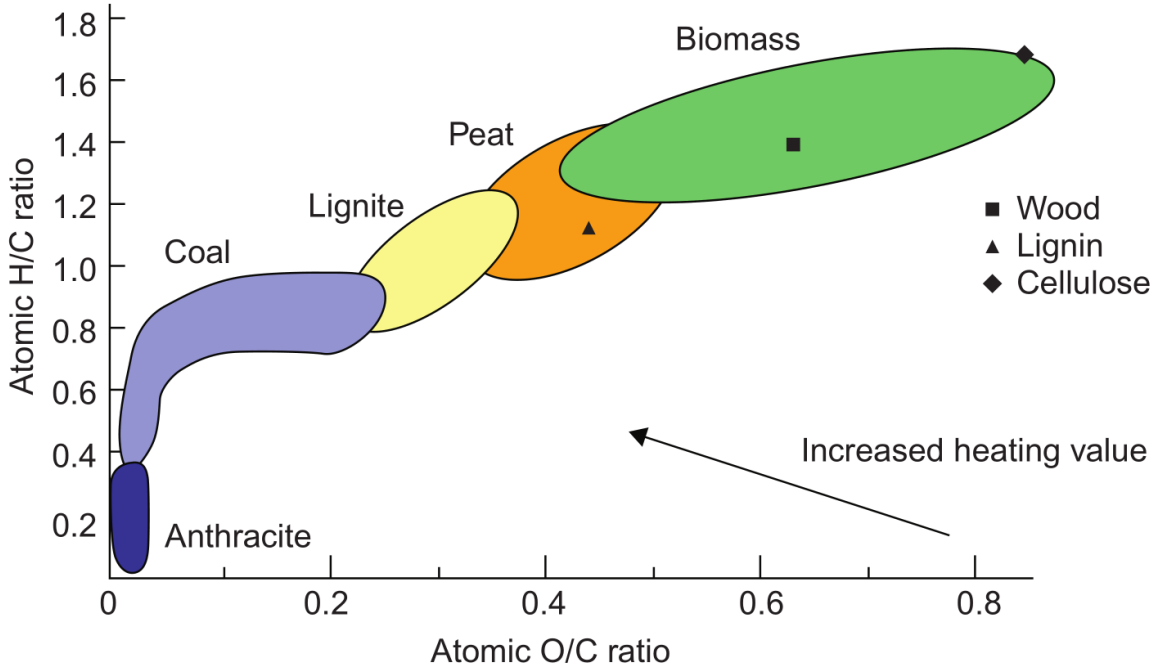

Figure 2.3: Krevelen diagram

2.2.1 Chemical analysis

Ultimate analysis: The ultimate analysis consists of measurements of chemical elements, such as carbon (C), hydrogen (H), oxygen (O), sulphur (S) and nitrogen (N). It is generally expressed in mass percentage on dry material (dry weight %) or on dry and ash free material (weight % daf) or always in mass percentage as received material (weight% ar). Depending on the type of biomass, the elemental composition can be significantly different and the ash content can vary greatly. In table 2.2[8] the composition of common biomasses are reported. The moisture content is also measured by drying the raw material at 105°C. The ash content, which also varies considerably, is measured by combustion of raw material at 550°C.

Proximate analysis: Proximate analysis is a simple and inexpensive process which gives the gross composition of an "as-received" biomass sample. These are: the total moisture (M), the volatile matter (VM), the ash (ASH) and the fixed carbon (FC). The M and ASH percentages

Tabel 2.2: Ultimate analysis of different biomasses in % dry matter

Residue	**Ash(wt%)**	**C(wt%)**	**H(wt%)**	**O(wt%)**	**N(wt%)**	**S(wt%)**
Black oak	1.34	49.0	6.0	43.5	0.15	0.02
Douglas-fir	0.10	50.6	6.2	43.0	0.06	0.02
Red alder	0.41	49.6	6.1	43.8	0.13	0.07
Cotton gin trash	14.7	42.8	5.1	35.4	1.53	0.55
Grape pomace	4.85	54.9	5.8	32.1	2.09	0.21
Peach pits	0.05	49.01	6.3	43.5	0.48	0.02
Rice hulls	21.0	38.3	4.4	35.5	0.83	0.06
Wheat straw	6.53	48.5	5.5	39.1	0.28	0.05
Rice straw	17.40	41.4	5.1	39.9	0.67	0.13
Sugarcane bagasse	3.90	47.0	6.1	42.7	0.30	0.10
Coconut shell	1.80	51.1	5.7	41.0	0.35	0.10
Potato stalks	12.92	42.3	5.2	37.2	1.10	0.21
Lignite	9.0	70.0	5.2	22.8	1.99	-
Bituminous Coal	10.0	80.9	6.1	9.6	1.55	1.88

which are determined by the proximate analysis are the same as that obtained by the ultimate analysis. The Volatile matter (VM) is composed of condensible and non-condensible vapours released by the fuel when heated; it is the largest mass fraction of woody biomass. However, the fixed carbon in proximate analysis is different from the carbon in the ultimate analysis because it does not include the carbon in the volatile matter. For gasification analysis, FC is an important parameter because in most gasifiers the conversion of fixed carbon into gases determines the rate of gasification and its yield. This conversion reaction is the slowest and it is used to determine the size of the gasifier. The figure 2.4 shows the relation between ultimate and proximate analysis. Known

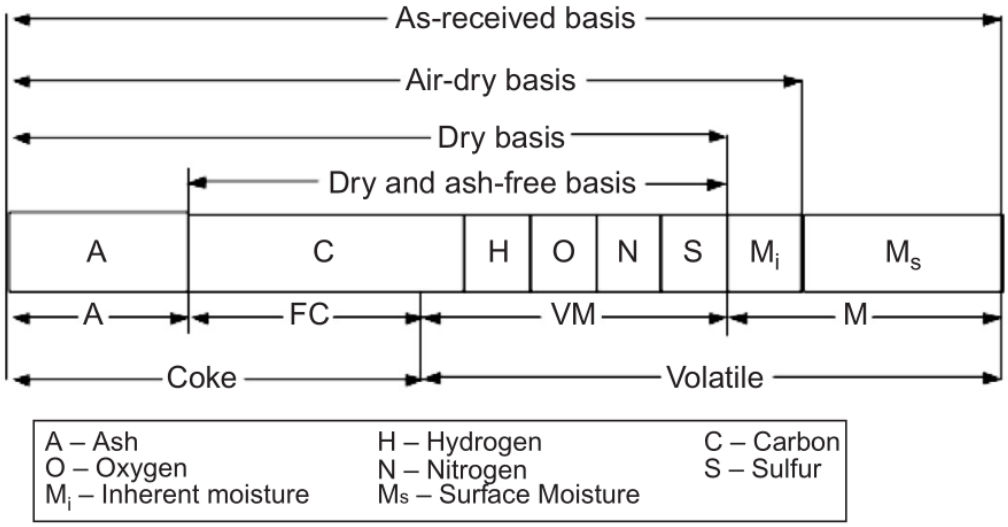

Figure 2.4: Proximate and ultimate analysis correlation

the weight percentage of VM, ASH and moisture, the fixed carbon can be calculated according the equations 2.2 and depending on weight percentage basis.

As received (ar)	$FC = 100 - VM - M - ASH$
Total dry (db)	$FC = 100 - VM - ASH$
Dry ash-free (daf)	$FC = 100 - VM$

(2.2)

Thermogravimetric analysis: The thermogravimetric analysis (TGA) was proposed by Klass in 1998 as an alternative to more complex and extremely expensive methods provided by the relative standards by the approximate analysis[5]. This method of analysis uses thermogravimetry (TG) or differential thermogravimetry (DTG) and involves heating a fuel sample in a specific atmosphere, usually inert atmosphere like N_2, at the desired speed. During the entire measurement process the sample is placed on an electronic micro-scale that detects the weight variations resulting from the devolatilization of the solid. In this way it is possible to monitor continuously the sample modifications according to its thermal history. Starting from the graphs just obtained, it is therefore possible to determine the moisture, volatile matter, ash and carbon content of the raw material. This approach is not a recognized standard, however it can quickly provide information about the thermochemical conversion of a fuel and additional information about reaction mechanisms, kinetic parameters, thermal stability and reaction heat.

2.2.2 Ternary diagram

The ternary diagram, although not developed to classify biomass, can reveal itself a very useful tool for evaluating and comparing the different types of fuel. It looks like a triangle whose corners depict pure components, that is with a 100% concentration, which can be for example three elements such as carbon, hydrogen and oxygen. The points inside the triangle describe the combinations of these three components, while the points on the perimeter show the concentrations in the element placed in the opposite corner. Figure 2.6 shows an example of a ternary diagram in which biomass, coal, char, gaseous fuel and combustion products are represented, according to their content of carbon, hydrogen and oxygen. It can be noted, based on its position in the diagram, that it is a fuel derived from the biomass and it is generally very rich in carbon and has very low percentages of oxygen, while a gaseous fuel has a lower carbon content and a very variable content of hydrogen and oxygen. Finally, the combustion products, generally consisting of water and carbon dioxide,

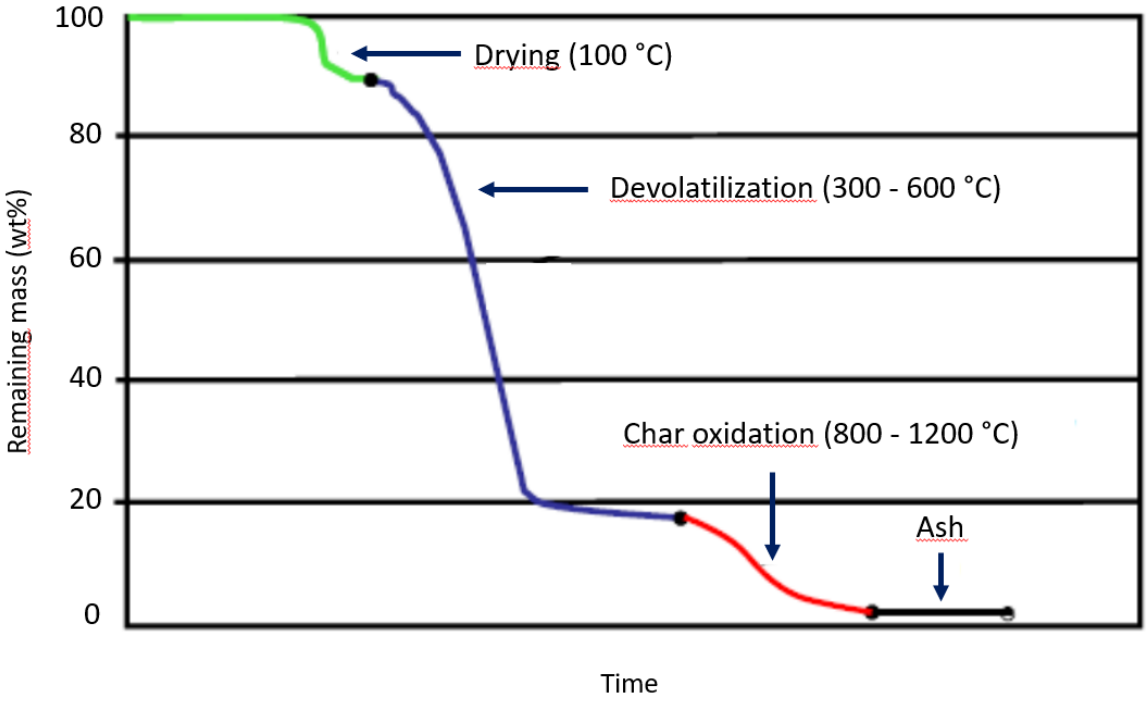

Figure 2.5: Typical thermogravimetric profile

are found in the right corner, delimited by two sides with a concentration of hydrogen and zero oxygen.

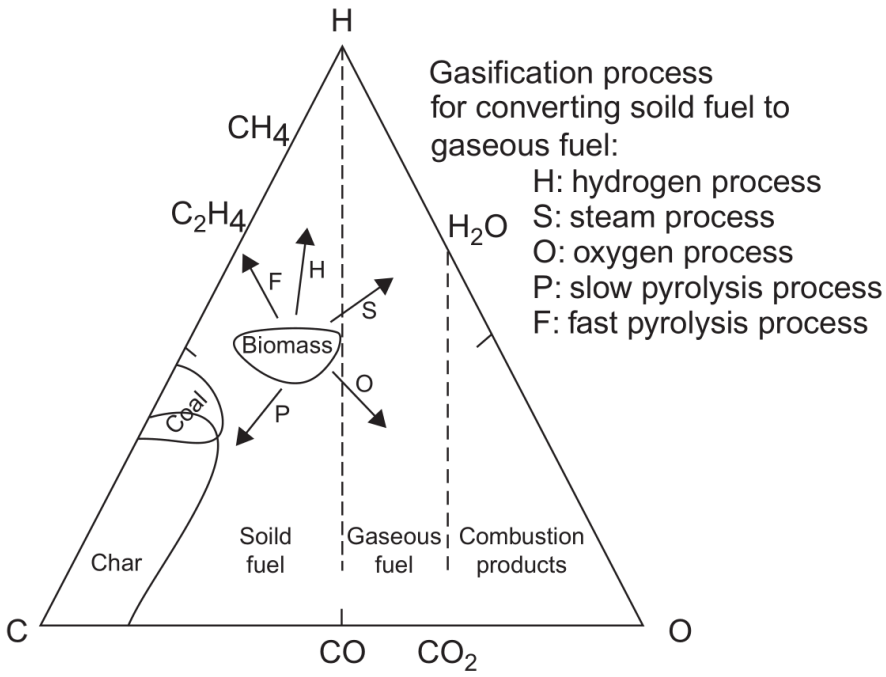

Figure 2.6: C-H-O ternary diagram of biomass showing the gasification process

2.3 Thermo-physical properties

Thermo-physical properties are very important when we talk about biomass gasification or pyrolysis. Many factors such as permeability, porosity and density mainly influence how chemical reactions progress, even as pyrolysis gases become trapped in the pores of the particles biomass packing. Many thermodynamic properties also affect the thermochemical processes: the specific heat and thermal conductivity influence the transmission of heat in the porous matrix of the biomass, thus conditioning the temperature in the entire gasifier, being the temperature itself the main accelerator of the reaction kinematics. Biomasses release more volatile matter in primary pyrolysis than carbonaceous solids, which makes the gasification process much simpler.

2.3.1 Moisture

In first approximation, an important parameter to take into account is the moisture present in the biomass. The moisture of the biomass expresses its water content and can be assessed on as received (wet basis) or on dry basis. The moisture in biomass can remain in two forms: free or external and inherent or equilibrium moisture.
In wet-basis moisture is expressed as:

$$M_{wet} = \frac{W_{wet} - W_{dry}}{W_{wet}} \quad [\%] \tag{2.3}$$

Instead, if we want to express the moisture content in wet basis the formula becomes:

$$M_{dry} = \frac{W_{wet} - W_{dry}}{W_{dry}} \quad [\%] \tag{2.4}$$

The latter formula can give a percentage value of moisture even higher than 100% for biomass with high water content. For this reason, the basis of moisture content must be always specified. The two formulae are linked each other by the following correlation:

$$M_{dry} = \frac{M_{wet}}{1 - M_{wet}} \quad [\%] \tag{2.5}$$

The following table shows some examples of typical moisture content of some biomass.

Tabel 2.3: Typical moisture content of some biomass

	Corn Stalks	Wheat Straw	Rice Straw	Rice Husk	Dairy Cattle manure	Wood Bark	Sawdust	Food Waste	RDF Pellets	Water Hyacinth
Moisture (wet basis)	40-60	8-20	50-80	7-10	88	30-60	25-55	70	25-30	95.3

2.3.2 Densities

One of the most important thermophysical properties to consider is density. Considering granular biomass, three different density definitions are established:

- True density
- Apparent density
- Bulk density

True density: Is the weight per unit volume occupied by the solid constituent of the biomass. Anyway, measuring the true density is not at all a simple calculation. It can be measured with a pycnometer or it can be estimated through ultimate analysis.

$$\rho_{true} = \frac{\text{Total mass of biomass}}{\text{Solid volume in biomass}} \quad \left[\frac{kg}{m^3}\right] \tag{2.6}$$

Apparent density: Is based on the apparent volume of the biomass which includes the volume of pores and microcavities in addition to the solid part. The apparent density considers the internal pores of a biomass particle but not the interstitial volume present between the biomass particles packed together.

$$\rho_{apparent} = \frac{\text{Total mass of biomass}}{\text{Apparent volume of biomass including solids and internal pores}} \quad \left[\frac{kg}{m^3}\right] \tag{2.7}$$

Apparent density is most commonly used for design calculations because it is simpler to measure than true density, and it gives the real volume occupied by a biomass particle.

Bulk density: Is based on the overall space occupied by an amount or a group of biomass particles. The bulk volume incorporates interstitial volume between the biomass particles and it

depends on how closely the particles are packed to each other.

$$\rho_{bulk} = \frac{\text{Total mass of biomass particles or stack}}{\text{Bulk volume occupied by biomass particles or stack}} \quad \left[\frac{kg}{m^3}\right] \tag{2.8}$$

The three definitions of density are related to each other, but two other parameters must be defined: ε_p is the void fraction in a biomass particle and ε_b is the voidage of particle packing.

The formulae are the following:

$$\rho_{apparent} = \rho_{true}(1 - \varepsilon_p) \quad \left[\frac{kg}{m^3}\right] \tag{2.9}$$

$$\rho_{bulk} = \rho_{apparent}(1 - \varepsilon_b) \quad \left[\frac{kg}{m^3}\right] \tag{2.10}$$

2.3.3 Thermal conductivity and specific heat

Thermal conductivity greatly influences the behaviour of biomass during the pyrolysis or gasification process. It changes with moisture, with density and above all with temperature. There are many correlations that describe the trend of thermal conductivity; in particular, figure 2.7 shows the variation of the latter as a function of the density of the dry biomass in a parallel or perpendicular direction to the grains of the biomass. Also the specific heat is very important for a gasification model. The two parameters that most influence the specific heat are the moisture and the temperature. The specific heat of general wood can be calculated according to the following equations:

$$C_{p,T} = 0.266 + 0.00116 \cdot T \quad \left[\frac{kJ}{kgK}\right] \tag{2.11}$$

$$C_p = M_{wet}C_w + (1 - M_{wet})C_{p,T} \quad \left[\frac{kJ}{kgK}\right] \tag{2.12}$$

where T [K] is the temperature; M_{wet} [% wt] is the total moisture fraction on wet basis and C_w is the specific heat of water. In figure 2.8 the variation of the specific heat of the biomass with the temperature is shown.

2.3.4 Heat of formation and heat of reaction

The Heat of Formation (HF), also known as enthalpy of formation, is the variation of enthalpy that occurs when a mole of product reacts with reagent substances in an environment under standard

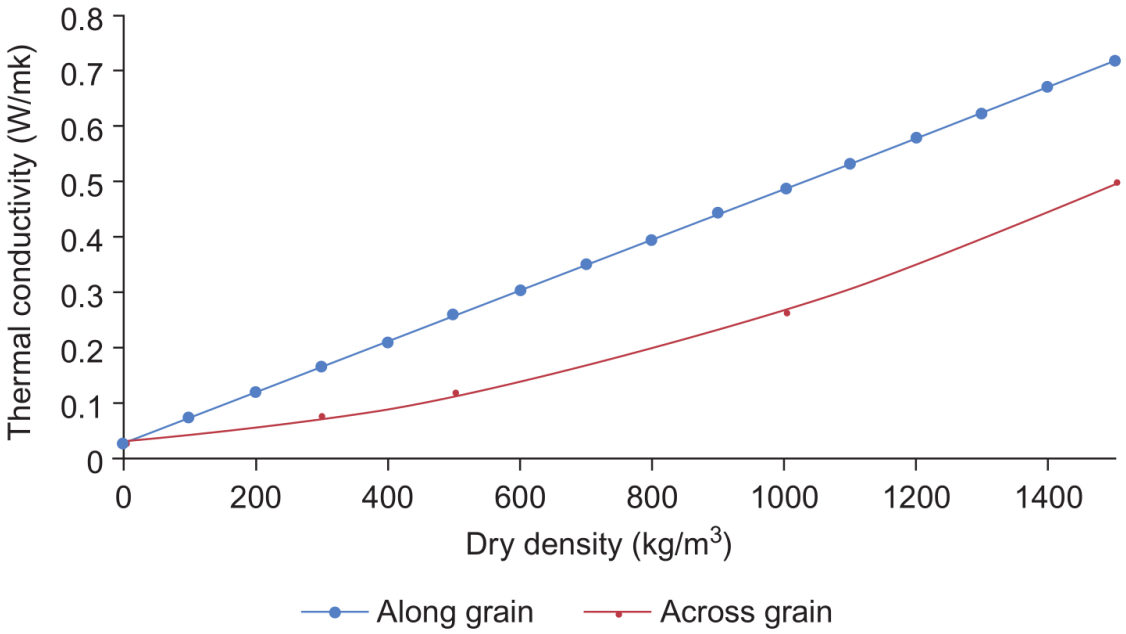

Figure 2.7: Thermal conductivity of biomass along the grain and across the grain increases with the dry density of the biomass

conditions at 25°C and 1 atm. If the compound was formed in several steps, then the HF is the sum of the enthalpy variation of each single step of the process. The HF of some simple gases such as H_2, O_2, N_2 etc. is zero because they cannot be considered compounds. To calculate the biomass HF, you need to know the biomass Heat of Reaction (HR) of combustion first. HR is the total heat released or absorbed in a chemical reaction without temperature variation. For a combustion reaction, the reaction heat is also known as heat of combustion ΔH_{comb}, which can be calculated as follows:

$$HR = \Delta H_{comb} = \sum HF_{products} - \sum HF_{reactants} \tag{2.13}$$

For instance if we assume $CH_{1.35}O_{0.617}$ as the chemical formula of sawdust, its heat of formation results -80.5 kJ/mol. Another parameter noticeably for a fuel is the ignition temperature. When a fuel is heated up, the heat produced by exothermic reactions increases proportionally to the increase in heat generated. Above a certain temperature when the heat produced exceeds the thermal losses, the process becomes self-sufficient and therefore can be self-powered. The temperature in question is known as the ignition temperature. The latter becomes lower and lower the higher becomes volatile matter content in the biomass. The biomass particles contain a percentage of volatile material (about 70%) which means an ignition temperature equal to 250°C

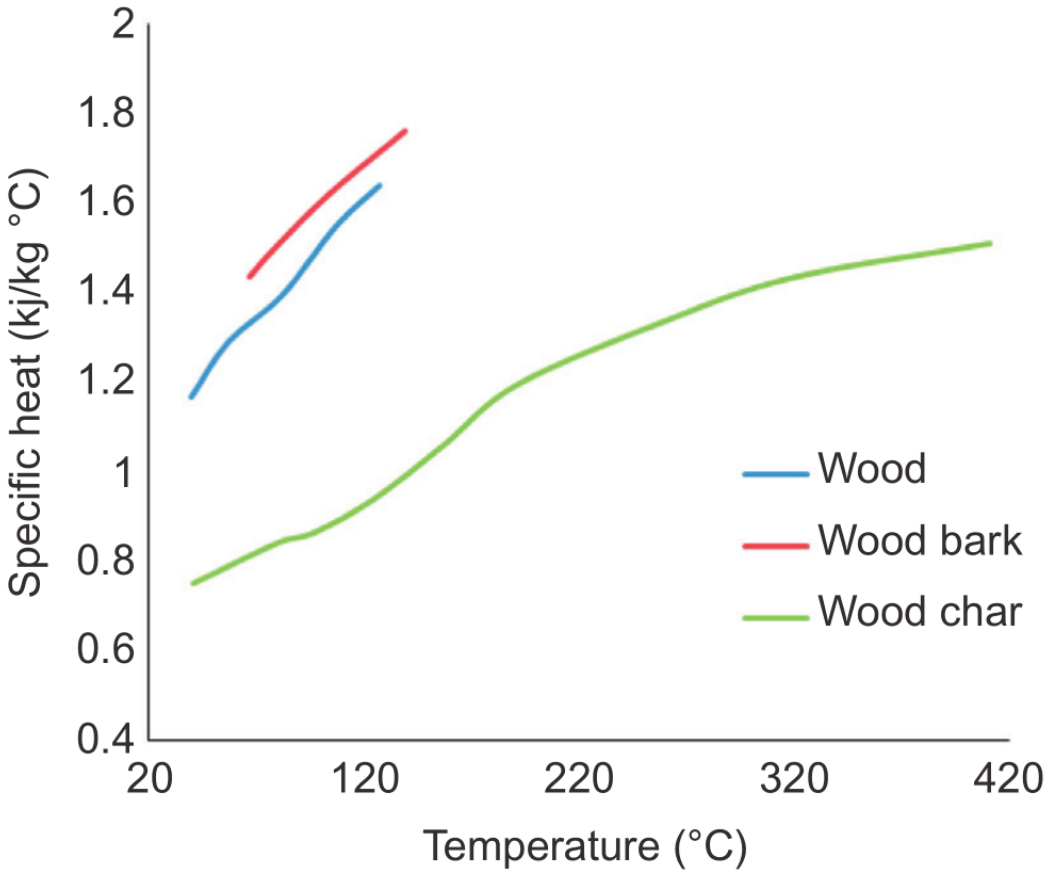

Figure 2.8: Specific heat of biomass as function of temperature

2.3.5 Higher and lower heating values - HHV & LHV

The heating value of a fuel is defined as the quantity of heat developed per unit of weight (or volume in the case of a gas) from the fuel when it is completely burned and the combustion products are cooled to a standard temperature of 15°C. Generally two types of heating value are considered: Higher heating value (HHV) and Lower heating value (LHV). The difference between the two types is linked to the latent heat of condensation of the water vapor during the combustion process. We are talking about the HHV, when all the steam produced during the fuel combustion is completely condensed. Instead, we speak of LHV when the latent heat of condensation of the steam is not recovered. Biofuels HHV can be measured by legislation using a calorimeter. There is a relationship between the HHV and the LHV of a general biomass fuel:

$$LHV = HHV - h_g \left(\frac{9H}{100} - \frac{M}{100} \right) \tag{2.14}$$

where apart HHV and LHV of which we know the meaning, H and M are the hydrogen and moisture percentage on wet basis, and h_g is the latent heat of steam in the same units of HHV and LHV. With the reference temperature of 100°C, h_g becomes equal to 2260 kJ/kg. During the last decades, many academics have tried to find a relationship that allows to find the HHV of the fuels knowing only the ultimate analysis of a generic fuel[9]. One of the most used empirical correlation to calculate the calorific value through the ultimate analysis is:

$$HHV = 0.3491 \cdot C + 1.1783 \cdot H + 0.1005 \cdot S - 0.1034 \cdot O - 0.0151 \cdot N - 0.0211 \cdot Ash \quad \left[\frac{kJ}{kg}\right] \quad (2.15)$$

Where C, H, S, O, N, Ash respectively represent the mass percentages on a dry basis of carbon, hydrogen, sulphur, oxygen, nitrogen and ash. The above relationship applies in the following ranges:

- 0.00 % ≤ C ≤ 92.25 %
- 0.43 % ≤ H ≤ 25.15 %
- 0.00 % ≤ S ≤ 94.08 %
- 0.00 % ≤ O ≤ 50.00 %
- 0.00 % ≤ N ≤ 5.60 %
- 0.00 % ≤ Ash ≤ 71.40 %
- 4.745 MJ/kg ≤ HHV ≤ 55.345 MJ/kg

The HHV of soft wood is about 17 MJ/kg and of hard woods is about 20 MJ/kg. The figure 2.9 shows the dependence of the LHV and HHV from the moisture content of the biomass.

2.3.6 Biomass availability for DB-SOFC project

As previously mentioned, the DB-SOFC project is mainly based on the use of three types of fuel: olive kernel, branches of vineyards residues from pruning, and organic fraction of municipal solid waste (OFMSW). The first two belong to the category of agro-food residues, while the last one belongs to another category of waste. The two categories are very different from each other also for the type of syngas developed, having very different characteristics. For the development of this thesis, the analysis of the syngas produced by the biofuels deriving from the agro-food waste

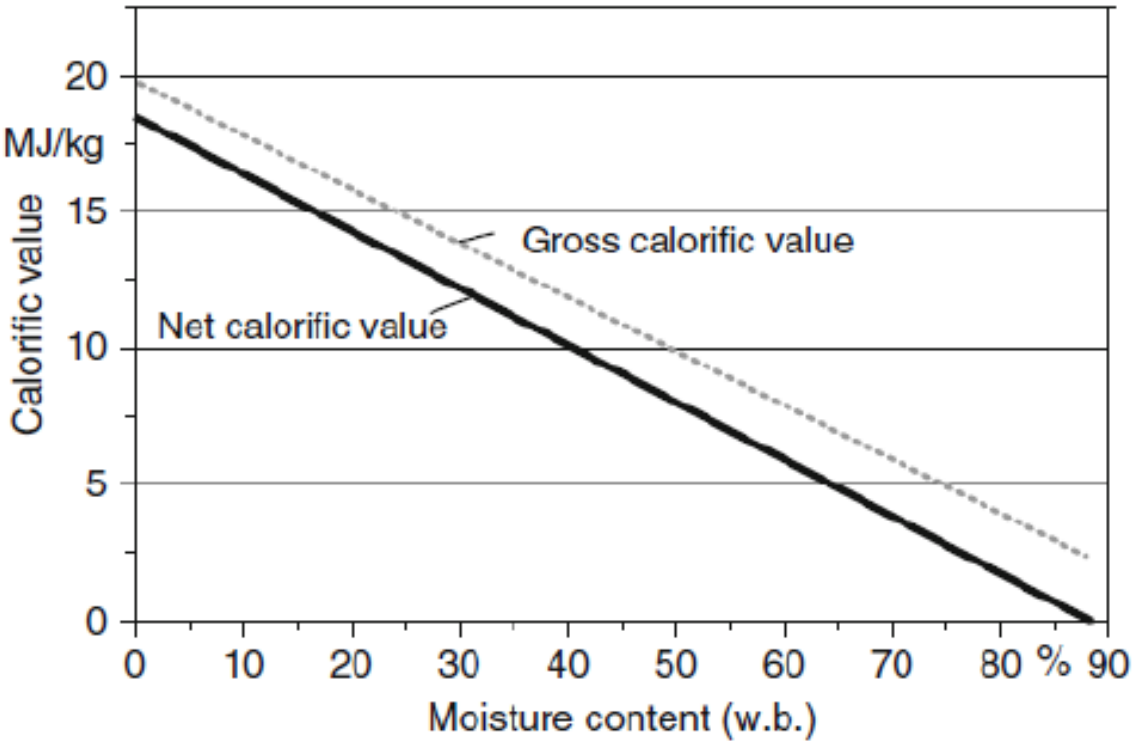

Figure 2.9: HHV and LHV of biomass varying with moisture content

will be taken into consideration, and in particular the residue of the olive cultivation, called OK (olive kernel) will be taken as a reference for carrying out a numerical analyzes. To answer the question of why this type of biomass was chosen, it is necessary to make an excursus regarding its availability in the Euro-Mediterranean area. In this regard, a report was made by the Polytechnic Mohammed VI located in Morocco on the availability of residual biomass from vineyards and olive groves[10].It can certainly be said that belonging to the same geographical area, the assessments made for the region of Morocco will also apply to all the high regions bordering the Mediterranean area. This report asserts that the agriculture in Morocco represents one of the most important sectors in the national economy and thus the available biomass represents a great potential that can be fully exploited. The main solid wastes produced during the olive oil production process are:

- Olive kernels: Olive pits or olive stones
- Olive pomace: It is the residual paste after oil extraction, it is made from a mixture of olive pits, olive pulp and skin.

As we can see in table 2.5, all the euro-mediterranean countries own over 70% on the total percentage of world of olive production. This fact explains why the DB-SOFC project has focused

the fuel research on this type of biomass.

Olive groves: Taking always Morocco as an example, the olive colture occupies 5% on the national agricultural GDP. The table 2.4 shows the growing production of olives.

Olive kernels (pits or stones): As mentioned above, olive kernels are very convenient to use as a biofuel, especially for the large cultivation of olive groves present throughout the Mediterranean area. Olive kernels are better than pomace olives because being solid, they are easier to handle, pack and transport and above all from a purely plant engineering point of view, having a low moisture content compared to pomace olives, they are more suitable for gasification. The production of olive pits for a country can be determined knowing the amount of olive production, because the total content of olive pits il the 10% of the weight of the olive fruit used for oil extraction.

Tabel 2.4: Cultivated area and total production of olives in Morocco, 2015 and 2020 projection

	2015	**2020**
Cultivated area (hectares)	1 100 000	1 220 000
Total production of olives (tons)	1 330 000	2 500 000
− Olive oil	138 000	330 000
− Tables olives	92 000	320 000

Tabel 2.5: Top five olive producing countries for the year 2012

Country	**Olive production 2012 (tons)**	**Percentage of world total (%)**
Spain	3 626 600	21.9
Italy	3 626 537	18.2
Greece	2 080 800	12.5
Turkey	1 820 000	10.9
Morocco	1 315 794	7.9

Chapter 3

Gasification and Fuel Cells Literature Review

This chapter briefly summarizes the physical principles behind the solid fuel gasification processes and the operating principles on which fuel cells are based. Gasification and fuel cells are closely related to each other because they are two technologies that are still taking up more and more space in the global energy scene due to their being clean and high efficient energy conversion methods.

3.1 Biomass conversion processes

The fact that biomass is very voluminous and has little energy density is an aspect that disadvantages its use compared to fossil fuels. So, over the centuries they have searched for ways to make biomass more user-friendly. Above all in the last century, technological goals have been achieved capable of converting solid biomass into liquid and gaseous fuels which are easier to handle. This conversion can be achieved through one of three major routes:

- Physical process such as drying and dewatering
- Thermo-chemical processes such as combustion, pyrolysis, gasification and liquefaction
- Bio-chemical processes such as digestion and fermentation

Physical processes are used only for the production of biodiesel, instead the thermo-chemical and

bio-chemical pathway is used for the production of both gaseous fuels and liquid fuels for various uses. In the next figure are summarized the thermo-chemical and bio-chemical pathways.

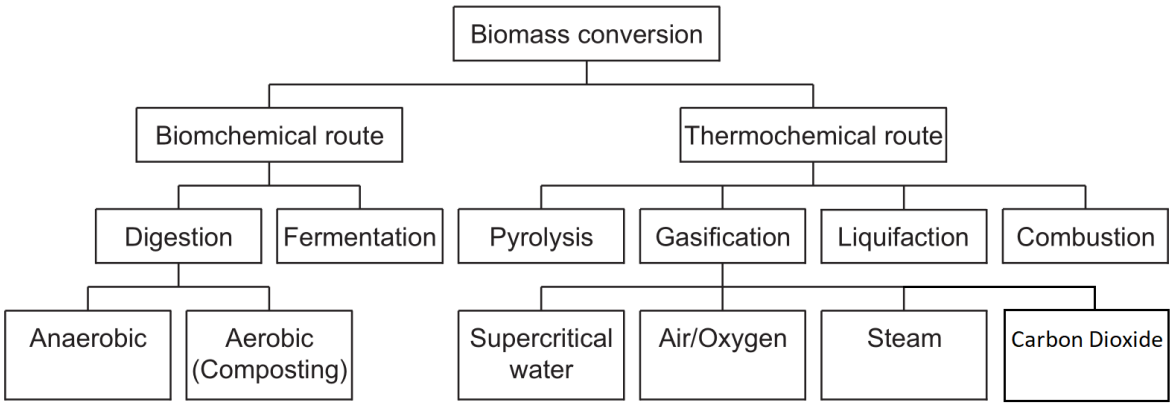

Figure 3.1: Thermo-chemical and Bio-chemical conversion processes

In this thesis we will focus mainly on the conversion by thermo-chemical route and in particular we will carry out gasification using carbon dioxide as medium. Thermochemical processes are based on the action of heat which allows the development of the reactions necessary for the transformation of matter into energy. Within these processes, the heating value of the biomass which depends on the moisture content plays a fundamental role, therefore it is necessary to provide, for the biomass used, a drying pretreatment in order to effectively exploit the chemical energy contained in it. The most suitable biomasses are wood and its processing waste such as: sawdust and shavings, lignocellulosic crops as eucalyptus, black locust, willow and common reed, lignocellulosic type and by-products or cereal straw, pruning residues of the vineyards and fruit trees and processing waste including chaff, shells and kernels. In reference thermochemical processes are, as mentioned above, combustion, pyrolysis, liquefaction and gasification.

3.1.1 Direct Combustion

Unlike the other thermochemical processes, the direct combustion process allows to transform the chemical energy contained within the biomass into thermal energy. This conversion takes place through a series of reactions of a comburent, generally oxygen, and oxidation of a fuel, with the release of energy and the formation of new compounds such as carbon dioxide and water in first place. Type and quantity of combustion products depends on fuel. In chronological order, the transformations that occur when starting a combustion reaction are as follows:

- Drying
- Pyrolysis
- Gasification
- Combustion

Then following a first heating step, the fuel dries up, then as the temperature rises, pyrolysis, gasification and finally real combustion processes take place inside the fuel particle. If combustion is complete, all the volatile matter initially present reacts with the oxidizing oxygen, thus remaining only of the carbonaceous material generally composed of inert matter. The released volatile matter is generally made up of carbon monoxide, carbon dioxide, hydrogen and some hydrocarbons. All this gaseous fraction is further oxidized according to the reactions:

$$2\,CO + O_2 \longleftrightarrow 2\,CO_2 + HEAT \tag{R 3.1}$$

$$C_xH_y + \left(x + \frac{y}{4}\right)O_2 \longleftrightarrow xCO_2 + \left(\frac{y}{2}\right)H_2O + HEAT \tag{R 3.2}$$

$$2\,H_2 + O_2 \longleftrightarrow 2\,H_2O + HEAT \tag{R 3.3}$$

In addition to the compounds listed above, the volatile fraction also contains condensible compounds such as water and carbonaceous compounds which tend to decompose into simpler substances with increasing temperatures. Direct biomass combustion is mainly used to create heat. It could also be used to create electricity through steam cycles.

3.1.2 Pyrolysis

Pyrolysis is a thermochemical process through which biomass decomposes into solid, liquid and gaseous products. To have the pyrolysis of a solid fuel, it is necessary to heat up the raw biomass to a certain temperature in the total absence of oxygen. Both the heating rate and the final temperature are variables to be taken into consideration based on the final products that we want to be obtained, but in general the minimum temperature is 400°C, as shown in table 3.1.

After reaching the final temperature, known as pyrolysis temperature, this value remains constant inside the reactor for a well-defined time, which can also vary according to the case. First the evaporation of the moisture present in the raw biomass occurs, then there is the release of the

Tabel 3.1: Characteristics of some thermal decomposition processes

Pyrolysis Process	**Residence Time**	**Heating Rate**	**Final Temperature [°C]**	**Products**
Torrefaction	10 - 60 min	Very small	280	Torrefied biomass
Carbonization	Days	Very low	> 400	Charcoal
Fast	< 2 s	Very high	~500	Bio-oil
Flash	< 1 s	High	< 650	Bio-oil, chemicals, gas
Ultrarapid	< 0.5 s	Very high	~1000	Chemicals, gas
Vacuum	2 - 30 s	Medium	400	Bio-oil
Hydropyrolysis	< 10 s	High	< 500	Bio.oil
Methanopyrolysis	< 10 s	High	> 700	Chemicals

volatile matter. The so-called primary volatiles derive from the thermal breakdown of the chemical bonds of the elements that make up the biomass, i.e. cellulose, hemicellulose and lignin. During this phase, the various products are formed, as permanent gases (CO, CO_2, CH_4), char and tar. This phase is known as primary pyrolysis, and can be followed by a subsequent phase where the primary pyrolysis products react with each other to create further compounds. An example may be the thermal cracking of tar created in primary pyrolysis, or reforming or polymerization reactions may occur; that starting from the above mentioned primary products, they create secondary products of pyrolysis. The distinction between primary pyrolysis and secondary pyrolysis is not exact, the two phases can even take place simultaneously within different zones of the fuel particles[11]. More in Generally, the pyrolysis process can be represented by the generic reaction:

$$\mathrm{C_nH_mO_p(Raw\ Biomass)} \longrightarrow \sum_{Liquid} \mathrm{C_xH_yO_z} + \sum_{Gas} \mathrm{C_aH_nO_c} + \mathrm{H_2O} + \mathrm{C(Char)} \qquad \text{(R 3.4)}$$

3.1.3 Types of pyrolysis

Depending on the heating rate of the biomass, the pyrolysis process can be defined as slow or fast. We are talking about slow pyrolysis, when the heating time required to bring the biomass

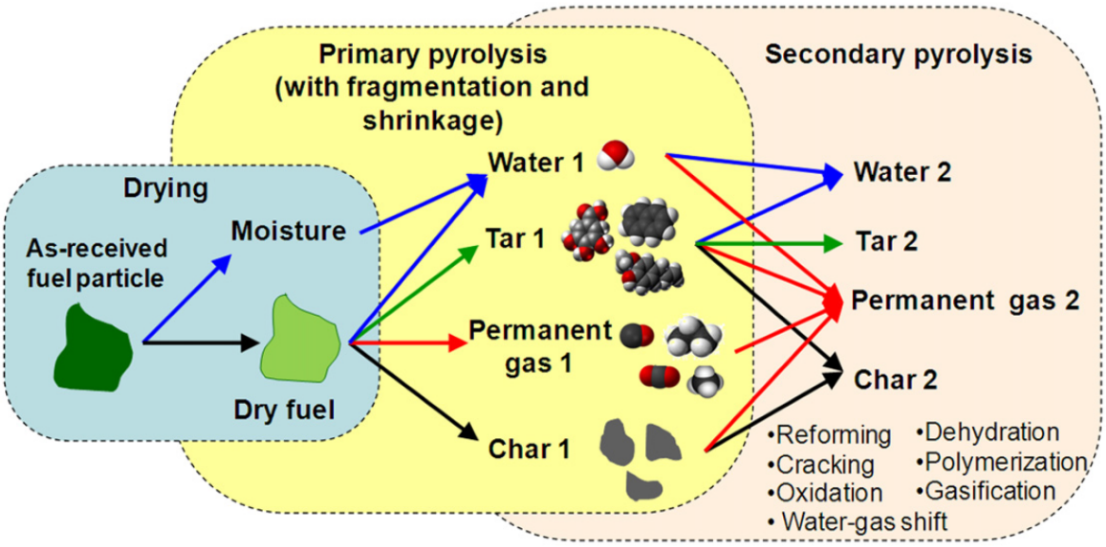

Figure 3.2: Thermal degradation of a biomass particle in a pyrolysis process

to the pyrolysis temperature is significantly longer than the characteristic reaction time of the process; instead the concept is the contrary when we talk about fast pyrolysis. Slow pyrolysis is characterized by very low heating rates and often occurs even at very low reaction temperatures (200 - 300°C) but with very long residence times. Slow pyrolysis is mainly used to maximize char production, while traditional pyrolysis is achieved thanks to the application of moderate heating rates (20°C/s) and equally moderate reaction temperatures (<600°C), with residence times varying between 10 seconds and 10 minutes. This type of pyrolysis, unlike the previous one, gives rise to comparable quantities of gas, tar and char. Fast pyrolysis has the objective of maximizing the production of bio-oil and gas. This is achieved by subjecting the raw biomass and a very rapid heating, followed by a very rapid cooling too. The peak temperature is decided on the basis of the products to be maximized:

- T < 650°C : Process aimed at the production of bio-oil
- T ≅ 1000°C : Process aimed to maximize the production of gas yield

The residence times for fast pyrolysis are very short and generally never more than a few seconds.

3.1.4 Pyrolysis products

Pyrolysis causes the breakdown of complex molecules to form smaller molecules, thus leading to a large number of substances generally divided into three categories:

- Solid (Char)
- Liquid (Tars, heavier hydrocarbons and water)
- Gas (CO_2 , CO , H_2 , H_2O , CH_4 , C_2H_2 , C_2H_4)

As mentioned, the relative quantities of these products depend on various factors, mainly on the pyrolysis temperature and on the heating rate.

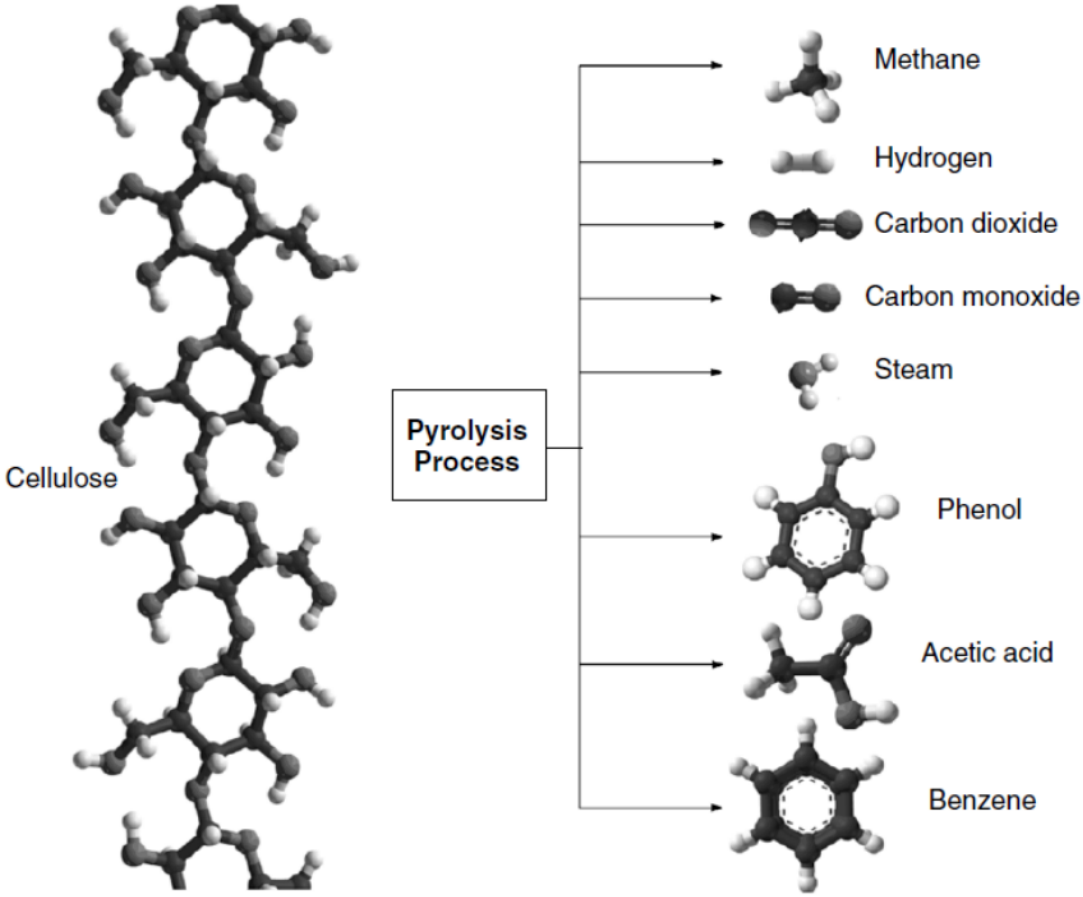

Figure 3.3: Pyrolysis products

Solid product: It is commonly called char. It is mainly composed of carbon, but it can also present traces of oxygen and, to a lesser extent, hydrogen. The approximate analysis, therefore, shows a high fixed carbon content and a low volatile matter content. Ash is very low in comparison to fossil fuels. Due to its high carbon content, the calorific value of the char is approx 32 MJ/kg; extremely higher than that of the starting wood biomass and liquid products obtained from the pyrolysis process.

Liquid product: The pyrolysis liquid product is known as bio-oil and derives from the rapid and simultaneous depolymerization and fragmentation of cellulose, hemicellulose and lignin. Typically, following a rather sudden heating, a rapid cooling is carried out, this to "freeze" the intermediate pyrolysis products and prevent further reactions between molecules of different types avoiding degradation processes. In literature there is still a widespread disagreement as to which is considered the most correct definition of bio-oil: the most used tends to refer to bio-oil as the sum of the entire liquid fraction, pyrolysis water and humidity. It is therefore possible to express the total fraction of bio-oil as[11]:

$$Y_{bio-oil} = Y_{tar} + Y_{\mathrm{H_2O}} + Y_M \tag{3.1}$$

During the pyrolysis and gasification processes many waste products are produced, including NO_x, $\mathrm{SO_2}$, ashes and tars. Among these, the tar is one of the most unwanted and difficult to treat. It looks like a thick and viscous liquid, black in color; the greater presence of volatile components in biomass compared to coal makes gasification of the former more subject to tar formation. The tar is a complex mixture of hydrocarbons, defined as: "All organic contaminants with a molecular weight larger than 78 [g/mol], which is the molecular weight of benzene". The reasons why tar represents an unwanted product are mainly two:

- Their composition
- Their condensation temperature

Since it is composed mostly of medium-long molecular chains, tar has a rather high carbon content. As seen for char, however, a high C content contributes substantially to increasing the heating value of the substance. The presence of tar at the exit of a process therefore reduces the LHV of the desired part of products, significantly affecting the overall performance of the system. In addition to this, the presence of a large number of heavy molecules inside it, causes the temperatures at which it condenses to be quite high, even above 120-130 °C. The presence of such a mixture is extremely unwanted inside an industrial plant, since cooling below these temperatures causes the condensation of the species contained in it and a consequent fouling of the internal surfaces of the equipment, which can lead from the simple reduction of the heat exchange characteristics to the actual occlusion of the component passage area. An example of fouling caused by tars is reported in figure 3.4. The greater presence of volatile components in biomass than coal means that the use

of the former as a source for exploitation by gasification is much more subject to tar formation than the use of the latter.

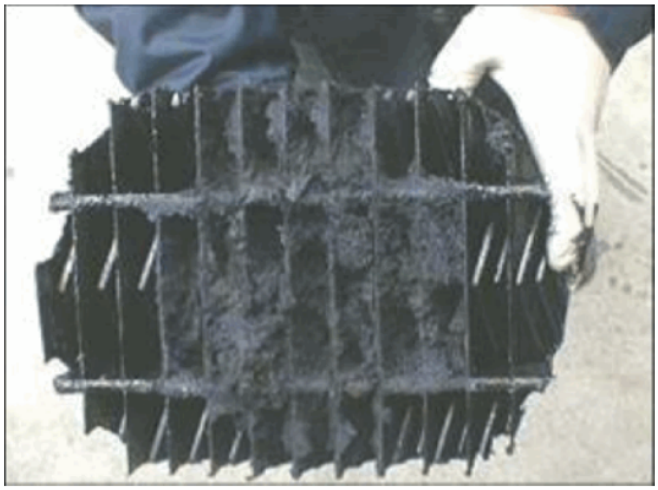

Figure 3.4: Fouling caused by tars

Gaseous product: From the decomposition of biomass both condensible and non-condensible gases are produced. The former, being made up of heavier molecules, after cooling condense and are therefore added to the liquid fraction. The other way around, the non-condensible fraction contains lighter molecules, such as carbon monoxide, carbon dioxide, methane, ethane, ethylene and a small fraction of hydrogen. To the gases produced directly by primary pyrolysis they are then added those formed by the secondary cracking of the initial gas mixture, called secondary gases. The LHV value of the pyrolysis gas can vary from 11 MJ/Nm^3 for primary gases to 20 MJ/Nm^3 (post cracking) for secondary gases.

3.1.5 Gasification

Gasification is a thermochemical process that occurs by incomplete oxidation at high temperatures of solid fuels. Usually, the temperature varies from 600 to 1000 °C and the goal of the process is to produce a low or medium HHV syngas essentially composed of combustion gases such as H_2, CO, CH_4 and diluting gases such as N_2, CO_2 and H_2O. Gasification also occurs in the combustion of woody biomass. For example, in a matchstick reported in figure 3.5 the gases and soot generated by the pyrolysis of the wood burn, provide the heat necessary to pyrolize the volatile matter of the biomass. The heat needed to start the process is given by the burning of the sulphur tip. The

flame is composed of different gases and soot combustion: the flame generated by soot is more orange and bright, instead the gas and tar combustion flame has a characteristic yellow color. The exhaust gases are transparent, while the pyrolysis gas generation is blue. Wood becomes before char and after ash during combustion[12]. The combustion of syngas has numerous advantages compared to the combustion of biomass. First of all, the control and regulation of combustion are very flexible and the exhausts have a high temperature which allows to achieve great efficiency according to the Carnot principle. Syngas combustion is clearer than biomass combustion in terms of soot and CO emissions. Furthermore, the gasification of wood biomass allows to obtain the maximum conversion efficiency of electric energy starting from wood biomass as raw material. Syngas is also suitable for synthetic liquids and for the production of pyrolysis oil and for the generation of steam. Air gasifiers generate low HHV gas with about 50% of N_2 and this is ideal for the production of energy and steam. The oxygen and hydrogen gasifiers are capable of producing medium HHV gas suitable for the generation of steam, the production of synthetic fuel and the use of energy carriers on site. Pyrolysis gasifiers have generated pyrolytic gas, pyrolysis oil and coal. Part of the carbon yield is used to produce the heat needed to provide the pyrolysis reaction. This chapter describes the biomass gasification process, the chemical reactions that occur and the most common fixed bed gasifier reactors are exposed. But the main purpose of the gasification which will be discussed in this thesis will be, as said in the introductory chapters, to feed solid oxide fuel cells integrated directly into the gasification system.

3.1.6 Processes in gasification

A general gasification reaction that occurs in gasifiers is a complex mechanism composed by five processes whose presence and succession depends on the reactor type:

- **Drying:** The total moisture of a freshly cut wood is between 30 and 60%. A minimum energy of 2.26 MJ is necessary to remove a kilo of water in the raw material and is not recoverable. Pre-drying of the wood at 10-20% humidity is required before gasification. The final drying takes place after the biomass has entered the gasifier, where it receives heat from the hot zone downstream. The surface humidity is removed above 100°C, at this temperature the VM starts to evaporate. The drying area in the gasifier ends at over 200°C.
- **Pyrolysis:** In the previous sections we have already widely spoken about the phenomenon of pyrolysis. When gasification takes place, pyrolysis is always an indispensable process that

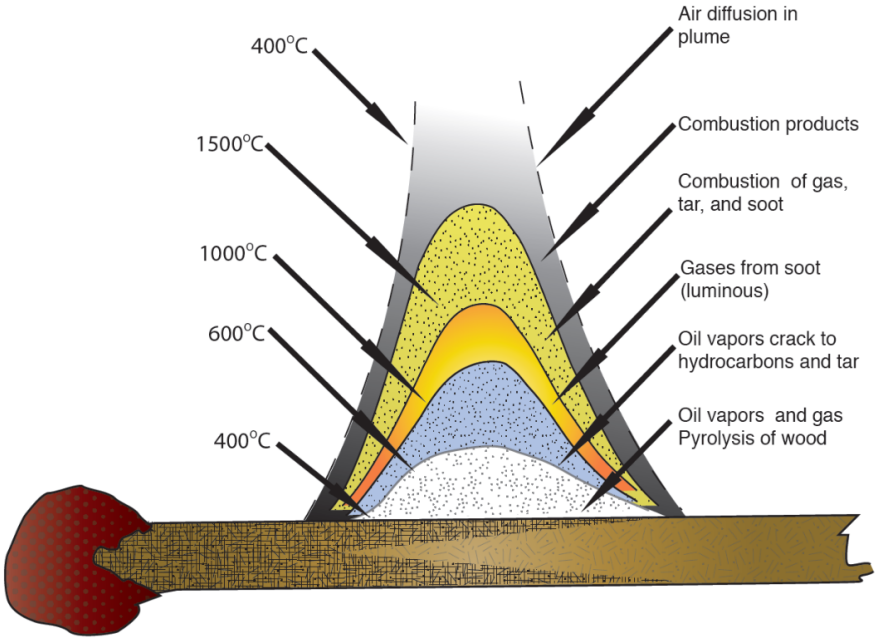

Figure 3.5: Gasification process in a matchstick combustion

occurs in conjunction with the gasification itself.

- **Combustion:** Part of char and tar produced by the pyrolysis is burned with air or oxygen. The products of combustion are H_2O and CO_2 which react in the reduction zone of the gasifier. The combustion zone is necessary to give the heat for pyrolysis and tar cracking.

- **Cracking:** As already explained above, tar is a complex mixture of condensible hydrocarbons including, among others, aromatic polyaromatic hydrocarbons and ring complexes. It looks like a thick, black, highly viscous liquid that condenses in the low temperature areas of a gasifier, obstructing the passage of gas and causing system interruptions. The tar produced in the pyrolysis process inside the gasifier, also known as tar gas, is in its gaseous phase and must be broken into small molecules such as H_2 and CO by the heat from combustion inside the reactor or from an external heat source. In addition, the syngas produced by the gasifier has a large amount of tar and one possible way to reduce it is by external heating. Generally, tar needs to be heated to 1200°C or 800°C with a catalyst to break the tar molecules.

- **Reduction:** These types of reactions are the real heart of the gasification process, they are reactions capable of reducing the oxidation number of a chemical species and therefore making it available to oxidize and release energy conserved in chemical potential. This process involves

chemical reactions between hydrocarbons, steam, carbon dioxide, oxygen and hydrogen in the reactor, as well as chemical reactions between the evolved gases. Of these, character reduction is the most important. The coal produced through the pyrolysis of biomass is not necessarily pure carbon. It contains a certain amount of hydrocarbon comprising hydrogen and oxygen. The character of biomass is generally more porous and reactive than coke. Its porosity is between 40 and 50%, while the porosity of coal varies between 2 and 18%. Therefore, its reaction behaviour is different from coal, brown coal or peat. The reduction of coal from biomass involves several reactions between coal and the gasifying media. Reduction reactions are generally endothermic, but some may also be exothermic.

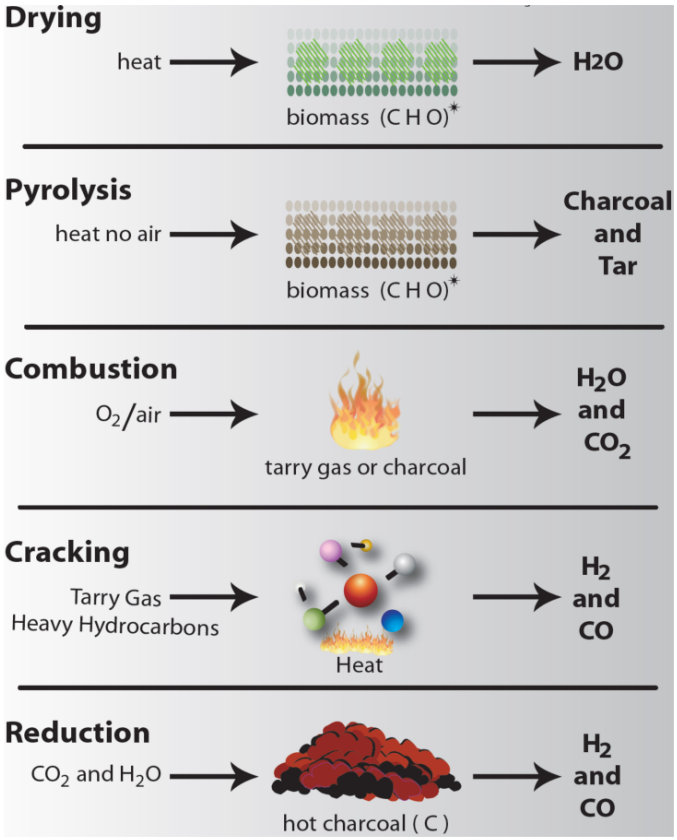

Figure 3.6: Processes in biomass gasification

3.1.7 Gasification chemical reactions

Inside gasifier reactors occur several chemical reaction which can be classified in five types depending on the reaction mechanisms: carbon, oxidation, shift, methanation and steam reforming[5].

Carbon reactions

There are four carbon reactions of interest in a gasification process:

$$\text{Boudouard:} \quad \mathrm{C + CO_2 \longleftrightarrow 2\,CO} \quad \Delta H^0 = +172 \text{ kJ/mol} \tag{R 3.5}$$

$$\text{Water-gas:} \quad \mathrm{C + H_2O \longleftrightarrow CO + H_2} \quad \Delta H^0 = +131 \text{ kJ/mol} \tag{R 3.6}$$

$$\text{Hydrogasification:} \quad \mathrm{C + 2\,H_2 \longleftrightarrow CH_4} \quad \Delta H^0 = -74.8 \text{ kJ/mol} \tag{R 3.7}$$

$$\text{Char-oxygen:} \quad \mathrm{C + \frac{1}{2}\,O_2 \longleftrightarrow CO} \quad \Delta H^0 = -111 \text{ kJ/mol} \tag{R 3.8}$$

Among the carbon reactions, the fastest is R 3.8, thus the combustion of carbon in oxygen. This process is so rapid that it leaves practically no trace of residual O_2 for the other reactions. The R 3.6 reaction, which involves carbon and H_2O, instead proceeds at a rate of 3-5 orders of magnitude lower than the previous one, while Boudouard reaction is slower by about 6-7 orders of magnitude than the first (R 3.8). The R 3.7 process, which involves carbon and H_2, is the slowest of the first group and it is particularly used in the production of SNG (Synthetic Natural Gas). In summary, the general picture is obtained from the considerations just made:

$$R_{C+\mathrm{O_2}} >> R_{C+\mathrm{H_2O}} > R_{C+\mathrm{CO_2}} >> R_{C+\mathrm{H_2}} \tag{3.2}$$

Oxidation reactions

Four exothermic oxidation reaction happen in the combustion zone for air and oxygen gasifiers:

$$\text{Char oxydation:} \quad \mathrm{C + O_2 \longleftrightarrow CO_2} \quad \Delta H^0 = -394 \text{ kJ/mol} \tag{R 3.9}$$

$$\text{Carbon monoxide oxydation:} \quad \mathrm{CO + \frac{1}{2}\,O_2 \longleftrightarrow CO_2} \quad \Delta H^0 = -284 \text{ kJ/mol} \tag{R 3.10}$$

$$\text{Methane oxydation:} \quad \mathrm{CH_4 + 2\,O_2 \longleftrightarrow CO_2 + 2\,H_2O} \quad \Delta H^0 = -803 \text{ kJ/mol} \tag{R 3.11}$$

$$\text{Hydrogen oxydation:} \quad \mathrm{H_2 + \frac{1}{2}\,O_2 \longleftrightarrow H_2O} \quad \Delta H^0 = -242 \text{ kJ/mol} \tag{R 3.12}$$

Char, carbon monoxide, methane and hydrogen generated by pyrolysis reaction with the oxygen of the gasifying agent to generate CO_2, water and heat necessary for the heating, drying and pyrolysis processes. Oxidation provides the highest amount of heat per mole of carbon consumed,

but char-oxygen reaction is also exothermic and produces CO of combustible gas. When carbon comes in contact with oxygen, both oxygenation and oxidation can occur, but their extent depends on the temperature. A partition coefficient θ can be defined to determine the division of oxygen between the two reactions. These reactions can be combined together:

$$\theta C + O_2 \longrightarrow 2\,(\theta - 1)CO + (2 - \theta)CO_2 \tag{R 3.13}$$

The variable θ can vary between 1 and 2 and it is affected by the temperature T [K] inside the reactor.

$$\theta = \frac{[CO]}{[CO_2]} = 2400 \cdot e^{[-(6234/T)]} \tag{3.3}$$

Water-gas shift reaction

The water-gas shift reaction is an important gas-phase reaction in a gasification process, it can be considered the most important among the gas-phase reaction. The purpose of this reaction is the increment of hydrogen content of the gasification product gas at the expense of carbon monoxide:

$$\text{Water-gas shift:} \quad CO + H_2O \longleftrightarrow CO_2 + H_2 \quad \Delta H^0 = -41.2 \ \text{kJ/mol} \tag{R 3.14}$$

Another important aspect of this reaction is to adjust the relationship between carbon monoxide and hydrogen in the product gas. The water-gas shift reaction is slightly exothermic and its equilibrium decreases slowly with temperature. An interesting aspect is given by the fact that depending on temperature, it may be driven in either direction. Above 1000°C it rapidly reaches equilibrium, but at a lower temperature it needs heterogeneous catalysts.

Methanation reactions

Two types of methanation reactions are considered in gasification:

$$2\,CO + 2\,H_2 \longleftrightarrow CH_4 + CO_2 \quad \Delta H^0 = -247 \ \text{kJ/mol} \tag{R 3.15}$$

$$CO_2 + 4\,H_2 \longleftrightarrow CH_4 + 2\,H_2O \quad \Delta H^0 = -165 \ \text{kJ/mol} \tag{R 3.16}$$

Steam-reforming reactions

The steam-reforming reactions considered in gasification are the following:

$$CH_4 + H_2O \longleftrightarrow CO + 3\,H_2 \quad \Delta H^0 = +206 \text{ kJ/mol} \tag{R 3.17}$$

$$CH_4 + \frac{1}{2}\,O_2 \longleftrightarrow CO + 2\,H_2 \quad \Delta H^0 = -36 \text{ kJ/mol} \tag{R 3.18}$$

3.1.8 Gasifier classification

A gasifier can be classified according to many factors, among which we remember:

- **Medium:** It represents the gasifying agent which is introduced inside a gasifier. The most used are air, pure oxygen, steam and carbon dioxide. Air has the advantage of being practically cost-free and constantly available. An air operated gasifier generates a syngas with HHV between 4 - 7 MJ/Nm^3 because the syngas is diluted with nitrogen which does not react because it is an inert gas; the reactor maintains temperatures between 800 and 1000 °C. A gasifier operating with pure oxygen generates a syngas with HHV between 12 - 28 MJ/Nm^3. The carbon monoxide and hydrogen content in an oxygen blown gasifier can reach the 90%. In a steam gasifier, there is a syngas with HHV between 10 - 18 MJ/Nm^3 but the reactions that take place are highly endothermic. Same thing happens in a carbon dioxide gasifier, where the main reaction is the Boudouard reaction, which is strongly endothermic.

- **Heat source:** The most important reduction reactions are endothermic, thus some heat is needed to balance the reactions. This heat can be given by exothermic oxidation reaction inside the reactor (auto-thermal) or outside the reactor (allo-thermal).

- **Design:** The design of a reactor is mainly based on the type of solid gas contact. There are three types: fixed bed, fluidized bed and entrained flow.The fixed gasifiers are further subdivided into specific types as shown in Figure 3.7

- **Purpose:** It is simply the final scope for the energy. It can be heat, electrical power and chemicals.

- **Scale:** It indicates the power size of the plant.

In this thesis the DB-SOFC project will be considered as a fixed bed reactor of design updraft where the gasifying agent is carbon dioxide. In the gasifier there is no combustion zone, in fact

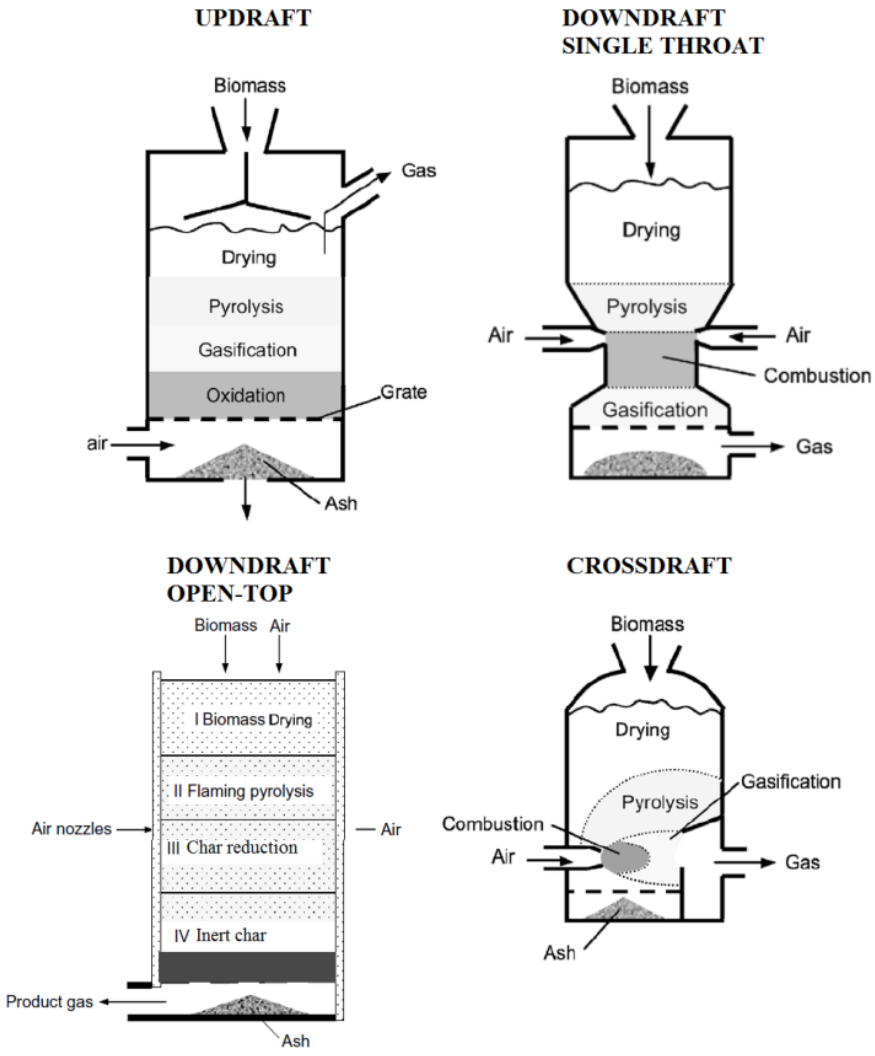

Figure 3.7: Fixed bed gasifier design

the heat needed to make the gasification reactions that takes place is given only by the SOFCs which are kept at a constant temperature of 800 °C. The aim of the project is to produce both electricity and syngas, and at the moment, the scale of the gasifier is to supply with syngas 25 SOFCs and exploit outside the gasifier the remaining syngas. In the gasification system of the DB-SOFC project, the reactor also has additional components in the part concerning the biomass bed. In fact, to mix the biomass and the gasifying agent well, a rotating distribution screw system is adopted which, in addition to serving as a biomass inlet, also serves to mix the compound. The gasification reactions and the advantages of having CO_2 gasification are illustrated in the following figure.

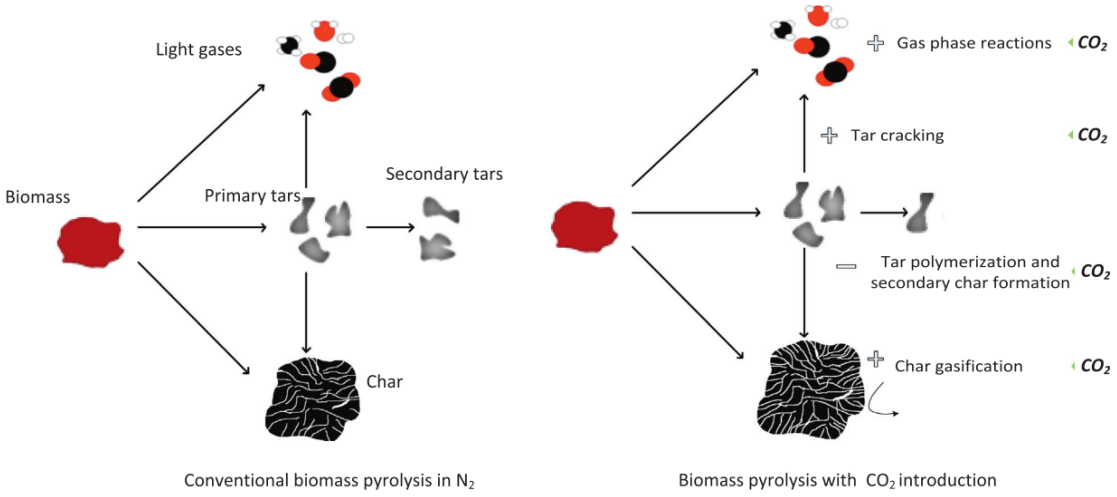

Figure 3.8: CO_2 gasification pathways

3.1.9 Kinetics of gasification

If we are considering the generic reaction:

$$\mathrm{nA} + \mathrm{mB} \xrightarrow{k_{for}} \mathrm{pC} + \mathrm{qD} \tag{3.4}$$

Where n, m, p and q are the stoichiometric coefficients of the reactants A, B and the the products C and D. The rate of reaction of this reaction is:

$$r_1 = k_{for} \cdot C_A^n \cdot C_B^m \tag{3.5}$$

Where C_A and C_B are the concentrations of the reactants. The unit of measure depends of the initial unit of measures of variables. The reaction can even move in the reverse direction:

$$\mathrm{pC} + \mathrm{qD} \xrightarrow{k_{back}} \mathrm{nA} + \mathrm{mB} \tag{3.6}$$

The rate of the reverse reaction is similar to the direct rate of reaction:

$$r_2 = k_{back} \cdot C_C^p \cdot C_D^q \tag{3.7}$$

When the reaction takes place, the concentration of reagents A and B is maximum and the concentration of products C and D is minimum. So the reaction rate in the direct direction is

higher than the reaction rate in the opposite direction. At a certain point, as the reaction progresses, the two reaction rates will be equal, and therefore there will be a state of chemical equilibrium. At equilibrium:

- The concentration of the chemical species present in the reaction no changes anymore.
- The Gibbs free energy of the system is minimum.
- The entropy is maximum.

Under equilibrium, we will get:

$$r_1 = r_2$$

$$k_{for} \cdot C_A^n \cdot C_B^m = k_{back} \cdot C_C^p \cdot C_D^q \tag{3.8}$$

A certain rate constant k_i is independent of the concentration of reactants or products but it depends only on the temperature T. The formula that shows this dependence is expressed in Arrhenius form:

$$k = A_0 \cdot \exp\left(-\frac{E}{RT}\right) \tag{3.9}$$

Where A_0 is knows as prexponential constant, R is the universal gas constant, and E is the activation energy for the reaction. Another parameter to report is the equilibrium constant:

$$K_e = \frac{k_{for}}{k_{back}} = \frac{C_C^p C_D^q}{C_A^n C_B^m} \tag{3.10}$$

The equilibrium constant can be expressed also through the Gibbs free energy:

$$\Delta G = \Delta H - T\Delta S \tag{3.11}$$

$$K_e = \exp\left(-\frac{\Delta G}{RT}\right) \tag{3.12}$$

3.2 Fuel cells

The fuel cell is an electrochemical system capable of converting the chemical energy of a fuel directly into electricity, without the intermediate intervention of a thermal cycle, thus obtaining higher conversion yields than those of conventional thermal machines. A fuel cell works similarly to a battery, in that it produces electricity through an electrochemical process; however unlike

the latter, it consumes substances from the outside and is therefore able to function without interruptions, as long as the system is supplied with fuel (H_2 or CO) and oxidant (O_2 or air). The cell is composed of two electrodes in porous material, separated by an electrolyte. The electrodes act as catalytic sites for cell reactions that basically consume carbonaceous fuel or hydrogen and oxygen, with the production of water and the passage of electric current in the external circuit. The electrolyte has the function of conducting the ions produced by one reaction and consumed by the other, closing the electrical circuit inside the cell, and at the same time preventing the mixing between anode and cathode gases. The final reaction that takes place inside the cell is exothermic, that is, it releases energy; this manifests itself in the form of heat and electricity. In the next figure we can see the fuel cell operating principle[13].

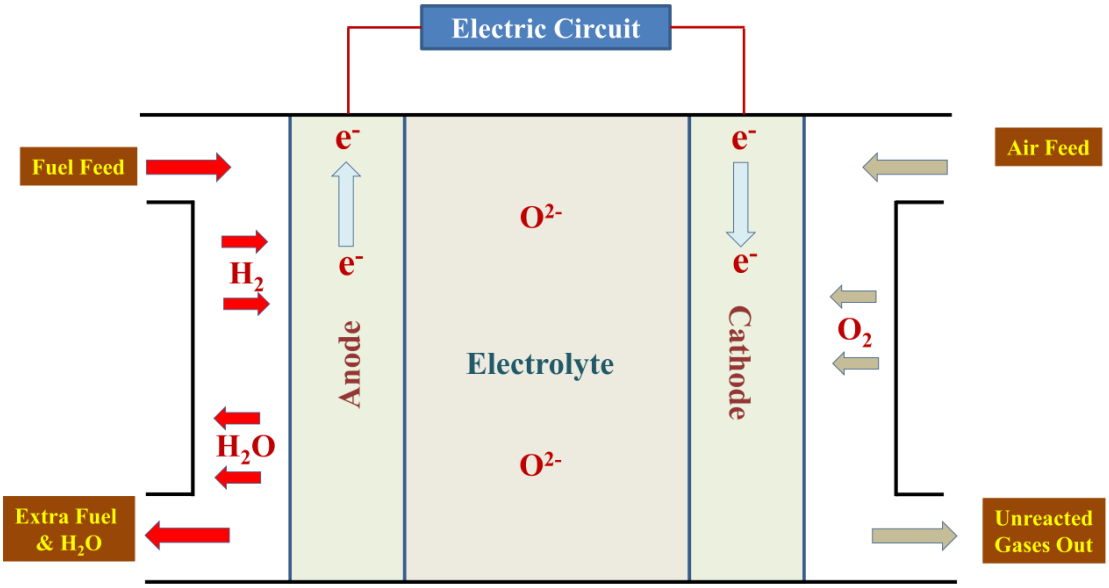

Figure 3.9: Fuel cell operating principle

So in this process occurs a charge separation, creating electrical fields on both electrodes. A voltage differential is established between the two electrodes. When the circuit will be closed also a current is created. the electrical power generated will be equal to:

$$W_{el} = \Delta V \cdot I \quad [W] \tag{3.13}$$

$$I = \dot{n_i} \cdot z \cdot F \quad [A] \tag{3.14}$$

where:

- $\dot{n}_i$ [mol/s] is the molar flow rate of species i
- z [-] is the number of electrons exchanged in the reaction
- F = 96486.7 [C/mol] is the Faraday's constant

3.2.1 Polarization curve

As mentioned above, inside a fuel cell, chemical energy is converted into electrical energy without passing through thermal energy, as is still the case today in most electrical energy production plants. The transformation from chemical energy to electricity is also subject to various types of losses. The formula that describes the total voltage differential is:

$$V = E - \eta_{act} - \eta_{ohm} - \eta_{diff} \quad [V] \tag{3.15}$$

Now we will analyze the various contributions within the formula:

- E is the reversible voltage that is the voltage which is present between the two electrodes in open circuit condition. When no current flows between the two electrodes, a chemical equilibrium is established between the anode and the cathode, therefore we speak of OCV (open circuit voltage). You can easily get to the final formula by going from the first and second principles of thermodynamics:

$$E = OCV = -\frac{\Delta g_{react}(T, p_0)}{z_f \cdot F} + \frac{R \cdot T}{z_f \cdot F} \cdot \ln \frac{\prod_1^n (\frac{p_i}{p_0})^{v_i}}{\prod_1^m (\frac{p_i}{p_0})^{v_i}} \quad [V] \tag{3.16}$$

  where

  - Δg_{react} [J/mol] is the molar Gibbs free energy for the reaction
  - F = 96486.7 [C/mol] is the Faraday's constant
  - R = 8.314 [J/(mol K)] is the universal gas constant
  - z_f is the number of electrons delivered by considered fuel
  - p_0 is the reference pressure
  - p_i is the pressure for a generic chemical species i
  - m and n are the number of products and reactants respectively

- v_i is the generic stoichiometric coefficient

- η_{act} are the activation overvoltages that represents the amount of voltage that has to be spent to overcome the energetic threshold of the activation of the electrochemical reaction.

- η_{ohm} are the ohmic overvoltages that are the losses due to both the resistances of electrodes and external circuit and to electrons transport and of electrolytic membrane to ions transport.

- η_{diff} are the diffusion overvoltages, due to the reduction in concentration of reactants in the point of reaction.

The voltage losses by diffusion and by activation must obviously be considered both for the anode and for the cathode. In the figure is shown a typical curve V-I for a fuel cell, it is known as Polarization Curve[14].

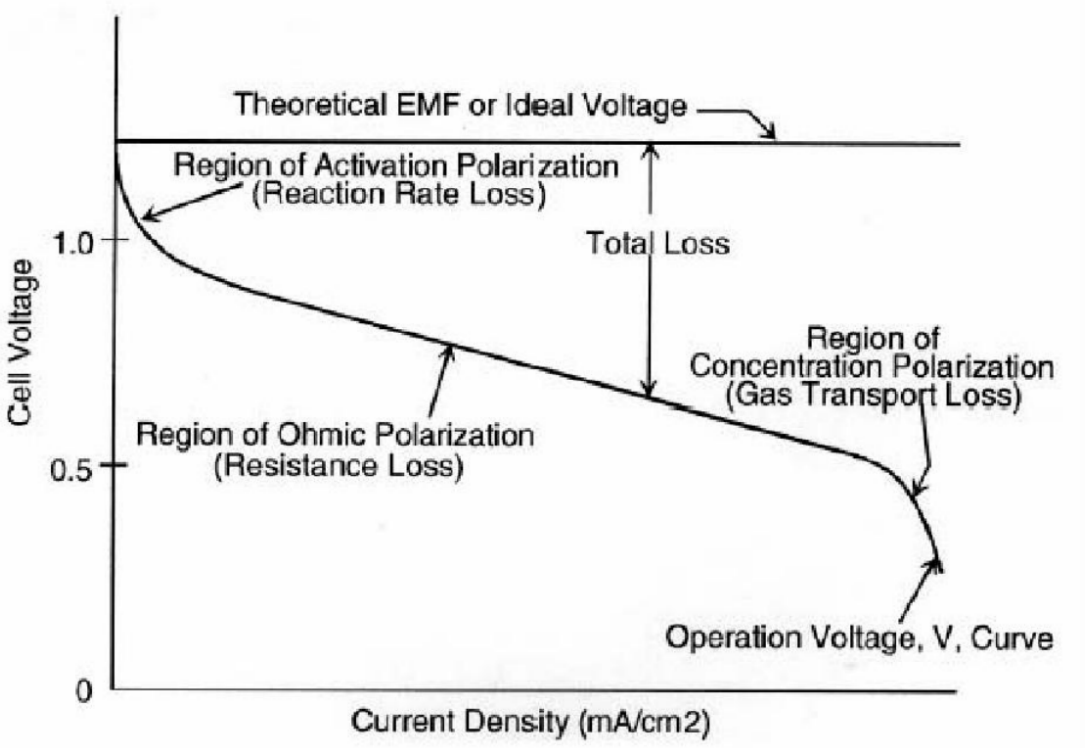

Figure 3.10: Typical fuel cell polarization curve

As we can notice, the fuel cell voltage starts to decrease when we increase the current density. In the OCV condition, there is no reactants conversion, when we close the circuit reactants reaction begins, also the polarization phenomena starts; these phenomena cause voltage drop respect the OCV value.

3.2.2 Solid Oxide Fuel Cell

Solid oxide fuel cells are defined as a "clean, pollution-free technology" for the electrochemical generation of high efficiency electric current. The advantages related to the use of these cells are tangible and mainly involve aspects of system design in which a SOFC can be used. The advantages are manifested in terms of: high efficiency, modularity, fuel adaptability, very low NOx and SOx emissions, possibility of reforming natural gas in the cells stack, possibility of integration in systems with gas or steam turbine or in systems for cogeneration heat. They are cells that use a solid state electrolyte, and reach the highest temperatures among all fuel cell technologies. The electrolyte used is a ceramic material (usually zirconium oxide, ZrO_2, stabilized with yttrium oxide, Y_2O_3) that conducts O^{2-} ions. This material is particularly suitable for its abundance in nature, chemical stability, non-toxicity and cost-effectiveness; on the other hand, it has drawbacks related to the high coefficient of thermal expansion, it is known as YSZ. The anode is usually made of cermet, a ceramic (ZrO_2) - metallic (Ni) composite material. Nickel, in addition to having good conductivity characteristics, acts as a catalyst for the internal reforming reaction. The cathode is made of a composite ceramic material, consisting in electron conducting oxides and ion conducting ceramic materials (Lanthanum Manganate, doped with strontium which acts as a semiconductor, it is called Perovskite). Unlike the other types of fuel cells, SOFCs can also operate on carbon fuel, typically the fuels used are H_2 and CO. The semireactions that take place inside the cell are:

- Anode: Hydrogen and carbon monoxide oxidation

$$2\,H_2 + 2\,O^{2-} \longrightarrow 2\,H_2O + 4\,e^- \tag{R 3.19}$$

$$2\,CO + 2\,O^{2-} \longrightarrow 2\,CO_2 + 4\,e^- \tag{R 3.20}$$

- Cathode: Oxigen reduction

$$O_2 + 4\,e^- \longrightarrow 2\,O^{2-} \tag{R 3.21}$$

Thus, the overall reactions are:

$$2\,H_2 + O_2 \longrightarrow 2\,H_2O \tag{R 3.22}$$

$$2\,CO + O_2 \longrightarrow 2\,CO_2 \tag{R 3.23}$$

The main feature of the cell is its high operating temperature: in addition to representing a cause

of problems (mechanical and chemical stability of the materials used, higher start-up times than in other cells) it allows the realization of internal reforming reactions to the cell itself and therefore the supply of the cell directly to natural gas. An essential aspect linked to SOFC cells is also the wide possibility of using the heat produced by the electrochemical reaction, mainly linked to the ohmic losses and to the activation of the electrodes. The heat produced is used to keep the cell operating temperatures high, to preheat the cathode reagent flow and to recover heat for cogeneration uses. Electric power and heat are useful products of a SOFC stack. The problem of thermal loads is also a general feature of this type of cell, given the use of ceramic materials, which resist limited mechanical efforts. Therefore, SOFCs lend themselves well to stationary operation. The basic scheme of a solid oxide cell is very simple, however the fundamental problem related to the definition of the cell configuration was to carry out a project that would allow to effectively put together a certain number of cells (cell stack) to have a significant electrical output power value. The absence of a liquid phase simplifies cell management and allows to develop different construction geometries.

There are two types of design for SOFC:

- **Planar cells:** In this configuration, the cell components are configured as flat plates which are connected in electrical series. A simple scheme of a planar configuration is shown below: This configuration is currently of great interest especially since progress has been made in

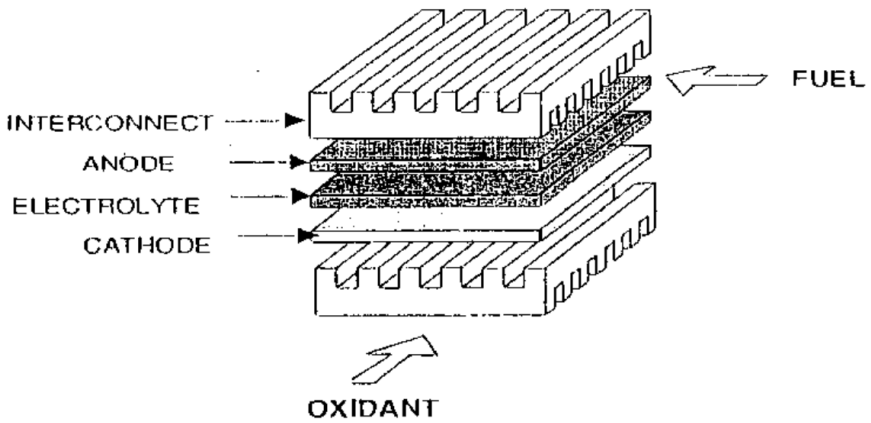

Figure 3.11: Planar configuration of SOFC

researching materials. However, the greatest problem in the design of planar configuration is related to the gas flows within the cell and to the reduction of leaks to the outside.

- **Tubular cells:** This configuration, compared to the planar configuration, presents a greater

constructive difficulty, but it also obtains considerable advantages such as the decrease if not almost no gas loss and the possibility of recirculation of the exhausted anodic flow favouring internal reforming. On the other hand, the connection between the various cells is more difficult.

In figure 3.12 such configuration is shown.

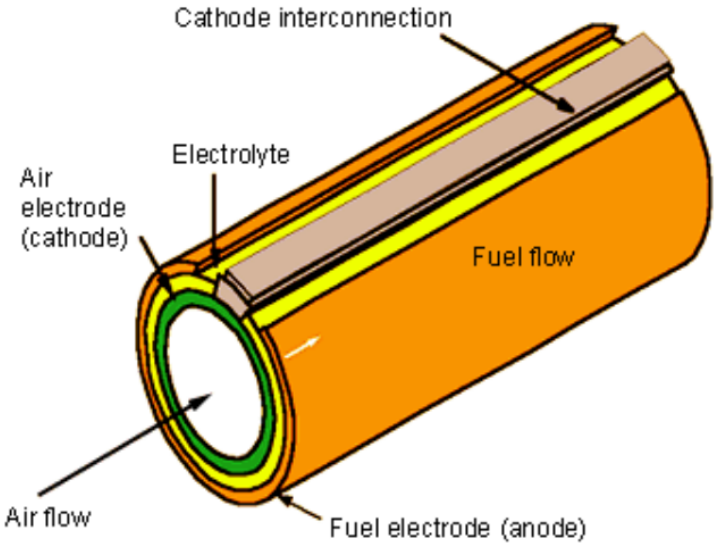

Figure 3.12: Tubular configuration of SOFC

In this thesis and therefore in the DB-SOFC project, this tubular, electrolyte supported cell configuration was chosen, due to its high efficiency.

Chapter 4

Numerical Assumptions and Multiphysics Modelling

The first step will be to model the physical problem concerning the DB-SOFC project, which will be articulated in different phases. It is necessary to initially choose the type of biomass and to establish its own chemical-physical properties through literature or already existing experiments. The software used to perform CFD simulations is a multiphysics software called COMSOL multiphysics®. In it, you have to transport the chosen geometry and use physical pre-established already implemented in the software. So at this point you will travel two parallel pathways: by modelling the reaction kinetics of the gasifier process with all the boundary conditions, and at the same time simulate the exchange of mass and energy that occurs at the boundary with the fuel cells. In this chapter we will make a systematic analysis of all these steps, providing all the formulas necessary to fully understand the transport of the real physical problem to the CFD model developed in the software.

4.1 Preliminary analysis

The preliminary analyzes will concern the biomass, the geometry and the dimensions of the system and the most basic physical assumptions.

4.1.1 Biomass for DB-SOFC project

As previously mentioned, three different types of biomass were used to power the system: olive kernel (OK), pruning from grape vine (GV) and the organic fraction of municipal solid waste (OFMSW). These three typologies were chosen for their availability in the whole area of interest of the project. In the next figure we can see the three biofuels.

Figure 4.1: The three types of biofuel

For numerical analysis, the olive kernel is the biomass analyzed and the one on which all the assumptions made will be based. As part of the DB-SOFC project, analyzes on chemical compositions have already been carried out by a Spanish research institute (INCAR-CSIC) and the following results have been highlighted regarding OK and GV[15]:

Tabel 4.1:Chemical analysis and heating value of raw biomass sample

	OK	**GV**
Elemental Analysis (wt%)		
C	50.2	47.0
H	5.9	5.7
N	0.7	1.0
O	40.2	41.4
S	0.02	0.06
Molar ratios		
H/C	1.41	1.6
O/C	0.60	0.66
Proximate analysis (wt%)		
Moisture	7.4	7.2
Ash Content	2.9	4.8
Volatile Matter	75.8	76.4
Fixed Carbon	13.9	11.6
HHV (MJ/kg) dry basis	20.03	18.41
LHV (MJ/kg) dry basis	18.82	17.24

Knowing elementary analysis is a very important result for advancing in biomass analysis. In fact, from the latter it is possible to know a raw formula of the raw biomass according to a form of the type CH_xO_y. The formulas to use are[16]:

$$x = \frac{HM_C}{CM_H} \qquad\qquad x = \frac{OM_C}{CM_O} \tag{4.1}$$

where C, H and O are the mass fraction, while M_C,M_H and M_O are the molecular weights of carbon, hydrogen and oxygen in the feedstock, respectively. So using the formulas above and also using the ultimate analyzes, it will be obtained that the raw formula of the raw biomass is $C_5H_7O_3$.

The scientific literature is full of articles about biomass and more generally in the process of gasification of the latter to obtain syngas for the most varied purposes. Therefore, since the characteristics of biomass are known, the other chemical-physical properties necessary to complete the numerical and mathematical model can easily be found in literature[17][18][19][20]. Below we will find the formulas used to find these parameters:

$$\text{Heat capacity:} \quad C_p^{biomass} = 1500 + T[K] \quad \left[\frac{J}{kgK}\right] \tag{4.2}$$

$$\text{Thermal conductivity:} \quad k_{biomass} = 0.056 + 2.6 \cdot 10^{-4} \cdot T[K] \quad \left[\frac{W}{mK}\right] \tag{4.3}$$

$$\text{Biomass Density:} \quad \rho_{biomass} = \rho_{apparent} = \rho_{bulk} = 650 \quad \left[\frac{kg}{m^3}\right] \tag{4.4}$$

$$\text{Biomass Permeability:} \quad \kappa_{\text{biomass bed}} = \kappa_{biomass} = \frac{d_0^2}{32} = 3.125 \cdot 10^{-10} \quad [m^3] \tag{4.5}$$

$$\text{Biomass Porosity:} \quad \varepsilon_{\text{biomass bed}} = \varepsilon_{biomass} = 0.4 \quad [-] \tag{4.6}$$

$$\tag{4.7}$$

Important observations can be made from the previous equations. The first consideration can be made on thermal capacity and thermal conductivity, in fact they are not constants but vary according to the temperature, more specifically, the higher the temperature, the larger these values will be. On the other hand, as far as density, permeability and porosity are concerned, the consideration that can be made is that in addition to the fact that it is constant, a very strong hypothesis has been made: the gasifier of the DB-SOFC project will be very close to the type of fixed bed, therefore the biomass particles will be packed in a fixed volume that will be kept

stationary at the same height, the hypothesis is that these three parameters are the same both for the single biomass particle and for the total volume occupied by the packed biomass. This hypothesis is reasonably due to a very small size of the biomass particle (100 - 200 [μm]), as we can see in the next figure.

Figure 4.2: Size of OK samples (100 - 200 [μm])

4.1.2 The design

After talking about the characteristics of the selected biomass, we may start talking about the geometry of the system. During the first months of work, the first creators of the project decided on a first configuration that the system could have, as shown in the figures 4.3 and 4.4.

This preliminary geometry is not fully forthcoming on the true shape that the complete system will have. It is therefore necessary to decide the 3D geometry that will be used as definitive geometry. In fact, the purpose of this thesis lies precisely here: to choose the geometry that manages to maximize the efficiency of the gasification system with built-in SOFCs. So to continue the analysis two fairly basic geometries have been chosen, but which will allow you to say safely which geometry is most suitable for this type of system.

Once the geometries are known and on which to simulate the gasification process, the geometry can be weighed and implemented on the COMSOL® software, where the same dimensions as in reality will be respected. An important computational simplification to be done concerns the software model. Given the complexity and variety of system components, it seems obvious that the model must be a 3D model. But a big simplification to be done is to divide the 3D domain in

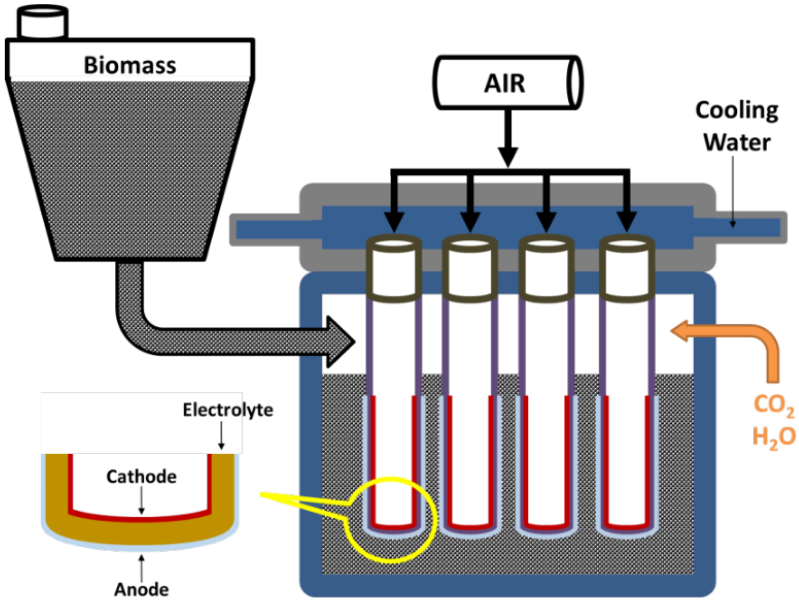

Figure 4.3: DB-SOFC initial stack configuration

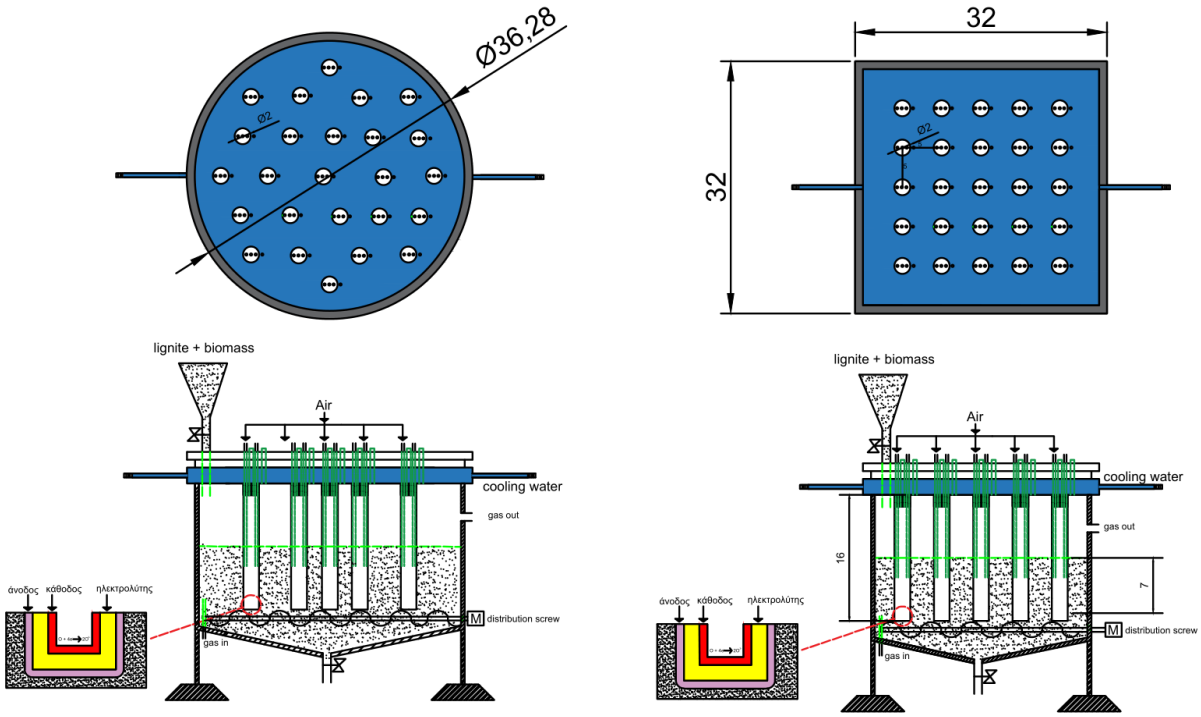

Figure 4.4: DB-SOFC analyzed geometries

half, being both the geometries analyzed symmetrical with respect to the zx plane. In the next figures the geometries implemented in the software are shown.

An important consideration is that all the measures have been chosen in order to keep the total volumes of both systems equal. As far as the components are concerned, the inlets, outlet, the

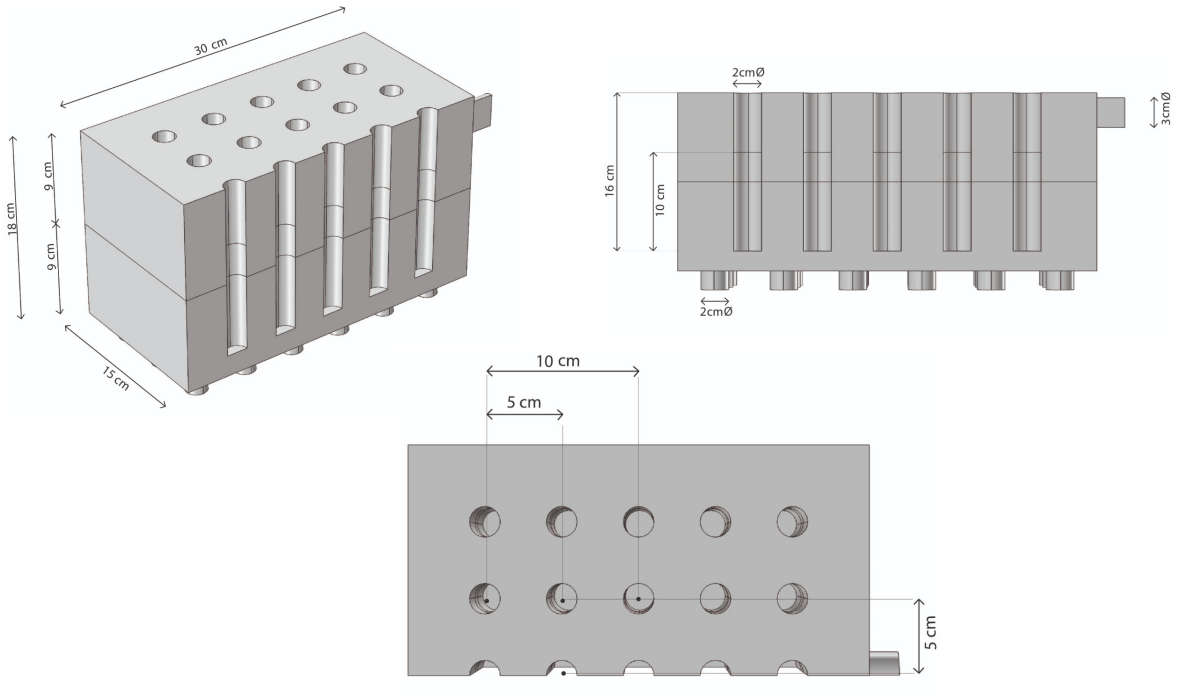

Figure 4.5: DB-SOFC square geometry

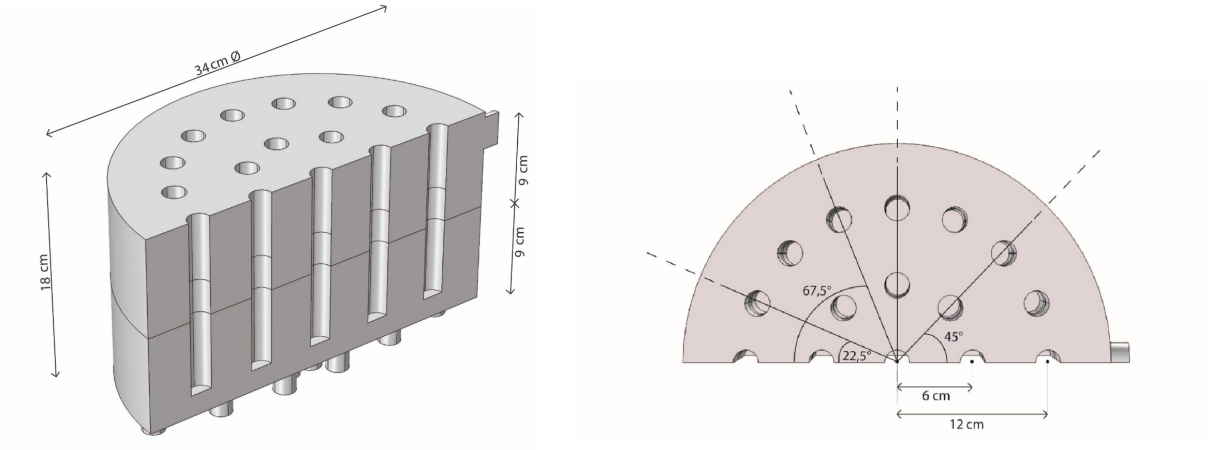

Figure 4.6: DB-SOFC circular geometry

cavities that act as an interchange with the SOFCs are present and the main domain is divided in half where the lower part corresponds to the biomass bed and the upper part corresponds to the free flow.

4.2 Physical and computational models

In this section we will analyze all the physical and mathematical models used, making the appropriate considerations on all the parameters that will influence their progress.

4.2.1 Fluid flow model

Studying fluid flow in CFD environment is always a very delicate and problematic topic. First we need to define the most suitable set of equations to best describe how the problem can be, in addition to also defining the physical properties and how the geometry of the problem has already been done. The basic equation set for any fluid dynamics problem are Navier-Stokes equations which are differential equations impossible to solve on paper, for this we need software that can solve with a certain degree of accuracy using appropriate solving algorithms. Whether it is cylindrical or cubic geometry, the domain will be divided into two parts. The lower part will be treated as a porous matrix with the same chemical-physical characteristics of biomass, instead the upper domain will be a free flow. So the equations will be of two types, those for the porous matrix and those for the free flow. Other premises are that the flow is considered laminar and compressible since it is CO_2 at low inlet speed. The problem to be solved will be in a steady state, being the DB-SOFC system designed to work in stationary conditions. The equations will be represented as follows[21]:

- Free fluid flow:

$$\begin{cases} \nabla \cdot (\rho \mathbf{u}) = 0 \\ \rho \mathbf{u} \cdot \nabla \mathbf{u} = -\nabla p + \nabla \cdot \left(\mu \left(\nabla \mathbf{u} + (\nabla \mathbf{u})^T \right) - \frac{2}{3} \mu (\nabla \cdot \mathbf{u}) \mathbf{I} \right) + \mathbf{F} \end{cases} \tag{4.8}$$

  Where:

  - ρ is the density of fluid $[kg/m^3]$
  - $\mathbf{u}$ is the velocity vector $[m/s]$
  - p is the pressure [Pa]
  - $\mathbf{I}$ is the identity matrix
  - μ is the dynamic viscosity of fluid $[Pa \cdot s]$
  - $\mathbf{F}$ is the volume force vector $[N/m^3]$

– T is the absolute temperature $[K]$

- Flow in porous matrix:

$$\begin{cases} \nabla \cdot (\rho \mathbf{u}) = Q_{br} \\ \frac{\rho}{\varepsilon_p} (\mathbf{u} \cdot \nabla) \frac{\mathbf{u}}{\varepsilon_p} = -\nabla p + \nabla \cdot \left[\frac{1}{\varepsilon_p} \left\{ \mu \left(\nabla \mathbf{u} + (\nabla \mathbf{u})^T \right) - \frac{2}{3} \mu (\nabla \cdot \mathbf{u}) \mathbf{I} \right\} \right] + \\ - \left(\kappa^{-1} \mu + \frac{Q_{br}}{\varepsilon_p^2} \right) \mathbf{u} + \mathbf{F} \end{cases} \tag{4.9}$$

Where:

– ε_p is the porosity of biomass bed

– κ is the permeability of biomass bed $[m^2]$

– Q_{br} is the mass source or mass sink $[kg/(m^3 \cdot s)]$

– The other parameters are the same of the previous set of equations

As mentioned above, the fluid flow at the entrance of the device is considered laminar. The Reynolds number is of important use to ascertain this hypothesis. The worst case scenario will be considered, that is when the inlet speed will be higher. In the case of the two geometries, the inlets will be 18 in the case of square geometry and 20 in the case of cylindrical geometry. the CO_2 flow rate will be maximum in the various simulations conducted at a value of 5 g/s and 800°C. So through the following formulas you can understand what is the maximum speed applied in the simulations:

$$\dot{m} = \frac{\dot{M}}{\#\text{ of Inlet}} \quad [kg/s] \tag{4.10}$$

$$u = \frac{\dot{m}}{\rho A} \quad [m/s] \tag{4.11}$$

$$Re = \frac{\rho u D}{\mu} \quad [-] \tag{4.12}$$

Where:

- $\dot{M}$ is the total mass flow entering in the system [kg/s]

- $\dot{m}$ is the single inlet mass flow [kg/s]

- A is the cross section area of the inlet $[m^2]$

- D is the diameter of the inlet $[m]$
- Re is the Reynolds number [-]

All the physical properties of CO_2 are taken for 800°C and therefore considering the worst case with a mass flow rate of 5 g/s, we will obtain a Reynolds number equal to:

$$Re = 427.2 < 2300 \quad [-] \tag{4.13}$$

So it can be said with certainty that the flow is certainly in laminar regime. In the next figure we can see the arrangement of the inlets in both geometries. The modelling choice was made to design multiple inlets to allow CO_2 to spread adequately within the porous domain.

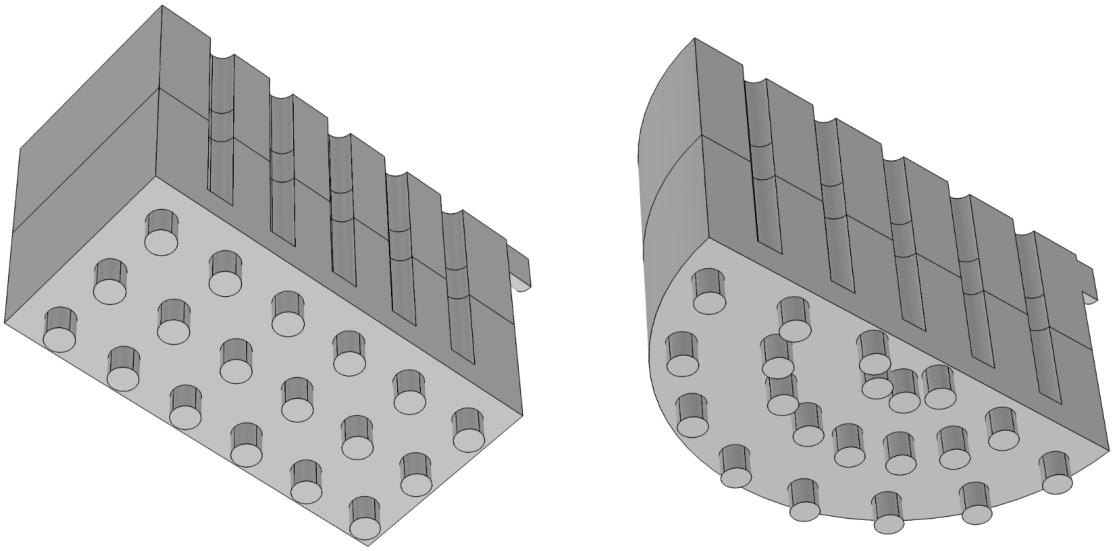

Figure 4.7: Inlet distribution in both geometries

Finally we talk about the pressure inside the system, it is set to atmospheric pressure. While the rest of the system boundaries that are nor inlets or outlets are considered to be walls.

4.2.2 Transport of chemical species

The previous physical model was useful for calculating the motion field and the pressure field within the system; now instead a physical model is needed to be coupled to the previous one to compute the transport, that is the diffusion of the chemical species involved and the aforementioned homogeneous or heterogeneous reactions that are created inside the reactor. To accomplish these

duties, we will use the COMSOL® interface dedicated to solving the mass transport equations. In addition to the motion fields, the mass fractions of each chemical species within the gas mixture will also be obtained. The basic equation of mass diffusion, also including convection, translates as follows in steady state condition:

$$\nabla \cdot (\rho \omega_i \mathbf{u}) = -\nabla \cdot \mathbf{j}_i + R_i \tag{4.14}$$

Where:

- ρ is the mixture density $[kg/m^3]$
- $\mathbf{u}$ is the mass averaged velocity of the mixture [m/s]
- ω_i is the mass fraction [1]
- $\mathbf{j}_i$ is the mass flux relative to the mass average velocity $[kg/(m^2 \cdot s)]$
- R_i is the rate expression describing mass production or consumption $[kg/(m^3 \cdot s)]$

The relative mass flux vector $\mathbf{j}_i$ can include contributions due to molecular diffusion and thermal diffusion. Summation of the transport equations over all present species gives the conservation of mass:

$$\nabla \cdot (\rho \mathbf{u}) = 0 \tag{4.15}$$

$$\sum_{i=1}^{Q} \omega_i = 1 \qquad \sum_{i=1}^{Q} \mathbf{j}_i = 0 \qquad \sum_{i=1}^{Q} R_i = 0 \tag{4.16}$$

To compute the mass fraction of the remaining species, COMSOL solves the equation:

$$\omega_1 = 1 - \sum_{i=2}^{Q} \omega_i \tag{4.17}$$

To describe the mass diffusion with a porous matrix and in a free flow, we have chosen to use the Fick's law which describes the vector $\mathbf{j}_i$ more specifically. By using the Fick's law approximation implemented in COMSOL, the relative mass flux $\mathbf{j}_i$ due to molecular diffusion is governed by a mole gradient:

$$\mathbf{j}_i = -\rho_i D_i^F \frac{\nabla x_i}{x_i} \tag{4.18}$$

Where x_i is the mole fraction. In this equation D_i^F could represents a general diffusion matrix describing the diffusion of species i into the mixture. In situation when the mass transport is dominated by diffusion and in particular in the problem that this thesis is handling, an useful alternative can be to use the diffusion coefficients at infinite dilution. The diffusion coefficient was considered equal for all the gaseous chemical species considered and was considered only dependent on the temperature according to the formula[22]:

$$D_i^F = 1.67 \cdot 10^{-5} \left(\frac{T[K]}{298} \right)^{1.75} \quad [m^2/s] \tag{4.19}$$

Obviously the mass diffusion equation will be modified according to the domain analyzed; in the case of the biomass bed the equation will also take into account the porosity. Finally considering also the other diffusion mechanisms, the final equations that will be obtained (in addition to equation 4.14 that will be always the same) are:

- Free flow:

$$\mathbf{j}_i = -\rho D_i^F \nabla \omega_i - \rho \omega_i D_i^F \frac{\nabla M}{M} + \rho \omega_i \sum_{i=1}^{N} \frac{M_i}{M} D_i^F \nabla x_i \tag{4.20}$$

  Where M [kg/mol] and M_i [kg/mol] are the molar mass of the mixtuire and of the single chemical species, respectively.

- Biomass bed:

$$\mathbf{j}_i = -\rho D_e^F \nabla \omega_i - \rho \omega_i D_e^F \frac{\nabla M}{M} + \rho \omega_i \sum_{i=1}^{N} \frac{M_i}{M} D_e^F \nabla x_i \tag{4.21}$$

$$D_e^F = f_e \cdot D_i^F \tag{4.22}$$

$$f_e = \frac{\varepsilon_p}{\tau_f} \tag{4.23}$$

$$\tau_f = \varepsilon_P^{-1/3} \tag{4.24}$$

  f_e and τ_f assumes this form by using "Millington and Quirk model" as effective diffusivity model.

4.2.3 Reactions of chemical species

In this section the whole chemical process and the gasification reactions that take place inside the DB-SOFC system are reported. The reactions that occur within the system are considered in the

term R_i within equation 4.14. The chemical process starts from the drying reaction of the biomass, passes through the coal gasification reactions created in the various pyrolysis processes and ends with the various gas phase reactions to create the final syngas at the exit of the gasifier. In the following figure we can see all the various reaction steps that take place in this specific gasification process.

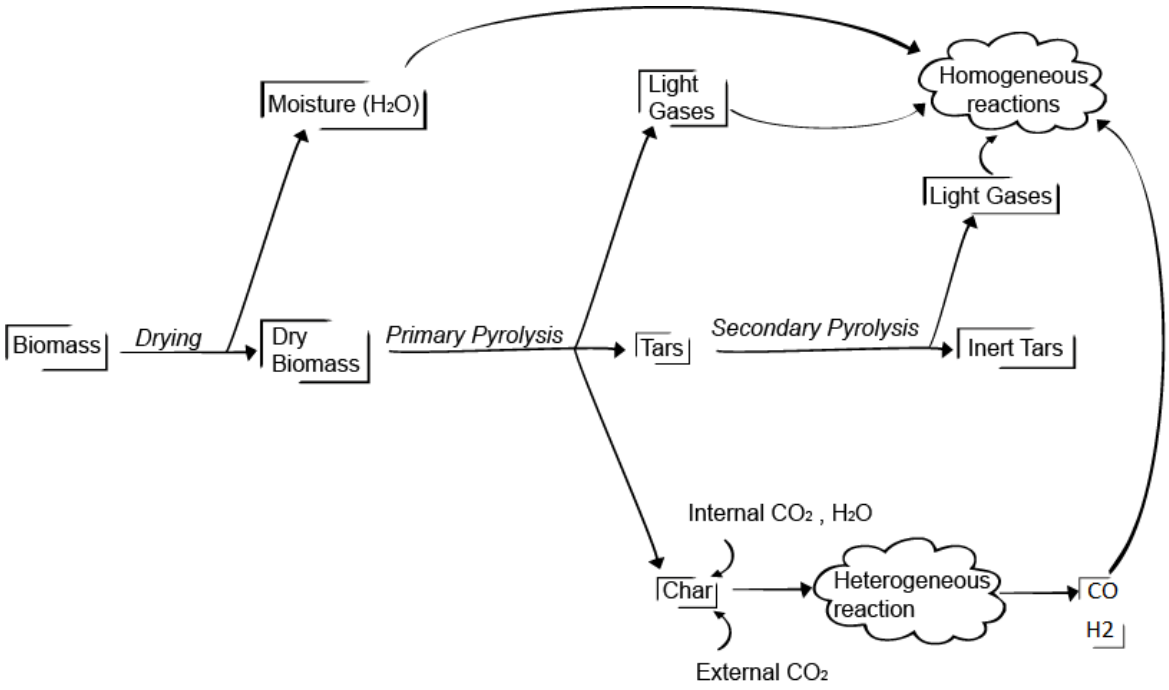

Figure 4.8: Step by step biomass gasification process

Each reaction will have its chemical kinetics with the values found in literature: In fact, the parameters behind the reaction kinetics cannot be established except through experimental research. Above all, the process that takes place in the gasification of biochar is a very tricky point, because the kinetic values depend strongly on the chemical-physical characteristics of the char itself and therefore consequently on the type of initial biomass. Regarding the initial biomass, we already know its chemical composition and its physical properties, in this way it is easier to find the kinetic parameters that best match the chosen biomass. The first important consideration is that the first two processes, that of drying and primary pyrolysis are instantaneous, in fact according to the kinetics found in literature, these processes are so fast as to be considered instantaneous. A tricky point, however, is to know in what quantity and in what products the biomass is divided after these processes. To satisfy this question it is necessary to rely on experimental campaigns[15].

After discovering the mass composition of the solid, liquid and gaseous fraction at a specific

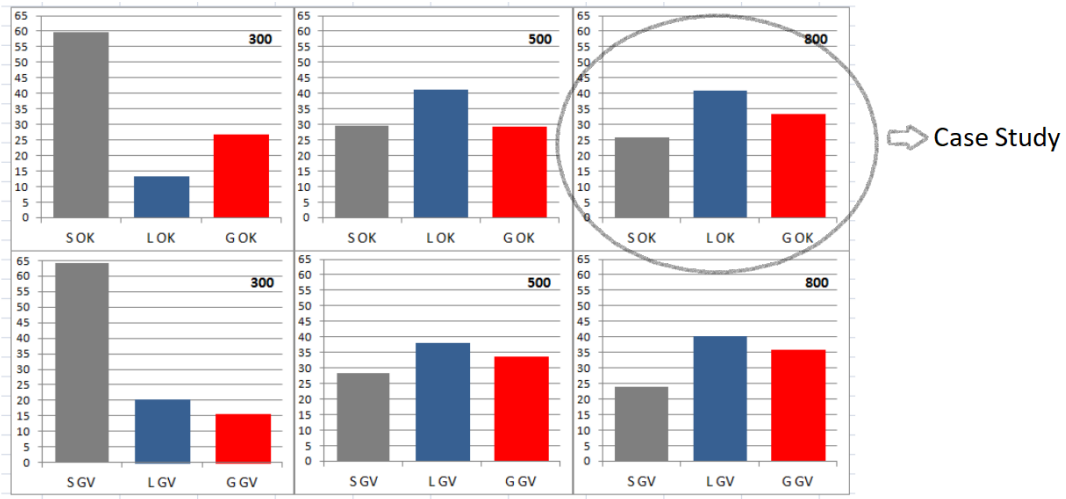

Figure 4.9: Solid (S), liquid (L) and gas (G) fraction yields after heat treatments at 300ºC, 500ºC and 800ºC of samples OK and GV

Tabel 4.2: Solid Liquid and gas fraction of OK pyrolysis at 800°C

	Solid (wt%)	**Liquid (wt%)**	**Gas (wt%)**
OK (800°C)	26.0	41.0	33.0

temperature for the case study on biomass, as shown in figure 4.9, the chemical composition of the latter must still be estimated to continue with the mass and molar balance of the raw biomass which, as we recall, had the formula $C_5H_7O_3$. In literature it is possible to find the mass composition of primary pyrolysis gases[23] which is an important finding to fully characterize the pyrolysis process. So starting from the chemical composition of the biomass and doing a stoichiometry analysis it is possible to obtain the total composition of the chemical mixture at the end of the primary pyrolysis. By knowing these mass fractions in this way, some hypotheses can be made to complete the characterization. Meanwhile, the biochar deriving from pyrolysis is considered as pure carbon, therefore with molar weight 12 (g/mol). The moisture present is considered as H_2O with the same mass percentage of the ultimate analysis; and finally the Tars were considered with a generic formula CHxOy based on the stoichiometry of the reaction. It was thus possible to create a pie chart that explains the mass fractions after drying and primary pyrolysis.

In the pie chart the H_2O involves the superficial moisture resulting from drying, in addition to the pyrolytic water formed by primary pyrolysis. Considering the stoichiometry of the problem, we can express the primary drying and pyrolysis through the reactions:

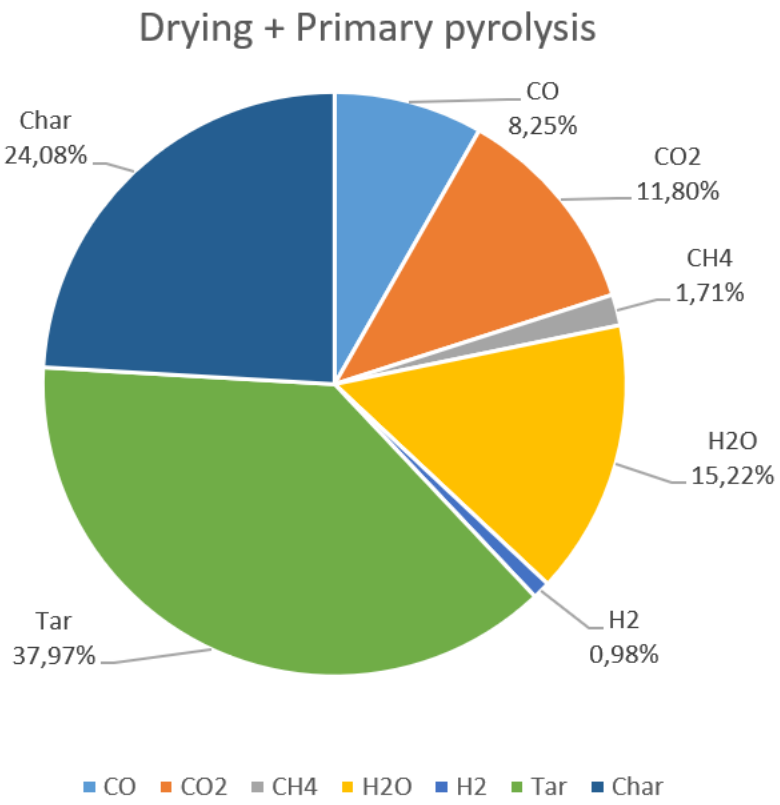

Figure 4.10: Pie chart of chemical species mass fractions for drying and primary pyrolysis

$$C_5H_7O_3 \longrightarrow 5\,CH_{1.221}O_{0.505} + 0.4728\ \text{Moisture}(H_2O) \quad \text{(R 4.1)}$$

$$5\,CH_{1.221}O_{0.505} \longrightarrow 0.339CO + 0.308CO_2 + 0.123CH_4 + 0.5H_2O + 0.56H_2 + 2.31\text{Char} + 1.92\text{Tar} \quad \text{(R 4.2)}$$

Where the minimum tars formula to comply with stoichiometry was:

$$\text{Tar} = CH_{1.789}O_{0.556} \quad \text{(R 4.3)}$$

Also the article published by S. Gerber[23] says that the tar produced by primary pyrolysis should be further decomposed into a so-called secondary pyrolysis, and therefore the tars would go into thermal cracking. Unlike the primary pyrolysis process, this process is not immediate this time but in spite of everything has a modest reaction rate, therefore it will be necessary to test its reaction rate through appropriate parameters. Obviously, the products of secondary pyrolysis depend also at temperature on which the process is carried on, therefore we have chosen

experimental data that also reflects the temperature of our case study, that is 800°C. Furthermore, the stoichiometry of the reaction was continued, thus obtaining a secondary pyrolysis reaction equal to:

$$\text{Tar} \longrightarrow 0.457\text{CO} + 0.057\text{CO}_2 + 0.125\text{CH}_4 + 0.196\text{H}_2 + 0.36Tar_{inert} \qquad (\text{R}\,4.4)$$

Always respecting stoichiometry it is clear that:

$$\text{Tar}_{\text{inert}} = \text{CH}_{2.48} \qquad (\text{R}\,4.5)$$

Speaking instead of mass fractions, the pie chart related to it is:

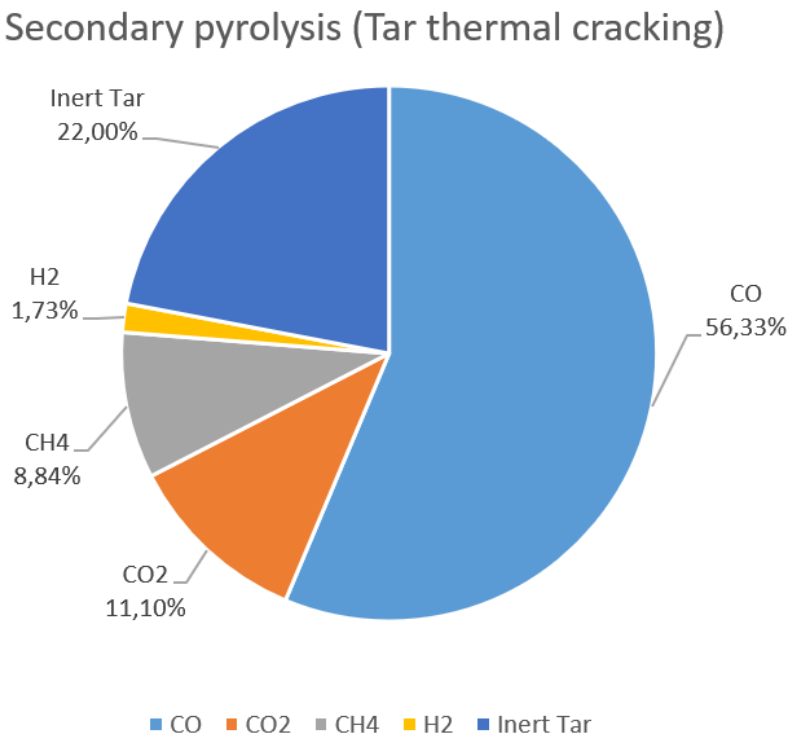

Figure 4.11: Pie chart of chemical species mass fractions for secondary pyrolysis

For "inert tars" is meant those tars in which the temperature has not managed to split the chemical bonds. This percentage of inert tar is mainly due to the fact that the temperature is not high enough (800°C) and therefore thermal cracking does not affect the whole mass of tars present. Regarding the kinetics of secondary pyrolysis, they can be expressed in the Arrhenius form with the parameters found in literature[24]:

$$R_{sp} = \rho_{tar} \cdot A_{sp} \cdot exp\left(-\frac{E_{sp}}{R \cdot T}\right) \quad \left[\frac{kg}{m^3 s}\right] \qquad (4.25)$$

Where:

- $A_{sp} = 2.076 \cdot 10^3 \quad [1/s]$ is the pre-exponential factor
- $E_{sp} = 66.3 \cdot 10^6 \quad [J/kmol]$ is the activation energy of the reaction
- $\rho_{tar} \quad [kg/m^3]$ is the mass concentration of tar

Homogeneous gas-phase reactions

The only one most important reaction between gas present in the reactor is the water gas shift. The other reactions between gases such as those of reforming will take place only in the vicinity of the cells where the nickel anode can catalyze the reactions. The WGS reaction is among the most relevant in a gasification reactor, because it allows to adjust the H_2/CO ratio. The reaction kinetics of the WGS considered in this thesis will be an equation which, based on the concentrations of the reagents or products, will be able to work in both directions and designed for non-catalyzed reactions[16]. Recalling the formula of the WGS:

$$\mathrm{CO} + \mathrm{H_2O} \longleftrightarrow \mathrm{CO_2} + \mathrm{H_2} \tag{R 4.6}$$

The kinetics will be:

$$R_{wgs} = A_{wgs} \cdot exp\left(-\frac{E_{wgs}}{RT}\right)\left(C_{CO}C_{\mathrm{H_2O}} - \frac{C_{\mathrm{CO_2}}C_{\mathrm{H_2}}}{K_p(T)}\right) \quad \left[\frac{mol}{m^3 s}\right] \tag{4.26}$$

- $A_{wgs} = 2.78 \cdot 10^3 \quad \left[\frac{m^3}{mol \cdot s}\right], \qquad E_{wgs} = 1.26 \cdot 10^4 \quad \left[\frac{J}{mol}\right]$
- $C_{CO}, C_{\mathrm{H_2O}}, C_{\mathrm{CO_2}}, C_{\mathrm{H_2}}$ are the molar concentration $\left[\frac{mol}{m^3}\right]$
- $K_p(T)$ is the equilibrium constant of the reaction that assumes the form:

$$K_p(T) = 0.0265 \cdot exp\left(\frac{4.55 \cdot 10^4 \quad [J/mol]}{RT}\right) \tag{4.27}$$

Heterogeneous solid-gas-phase reactions

The most relevant reactions in a gasification process are the heterogeneous processes that take place between the solid phase (Char) and the gas phase of the main gasifying agents such as carbon dioxide and steam. The gasification processes of the char have not yet been clarified 100%

because the process in which the gasifying agent diffuses within the pores of the char and the chemical reactivity between gas and solid within the internal sites in the pores of the char is still difficult to understand. Even more difficult to understand becomes the problem when the gasifying agents become more than one. According to a study carried out by Guizani[25], it can be stated through an experimental campaign that if you have CO_2 and H_2O as the gasifying agent, the two reactivities are completely independent of each other and the char reactivity in a mixed atmosphere of CO_2 and H_2O can be written as the sum of the single reactivities:

$$\text{Boudouard reaction:} \quad \mathrm{C} + \mathrm{CO_2} \longrightarrow 2\,\mathrm{CO} \tag{R 4.7}$$

$$\text{Water-gas reaction:} \quad \mathrm{C} + \mathrm{H_2O} \longrightarrow \mathrm{CO} + \mathrm{H_2} \tag{R 4.8}$$

$$React_{(\mathrm{CO_2}+\mathrm{H_2O})} = React_{\mathrm{CO_2}} + React_{\mathrm{H_2O}} \quad [1/s] \tag{4.28}$$

The peculiarity of the gasification of the char and that the reactivity to the single gasifying agent is that the reactivity itself changes according to the type of biomass from which the char derives. So we had to look in literature for parameters that corresponded to the biomass in question, therefore to the olive kernel. The equations that have been found in literature regarding the gasification in CO_2 and H_2O of char deriving from the pyrolysis of the olive kernel are[26][27]:

$$R_{br} = React_{\mathrm{CO_2}}^{(\chi=50)} \cdot \rho_{char} \quad \left[\frac{kg}{m^3 s}\right] \tag{4.29}$$

$$React_{\mathrm{CO_2}}^{(\chi=50)} = A_{br} \cdot exp\left(-\frac{E_{br}}{RT}\right) \cdot p_{\mathrm{CO_2}}^{n} \quad [1/s] \tag{4.30}$$

$$R_{wg} = React_{\mathrm{H_2O}}^{(\chi=50)} \cdot \rho_{char} \quad \left[\frac{kg}{m^3 s}\right] \tag{4.31}$$

$$React_{\mathrm{H_2O}}^{(\chi=50)} = A_{wg} \cdot exp\left(-\frac{E_{wg}}{RT}\right) \cdot p_{\mathrm{H_2O}}^{m} \quad [1/s] \tag{4.32}$$

In the equations seen above, reactivity is expressed as a function of another parameter seen as χ. This parameter indicates the conversion of the char as the gasification takes place: The reactivity varies according to the conversion, the lower the conversion the higher the reactivity, which translated means that in the initial stages of gasification, the reaction kinetics will be faster. In general, however, to have expressed the reactivity in a single number, reference is made to the conversion at 50%, as adopted in this case study.

Tabel 4.3: Kinetics parameters of Boudouard reaction and water-gas reaction

Boudouard reaction	**Water-gas reaction**
$A_{br} = exp(9.22) \quad [\frac{1}{bar \cdot s}]$	$A_{wg} = 1.71 \cdot 10^7 \quad [\frac{1}{bar \cdot s}]$
$E_{br} = 1.333 \cdot 10^5 \quad [\frac{J}{mol}]$	$E_{wg} = 2.11 \cdot 10^5 \quad [\frac{J}{mol}]$
$n = 0.43 \quad [-]$	$m = 0.51 \quad [-]$
p_{CO_2} = Partial pressure $CO_2 \quad [bar]$	p_{H_2O} = Partial pressure $H_2O \quad [bar]$

4.2.4 SOFC modelling

SOFC modelling is a fairly tricky point during this analysis and simulation of the DB-SOFC project. The previous work concerning this system, had already involved the modelling of a single SOFC feed to syngas coming from the gasification of the biomass which in turn comes from the agro-food residue, in particular the olive kernel. In the next figure we can see the geometry of the cells that will be used in the gasifier on which this analysis is based. Obviously, fully simulating the operation

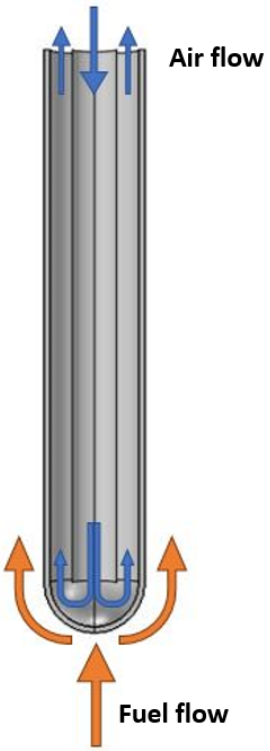

Figure 4.12: Geometry of tubular SOFC

of the cell would be redundant and in particular it would require a not indifferent effort, given

the complexity of the system, including the diversity of components (anode, cathode, electrolyte layer) as we can see in the figure 4.13. As we can see from the figure, given the complexity of the

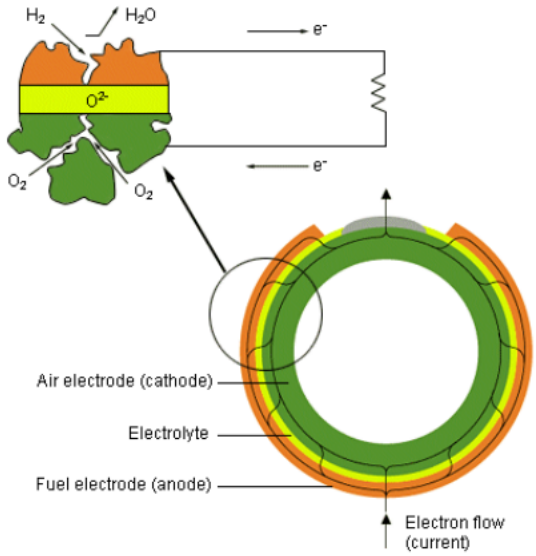

Figure 4.13: Components of tubular SOFC

system it would be very difficult to simulate both the fuel cells and the reactor in its entirety, not to mention the immense computational effort. So to facilitate the computational effort, the SOFC will be simulated as a boundary from which the rest of the reactor will exchange mass and energy; in the real physics of the problem this control will correspond to the anode of the cell. The mass exchange is so immediate to define because the polarization curve is available from the previous analyzes [28] and therefore it is possible to establish the nominal configuration. By inverting the formula it is possible to immediately obtain the consumption in moles of the SOFCs:

$$\dot{n}_{fuel} = \frac{I}{z \cdot F} = 1.0364 \cdot 10^{-6} \quad \left[\frac{mol}{s \cdot cm^2 \cdot cell}\right] \tag{4.33}$$

So simply by calculating the active surface of the cell, knowing its geometry (cell diameter is 2 cm), and multiplying it by the number of cells it is possible to know the total fuel consumption of all the cells. As the nominal configuration, 0.7 [V] and 0.2 $[A/cm^2]$ were considered as the cell nominal working point. So knowing the fuel flow rate, the key point is to know what fuel the cell will use, since SOFCs can work both with pure hydrogen and with hydrocarbons. The modelling choice is that, as happens in reality, the fuels that are electro-oxidized in the cell are hydrogen and carbon monoxide, while the other hydrocarbons will be reformed thanks to the nickel of the

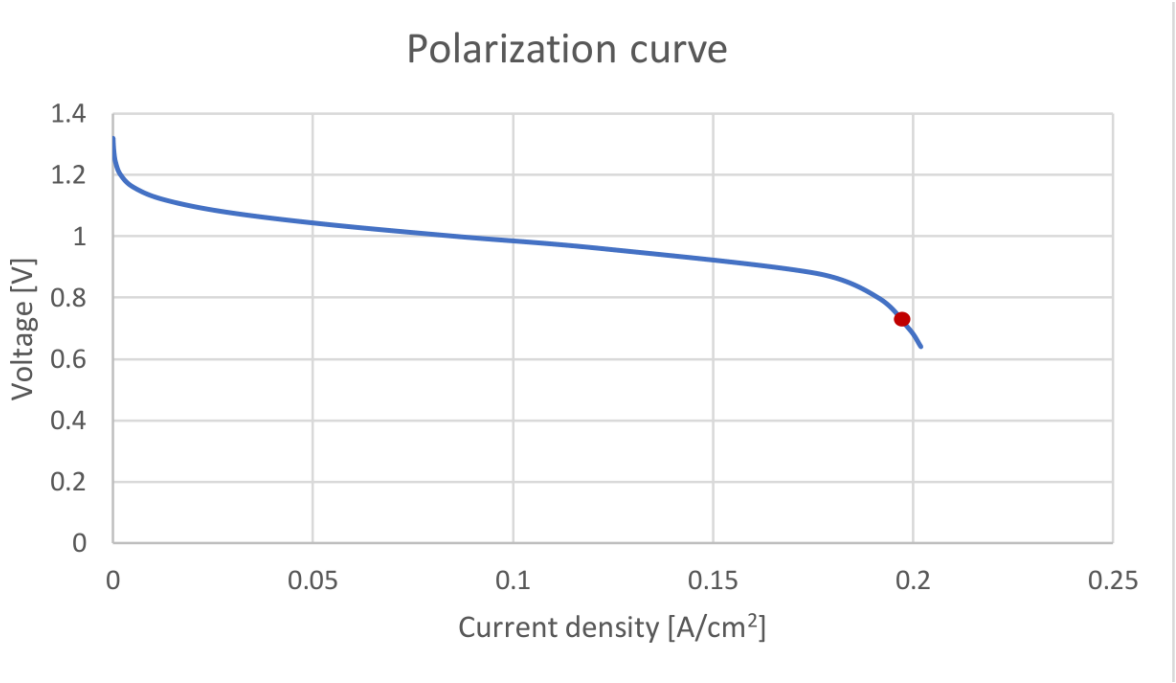

Figure 4.14: Polarization curve for nominal configuration

anode which will act as a reaction catalyst. The difficult point is to know in what proportions the cell will consume CO and H_2. If the cell had been simulated, each chemical species would have contributed to creating chemical potential based on the pressures exerted in the porous anode, and on the diffusion characteristics and reaction rate of CO and H_2 in the three-phase boundary. However, not having the possibility of simulating all the components of the cell, one way that can be followed is the theory behind the activation overvoltages. The activation overvoltages represent the amount of energy that has to be spent to overcome the energetic threshold of the activation of the electrochemical reaction. This means that both CO and H_2 will have their activation current and therefore the flow rate of each type of fuel will be proportional to it. The higher the fuel activation current the less the losses and more fuel it will be consumed. To evaluate the activation losses, just invert the Butler-Volmer equation, and we will obtain:

$$\eta_{act} = \frac{RT}{\alpha \cdot F} \cdot \sinh^{-1}\left(\frac{i}{2i_0}\right) \quad [V] \tag{4.34}$$

Where:

- i $[A/cm^2]$ is the current density produced by overpotential
- i_0 $[A/cm^2]$ is the exchange current density produced by single fuel

- α $[-]$ is the transfer coefficients for each chemical species

So now all that remains is to evaluate the exchange current densities for CO and H_2. Regarding SOFCs, in literature[29][30] we found that for the two electrochemical reactions:

$$\mathrm{H_2 + O^{2-} \longrightarrow H_2O + 2\,e^-} \tag{R 4.9}$$

$$\mathrm{CO + O^{2-} \longrightarrow CO_2 + 2\,e^-} \tag{R 4.10}$$

$$i_0^{\mathrm{H_2}} = i^*_{\mathrm{H_2}} \cdot \frac{\left(\frac{P_{\mathrm{H_2}}}{P^*_{\mathrm{H_2}}}\right)^{1/4} \cdot \left(P_{\mathrm{H_2O}}\right)^{3/4}}{1 + \left(\frac{P_{\mathrm{H_2}}}{P^*_{\mathrm{H_2}}}\right)^{1/2}} \quad [A/cm^2] \tag{4.35}$$

$$P^*_{\mathrm{H_2}} = \frac{A_{des}\Gamma^2\sqrt{2\pi RTM_{\mathrm{H_2}}}}{\gamma_0} \cdot \exp\left(-\frac{E^{\mathrm{H_2}}_{des}}{RT}\right) \quad [atm] \tag{4.36}$$

$$i_0^{CO} = i^*_{CO} \cdot \exp\left(-\frac{E^{\mathrm{CO}}_{act}}{RT}\right) \cdot P_{CO}^{-0.058} \cdot P^{1/4}_{\mathrm{CO_2}} \quad [A/cm^2] \tag{4.37}$$

Tabel 4.4: Value of parameters in equations

Values	
$i^*_{\mathrm{H_2}}$	$8.5 \quad [A/cm^2]$
A_{des}	$5.59 \cdot 10^{19} \quad [cm^2/(mol \cdot s)]]$
Γ	$2.6 \cdot 10^{-9} \quad [mol/cm^2]$
γ_0	$0.01 \quad [-]$
$E^{\mathrm{H_2}}_{des}$	$88 \quad [kJ/mol]$
i^*_{CO}	$4.56 \cdot 10^6 \cdot T[K] \quad [A/m^2]$
E^{CO}_{act}	$118 \quad [kJ/mol]$

In all the previous equations the partial pressures were expressed in atmospheres. Thus, knowing the value of the activation currents, the flow rates of the individual fuels in the SOFC can be expressed:

$$\dot{n}_{CO} = \frac{1}{\frac{i_0^{\mathrm{H_2}}}{i_0^{CO}} + 1}\dot{n}_{fuel} \quad \left[\frac{mol}{s \cdot cm^2 \cdot cell}\right] \tag{4.38}$$

$$\dot{n}_{\mathrm{H_2}} = \dot{n}_{fuel} - \dot{n}_{CO} \quad \left[\frac{mol}{s \cdot cm^2 \cdot cell}\right] \tag{4.39}$$

The fuel flows in the SOFCs have been modelled as mass flows through the boundary. The next step is to model the reforming of the other hydrocarbons present, and to reshape the catalyzed water gas shift on the catalyst nickel layer. Catalyst activity is influenced by temperature, chemical species particles size, and the chemical composition of the gas. The optimum operating temperature for a nickel catalyst is about 800°C[5]. Steam-reforming nickel catalysts for heavy hydrocarbons are effective for reduction of tar while nickel catalysts for light hydrocarbons are effective for methane reduction. Deactivation due to carbon deposition and particle growth is a problem for nickel-reforming catalysts, but we will talk about this later. So the reactions if catalyzed in the vicinity of the cell will be[31]:

- Catalyzed Water-gas shift:

$$\mathrm{CO + H_2O \xrightarrow{k_{cwgs}} H_2 + CO_2} \tag{R 4.11}$$

$$R_{cwgs} = k_{cwgs}\left(p_{CO} \cdot p_{\mathrm{H_2O}} - \frac{p_{\mathrm{CO_2}} \cdot p_{\mathrm{H_2}}}{K_{cwgs}}\right) \quad \left[\frac{mol}{m^3 s}\right] \tag{4.40}$$

$$k_{cwgs} = 0.0171 \exp\left(-\frac{103191 \quad [J/mol]}{RT}\right) \quad \left[\frac{mol}{m^3 \cdot Pa^2 \cdot s}\right] \tag{4.41}$$

Where K_{cwgs} is the equilibrium constant defined according to the following empirical equation:

$$K_{cwgs} = \exp\left(-0.2935 \cdot Z^3 + 0.6351 \cdot Z^2 + 4.1788 \cdot Z + 0.3169\right) \quad [-] \tag{4.42}$$

With:

$$Z = \frac{1000}{T[K]} - 1 \quad [-] \tag{4.43}$$

- Steam methane reforming:

$$\mathrm{CH_4 + H_2O \xrightarrow{k_{smr}} 3\,H_2 + CO} \tag{R 4.12}$$

$$R_{smr} = k_{smr}\left(p_{\mathrm{CH_4}} \cdot p_{\mathrm{H_2O}} - \frac{p_{\mathrm{CO}} \cdot p_{\mathrm{H_2}}^3}{K_{smr}}\right) \quad \left[\frac{mol}{m^3 s}\right] \tag{4.44}$$

$$k_{smr} = 2395 \exp\left(-\frac{231266 \quad [J/mol]}{RT}\right) \quad \left[\frac{mol}{m^3 \cdot Pa^2 \cdot s}\right] \tag{4.45}$$

Where K_{smr} is the equilibrium constant defined according to the following empirical equation:

$$K_{smr} = P_{ref}^2 \cdot \exp\left(-0.2513 \cdot Z^4 - 0.3665 \cdot Z^3 + 0.5810 \cdot Z^2 - 27.134 \cdot Z + 3.277\right) \quad [Pa^2] \tag{4.46}$$

With:

$$Z = \frac{1000}{T[K]} - 1 \quad [-] \tag{4.47}$$

- Dry methane reforming[32]:

$$\mathrm{CH_4 + CO_2} \xrightarrow{k_{dmr}} \mathrm{2\,H_2 + 2\,CO} \tag{R 4.13}$$

$$R_{dmr} = k_{dmr} \cdot \left[\frac{K_{\mathrm{CO_2}} K_{\mathrm{CH_4}} p_{\mathrm{CO_2}} p_{\mathrm{CH_4}}}{(1 + K_{\mathrm{CO_2}} p_{\mathrm{CO_2}} + K_{\mathrm{CH_4}} p_{\mathrm{CH_4}})}\right] \cdot \left[1 - \frac{\left(p_{\mathrm{CO}} p_{\mathrm{H_2}}\right)^2}{K_1 p_{\mathrm{CH_4}} p_{\mathrm{CO_2}}}\right] \tag{4.48}$$

Where:

$$K_{\mathrm{CO_2}} = 2.64 \cdot 10^{-2} \cdot \exp\left(\frac{37641 \quad [J/mol]}{RT}\right) \quad \left[\frac{1}{atm}\right] \tag{4.49}$$

$$K_{\mathrm{CH_4}} = 2.63 \cdot 10^{-2} \cdot \exp\left(\frac{40684 \quad [J/mol]}{RT}\right) \quad \left[\frac{1}{atm}\right] \tag{4.50}$$

$$k_{dmr} = 1290 \cdot 5000 \cdot \exp\left(-\frac{102065 \quad [J/mol]}{RT}\right) \quad \left[\frac{mol}{m^3 s}\right] \tag{4.51}$$

$$K_1 = \exp(34.011) \cdot \exp\left(-\frac{258598 \quad [J/mol]}{RT}\right) \quad \left[atm^2\right] \tag{4.52}$$

- Tar dry and steam reforming[33]: As for tar reforming, an important hypothesis that has been made is that both the reaction with CO_2 and the reaction with H_2O advance at the same rate of reaction $k_{\mathrm{tar\ ref}}$:

$$\mathrm{C_nH_x + nH_2O} \xrightarrow{k_{\mathrm{tar\ ref}}} \left(n + \frac{x}{2}\right)\mathrm{H_2 + nCO} \tag{R 4.14}$$

$$\mathrm{C_nH_x + nCO_2} \xrightarrow{k_{\mathrm{tar\ ref}}} \left(\frac{x}{2}\right)\mathrm{H_2 + 2\,nCO} \tag{R 4.15}$$

With:

$$k_{\mathrm{tar\ ref}} = 50.869 \cdot \exp\left(-\frac{76161 \quad [J/mol]}{RT}\right) \quad \left[\frac{m^3}{mol \cdot s}\right] \tag{4.53}$$

So the reaction rates will be equal to:

$$R_{\text{tar dry ref}} = k_{\text{tar ref}} \cdot C_{Tar} \cdot C_{\text{CO}_2} \quad \left[\frac{mol}{m^3 s}\right] \tag{4.54}$$

$$R_{\text{tar steam ref}} = k_{\text{tar ref}} \cdot C_{Tar} \cdot C_{\text{H}_2\text{O}} \quad \left[\frac{mol}{m^3 s}\right] \tag{4.55}$$

With $C_{\text{H}_2\text{O}}$, C_{CO_2}, C_{Tar} are the molar concentration in $[mol/m^3]$ of steam, carbon dioxide and tar, respectively.

As these reactions take place in the immediate vicinity of the cell, in the modelling concerning this thesis they will be transformed into mass flux through the boundary. To transform them into mass flux, we just multiply them by the volume of the anode and divide them by the useful surface of the anode, thus obtaining a value in $\left[\frac{mol}{m^2 s}\right]$.

4.2.5 Heat transfer modelling

To model the heat transmission interface, reference will always be made to the two types of domain, the porous medium corresponding to the biomass bed in the lower part of the system, and the free flow in the upper part. Each domain will have its physics and its equations to simulate the exchange and transport of thermal energy. As far as free flow is concerned, the equation assumes the known form of heat transfer in fluids[34]:

$$\rho_f C_{p,f} \mathbf{u}_f \cdot \nabla T_f + \nabla \mathbf{q}_f = Q_f + Q_{p,f} + Q_{vd,f} \tag{4.56}$$

$$\mathbf{q}_f = -k_f \nabla T_f \tag{4.57}$$

Were the terms in the equation are:

- ρ_f $[kg/m^3]$ is the density of fluid
- $C_{p,f}$ $[J/(kg \cdot K)]$ is the specific heat at constant pressure of fluid
- T_f $[K]$ is the temperature of fluid
- $\mathbf{u}_f$ $[m/s]$ is the velocity vector
- $\mathbf{q}_f$ $[W/m^2]$ is the heat flux by conduction
- Q_f $[W/m^3]$ is the heat source or sink

- $Q_{p,f}$ $[W/m^3]$ is the heat source for pressure changes that in general is low for small Mach number flows. It assumes in stationary conditions the form:

$$Q_{p,f} = \alpha_p T_f \mathbf{u}_f \cdot \nabla p \tag{4.58}$$

  With α_p $[1/K]$ the coefficient of thermal expansion

- $Q_{vd,f}$ $[W/m^3]$ is the heat source due to the viscous dissipation in the fluid, it is equal to:

$$Q_{vd,f} = \tau : \nabla \mathbf{u}_f \tag{4.59}$$

  With τ $[Pa]$ is the viscous stress tensor

- p [Pa] is the pressure

Instead the heat transfer in the porous medium is a set of the equation of energy in the solid and the equation of energy in the fluids:

- Biomass bed:

  Regarding the solid porous matrix the equation is:

$$\nabla \cdot \mathbf{q}_s = Q_s \tag{4.60}$$

$$\mathbf{q}_s = -k_s \nabla T_s \tag{4.61}$$

  Instead, for the fluid that is the interstices of the porous matrix the equation is:

$$\rho_f C_{p,f} \mathbf{u}_f \cdot \nabla T_f + \nabla \mathbf{q}_f = Q_f \tag{4.62}$$

$$\mathbf{q}_f = -k_f \nabla T_f \tag{4.63}$$

  The main hypothesis on which the theory of heat transfer in porous media is based is that, there is a thermal balance between liquid and solid:

$$T_f = T_s = T \tag{4.64}$$

So the equations mentioned above can merge into a single equation:

$$\rho C_p \mathbf{u} \cdot \nabla T + \nabla \mathbf{q} = Q \tag{4.65}$$

$$\mathbf{q} = -k_{eff} \nabla T \tag{4.66}$$

Where:

- ρ $[kg/m^3]$ is the fluid density
- C_p $[J/(kg \cdot K)]$ is the specific heat at constant pressure of fluid
- $\mathbf{u}$ $[m/s]$ is the velocity field inside the porous matrix from a fluid flow interface
- $\mathbf{q}$ $[W/m^2]$ is the heat flux by conduction
- Q $[W/m^3]$ is the heat source or sink
- k_{eff} $[W/(mK)]$ is the effective thermal conductivity

The effective thermal conductivity can be calculated starting from the values of the thermal conductivity of the solid and the fluid and choosing a mathematical model to be applied. For instance in this model, the volume averaged model was chosen, that is:

$$k_{eff} = \theta_p k_p + (1 - \theta_p) k_f \tag{4.67}$$

Where k_p and k_f are respectively the thermal conductivity of solid and fluid. Instead θ_p is the volume fraction of the porous solid matrix:

$$\theta_p = 1 - \varepsilon_p \quad [-] \tag{4.68}$$

Therefore, after defining therefore the equations that define the physics of the problem, we need to deepen the hypotheses made in the domain of our system. By removing inlets, outlets and plane of symmetry, all the other boundaries of the domain are considered thermally isolated, thus there are no thermal losses. The CO_2 enters the system at 800°C and fuel cells are also considered isothermal at 800°C as the main energy source of the system. Furthermore, once the fixed temperatures have been defined, the energy sinks of the system must be defined. The main events that remove heat from the system are chemical reactions. The last hypothesis to affirm is that in the heterogeneous

reactions between char and gas phase, have been modelled in the lower part of the system, that is the biomass bed, instead it is hypothesized that the reactions between gas phases take place in the whole reactor. All the chemical reactions and its heat of reaction used during this simulation have been summarized in the table 4.5. The heats of reactions have been assumed with a positive sign if they are endothermic reactions, instead with a negative sign if they are exothermic reactions. In the next chapter we will pass on to see the results obtained by numerical simulations.

Tabel 4.5: Endothermic or exothermic reactions

Reactions
Drying
$C_5H_7O_3 \longrightarrow 5\,CH_{1.221}O_{0.505} + 0.4728\ \text{Moisture}(H_2O)$
Endothermic reaction $\Delta H_0 = +2250 \quad [kJ/kg_{moisture}]$
Primary Pyrolysis
$5\,CH_{1.221}O_{0.505} \longrightarrow 0.339CO + 0.308CO_2 + 0.123CH_4 + 0.5H_2O + 0.56H_2 + 2.31\text{Char} + 1.92\text{Tar}$
Endothermic reaction $\Delta H_0 = +255.5 \quad [kJ/kg_{biomass}]$[19]
Secondary Pyrolysis
$\text{Tar} \longrightarrow 0.457CO + 0.057CO_2 + 0.125CH_4 + 0.196H_2 + 0.36Tar_{inert}$
Exothermic reaction $\Delta H_0 = -42 \quad [kJ/kg]$[35]
Water-gas shift
$CO + H_2O \longleftrightarrow CO_2 + H_2$
Exothermic reaction $\Delta H_0 = -41.5 \quad [kJ/mol]$
Boudouard reaction
$C + CO_2 \longrightarrow 2\,CO$
Endothermic reaction $\Delta H_0 = +172 \quad [kJ/mol]$
Water-gas reaction
$C + H_2O \longrightarrow CO + H_2$
Endothermic reaction $\Delta H_0 = +131 \quad [kJ/mol]$
Catalyzed WGS
$CO + H_2O \longrightarrow CO_2 + H_2$
Exothermic reaction $\Delta H_0 = -(45063 - 10.28 \cdot T) \quad [J/mol]$[31]
Steam methane reforming
$CH_4 + H_2O \longrightarrow CO_2 + 3\,H_2$
Endothermic reaction $\Delta H_0 = +206205.5 + 19.5175 \cdot T \quad [J/mol]$[31]
Dry methane reforming
$CH_4 + CO_2 \longrightarrow 2\,CO + 2\,H_2$
Endothermic reaction $\Delta H_0 = +260 \quad [kJ/mol]$[36]
Tar dry reforming
$C_nH_x + nCO_2 \longrightarrow (\frac{x}{2})H_2 + 2\,nCO$
Endothermic reaction $\Delta H_0 = +948 \quad [kJ/mol]$[37]
Tar steam reforming
$C_nH_x + nH_2O \longrightarrow (n + \frac{x}{2})H_2 + nCO$
Endothermic reaction $\Delta H_0 = +753 \quad [kJ/mol]$[37]

Chapter 5

Results

After having completely set the simulation on the COMSOL multiphysics® software, therefore having decided the physics to be used and having completely defined the thermophysical properties of the materials, you can go on simulating the different operating conditions at which the system can operate. In the previous chapters we have already defined the nominal parameters at which the system must operate, and for which they are the basis from which to start. The next table will list the design parameters for which the SOFCs are designed and the parameters of the gasifier that are the basis for exploring the various possibilities of use.

Tabel 5.1: Nominal configuration parameters

Parameters	**Value**
Cells Operating Temperature	1073 $[K]$
Cells Operating current density	0.2 $[A/cm^2]$
Cells operating Voltage	0.7 $[V]$
Inlet Temperature of CO_2	1073 $[K]$
Numbers of Cells	25 $[-]$
Reactor Reference Pressure	1 $[atm]$
Cell Diameter	2 $[cm]$
Cells Height	16 $[cm]$
Cells Active Height	10 $[cm]$
Nominal Electrical efficiency SOFC	48.4 [%]
Reactor Total Height	18 $[cm]$
Biomass Bed Height	9 $[cm]$
Reactor Cross Section Area	1024 $[cm^2]$

These are the parameters that must be kept fixed because they are design data already chosen and therefore future choices must be based on these parameters. The variables that can be varied to optimize the system are listed in the table 5.2 Regarding the parameters to be designed and

Tabel 5.2: Parameters to choose for optimization

Parameters
Number of CO_2 Inlet
Layout of Inlet
Cells Layout
Mass Flow of CO_2
Mass Flow of biomass
Reactor Geometry

optimized, some of them, especially the geometry ones, are easy to design. As mentioned in the previous chapters, the geometry will be of two types: square and circular; the characteristic lengths have been kept such as to keep the total volume of the reactor intact. The SOFCs, on the other hand, have already been totally characterized in the previous works, therefore it is sufficient to visualize a SOFCs' distribution in the system. The CO_2 inlet system is more difficult to design, because in addition to the layout, you must also think about the number of inlets to put in the system. As far as the mass flow of CO_2 and biomass is concerned, a parametric analysis will be carried out to see which system optimizes the characteristics of the system in relation to CO_2/biomass ratio. Regarding the square geometry, 18 inlets were designed and a square pattern was designed for both the SOFCs and the inlets themselves. As for circular geometry, 20 inlets were designed and a circular pattern with symmetrical angles was designed for both the SOFCs and the inlets themselves. We then analyze the mass flow rates of CO_2 and biomass, the only criteria to be respected is that of satisfying the needs of SOFCs. Therefore it was decided to take into consideration the mass flow range of CO_2 and biomass shown in the table 5.3.

Tabel 5.3: CO_2/Biomass ratios

	CO_2/Biomass Ratio									
	1.80	1.93	2.0	2.08	2.19	2.27	2.38	2.49	2.59	2.70
CO2 mass flow [g/s]	3.75	3.75	3.75	3.75	4.1	4.1	4.3	4.5	4.75	5
Biomass mass flow [g/s]	2.083	1.944	1.875	1.805	1.875	1.805	1.805	1.805	1.833	1.852

An important clarification to make is that biomass does not have a real physical inlet but is instantaneously generated isotropically everywhere in the volume designated exactly for biomass. Therefore, the biomass distribution screw was not taken into account; this simplification does not fully adapt the real physics to the simulation, because in this way the diffusion of the gaseous species in the biomass bed is slightly underestimated, but in any case we suppose that the hypothesis

made does not alter the results as much. Experimental analyzes have not yet been carried out in the laboratory regarding the DB-SOFC project and also literature does not contain studies made on similar systems. The only experimental analysis that has been done is the gasification according to the temperature of the olive kernel and its biochar pyrolysed at various temperatures in a gasifier test. The experiment was carried out by UoWM (University of Western Macedonia) in collaboration with TUC (Technical University of Crete) and took place in an atmosphere completely saturated with CO_2. In the next figure we can see the results obtained from the gasification test[15]: Obviously it is impossible to make a comparison with the results that can be

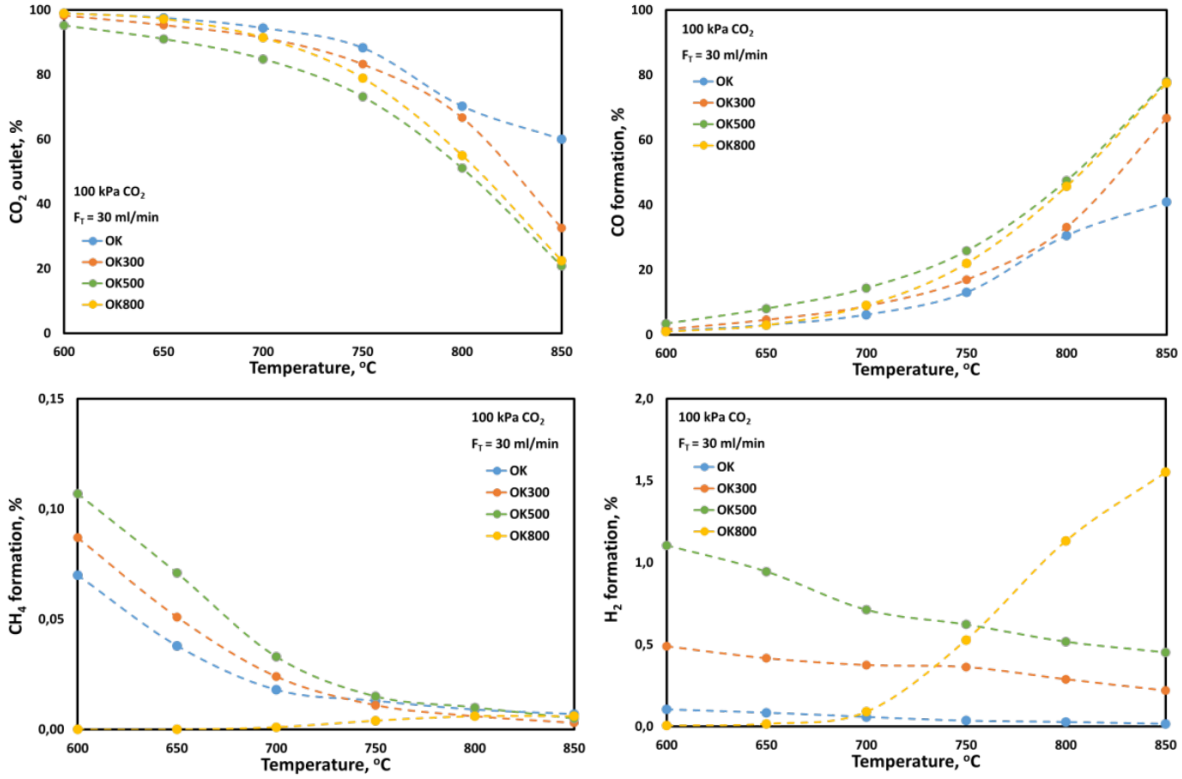

Figure 5.1: Effect on temperature on CO_2 gasification of OK

obtained from COMSOL multiphysics®, due to the diversity of the operating conditions, both geometric and physical, of the gasifier, however, a qualitative analysis can be made subsequently in future experimental analysis. An important aspect that we can immediately notice is the greater presence of CO compared to H_2. This is given by the fact that the most favoured reaction is the Boudouard reaction, and that the large presence of CO_2 favours the reverse WGS.

5.1 Main results

As mentioned in the previous section, the first step was to see how the main results vary as the CO_2/biomass ratio changes. First we see how the mass fractions of the chemical species involved in the system vary with the variation of the ratio itself. The following figures show the mass fractions at the reactor outlet of all the chemical species involved in the system.

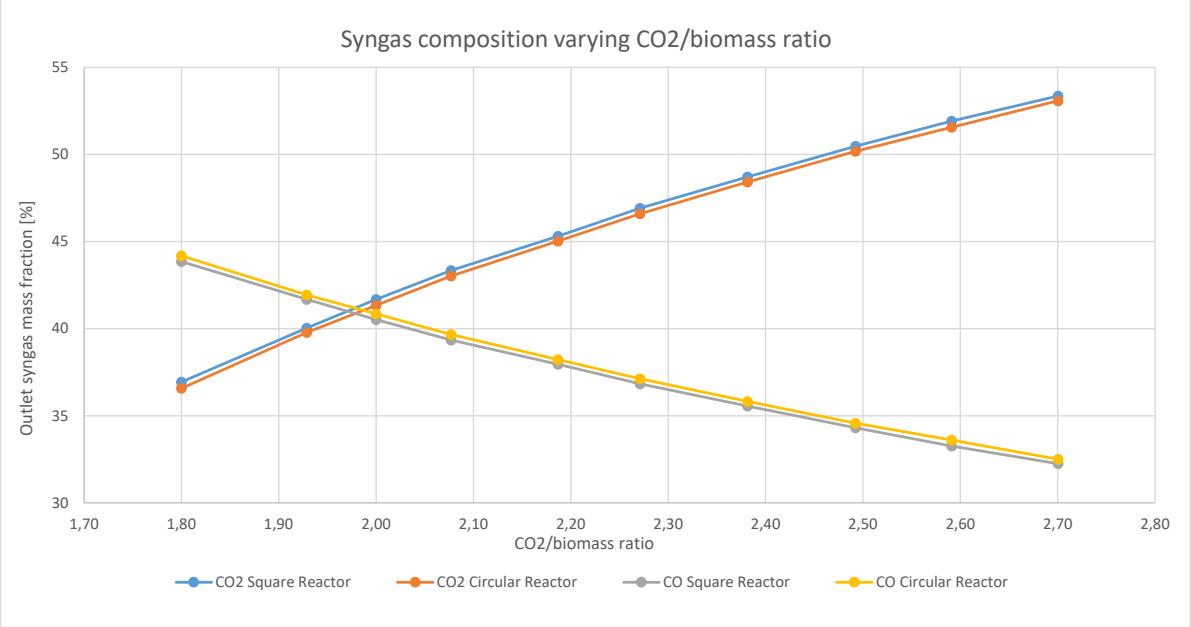

Figure 5.2: CO_2 and CO outlet mass fractions

As we can see from the figures, the mass fractions at the outlet of the reactor between the two geometries assume completely comparable values. While H_2O and tar assume identical values between the two geometries, methane, hydrogen and carbon monoxide have a slightly higher value in the circular geometry reactor. This is an advantage point for this type of reactor, because it allows to have a syngas with higher heating value. To refute the slight superiority of the circular geometry at the expense of the square one, you can refer to the heating value of the syngas, calculated as follows:

$$HHV_{syngas} = \omega_{\mathrm{CO}}^{outlet} \cdot HHV_{\mathrm{CO}} + \omega_{\mathrm{H_2}}^{outlet} \cdot HHV_{\mathrm{H_2}} + \omega_{\mathrm{CH_4}}^{outlet} \cdot HHV_{\mathrm{CH_4}} \quad [MJ/kg] \tag{5.1}$$

With:

- $HHV_{\mathrm{CO}} = 10.112 \quad [MJ/kg]$

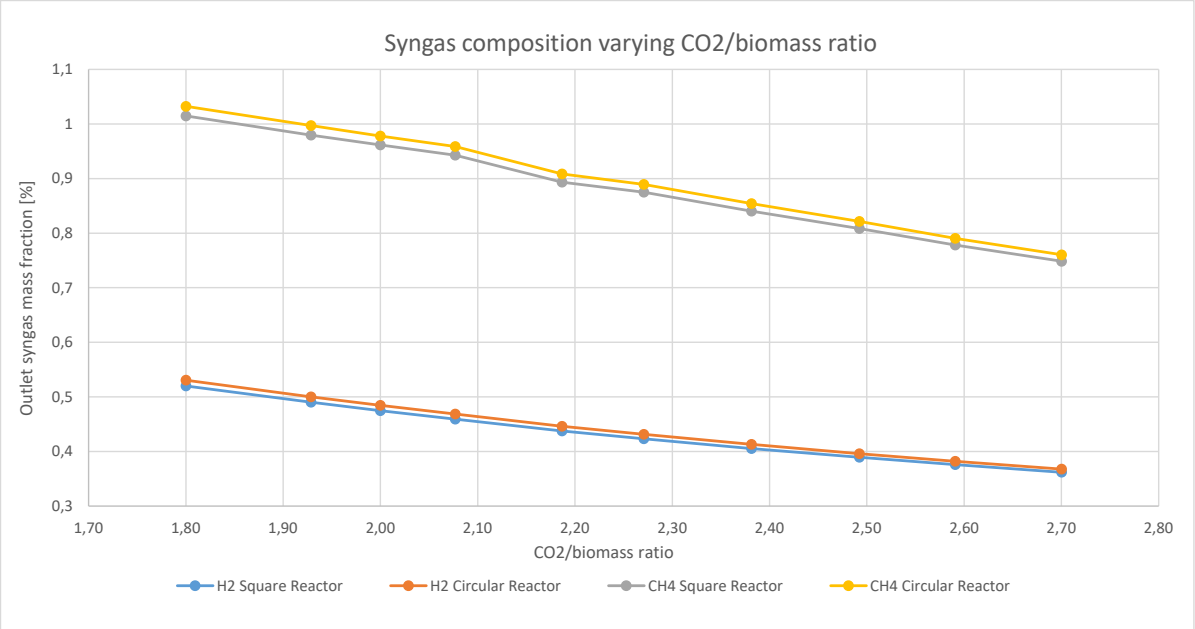

Figure 5.3: H_2 and CH_4 outlet mass fractions

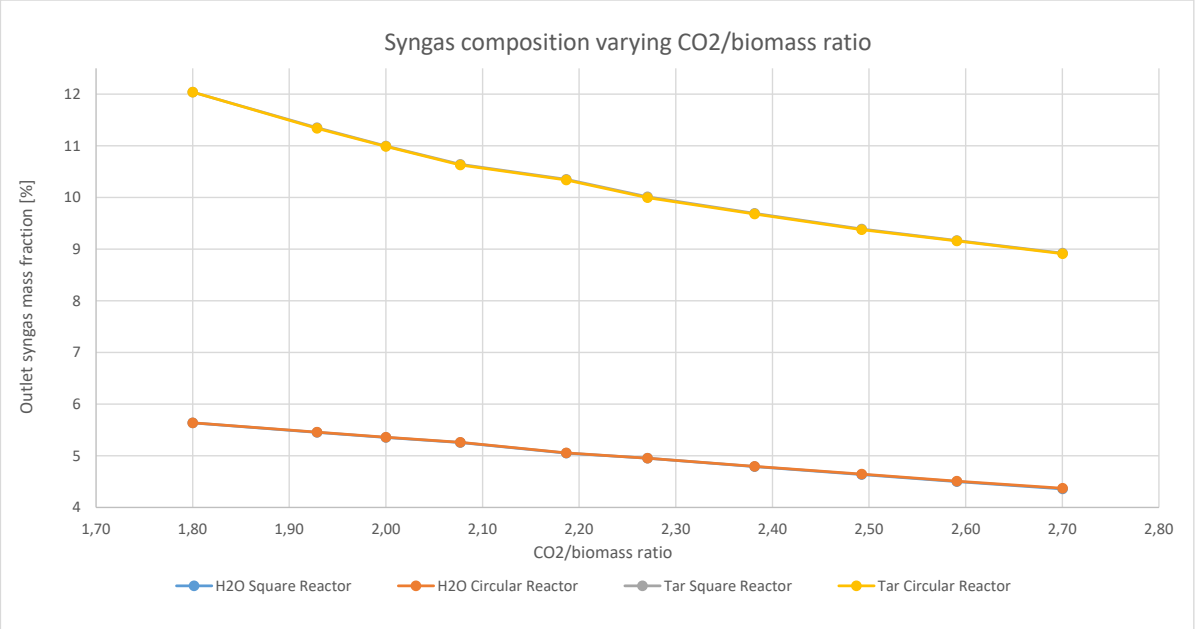

Figure 5.4: H_2O and Tar outlet mass fractions

- $HHV_{\mathrm{H_2}} = 141.8 \quad [MJ/kg]$
- $HHV_{\mathrm{CH_4}} = 55.5 \quad [MJ/kg]$

Therefore, knowing the mass fractions of the chemical species at the outlet, it is possible to draw the graph of the syngas HHV also based on the CO_2/biomass ratio.

As predicted by the mass fractions, it was quite obvious that the HHV of the syngas produced

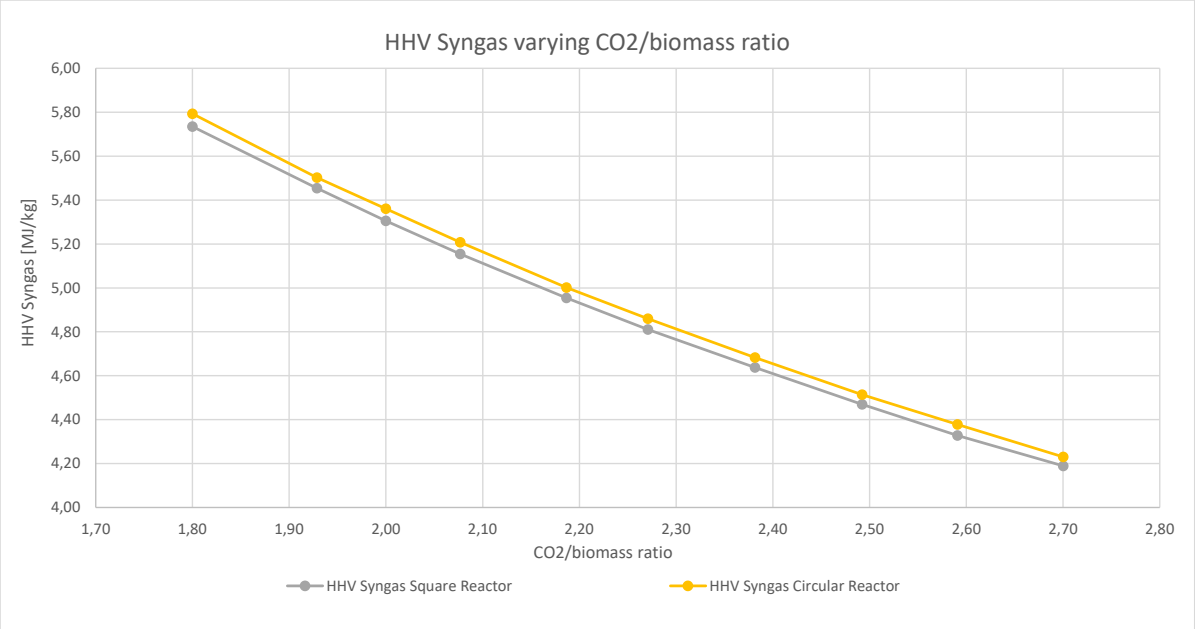

Figure 5.5: HHV Syngas at the outlet of the reactor

in the circular reactor was, although slightly, larger than the HHV of the syngas produced in the square geometry reactor. Now, knowing the HHV value of syngas and knowing the power developed by the SOFC and HHV of the initial biomass, it is possible to calculate the efficiency of the total system. The efficiency to be calculated includes the net power developed by the SOFCs and the power used to increase the inlet CO_2 temperature from the ambient temperature up to the system 800°C. By doing so, the calculated efficiency will include all the useful power and all the power spent. The final formula for calculating efficiency will be:

$$\eta_{system} = \frac{\text{Net power output}}{\text{Total power input}} = \frac{W^{el}_{SOFCs} + \dot{m}_{syngas} \cdot HHV_{syngas}}{\dot{m}_{biomass} \cdot HHV_{biomass} + C^{average}_{p,\mathrm{CO_2}} \cdot \Delta T \cdot \dot{m}_{\mathrm{CO_2},in}} \quad [-] \qquad (5.2)$$

Where:

- η_{system} $[-]$ is the net efficiency of the complete integrated system
- $W^{el}_{SOFCs}[W]$ is the total electrical power developed by the fuel cells
- $\dot{m}_{syngas}$ $[kg/s]$ is the mass flow of syngas exiting the system
- HHV_{syngas} $[J/kg]$ is the higher heating value of syngas
- $\dot{m}_{biomass}$ $[kg/s]$ is the mass flow of biomass entering in the system
- $HHV_{biomass}$ $[J/kg]$ is the higher heating value of biomass

- $C_{p,\mathrm{CO_2}}^{average}$ $[J/(KgK)]$ is the average heat capacity of CO_2 between the ambient temperature and 800°C
- ΔT $[K]$ is the temperature difference between the ambient temperature and 800°C
- $\dot{m}_{\mathrm{CO_2},in}$ $[kg/s]$ is the CO_2 mass flow as gasifying medium entering the system

A design choice aimed at optimizing the system and therefore with the scope of increasing efficiency, could be to recirculate the CO_2 at the output of the system itself, thus making less CO_2 to be used and less energy used to preheat CO_2. With this design choice the efficiency equation will become:

$$\eta_{system,r} = \frac{\text{Net power output}}{\text{Total power input - recovered power}} \quad [-] \tag{5.3}$$

$$\eta_{system,r} = \frac{W_{SOFCs}^{el} + \dot{m}_{syngas} \cdot HHV_{syngas}}{\dot{m}_{biomass} \cdot HHV_{biomass} + C_{p,\mathrm{CO_2}}^{average} \cdot \Delta T \cdot (\dot{m}_{\mathrm{CO_2},in} - \dot{m}_{\mathrm{CO_2},out})} \quad [-] \tag{5.4}$$

Where:

- $\eta_{system,r}$ $[-]$ is the net efficiency of the complete integrated system with the CO_2 recovery system
- $\dot{m}_{\mathrm{CO_2},out}$ $[kg/s]$ is the CO_2 mass flow fraction of exiting gas to recovery

With these premises, the efficiency of the system will be represented in the figure 5.6

After analyzing all these factors, one thing immediately jumps out, that is that as the CO_2/biomass ratio increases, all the parameters analyzed so far tend to decrease the performance of the system, instead results that the circular geometry are much better than the square geometry due to various factors. Finally, to decide which ratio is the best, it is necessary to analyze a parameter that is quite unrelated to the amount of CO_2 that is present in the system. The fact that the total number of heat sinks in the system can be analyzed and therefore be taken into consideration. In the next figure is shown the thermal power consumed in the reactor.

As we can see from the figure 5.7 and the table 5.3, less energy is used where where both the biomass entering the system and the CO_2 entering the system are minimal. So it seems easy to understand the design choice to choose a CO_2/biomass ratio, which is at the same time a good compromise between thermal efficiency and system performance, because it consumes less biomass and less CO_2. The last parameters to analyze are the bulk density of the biochar resulting from the OK pyrolysis and the average temperature inside the device. As we can see from the figures

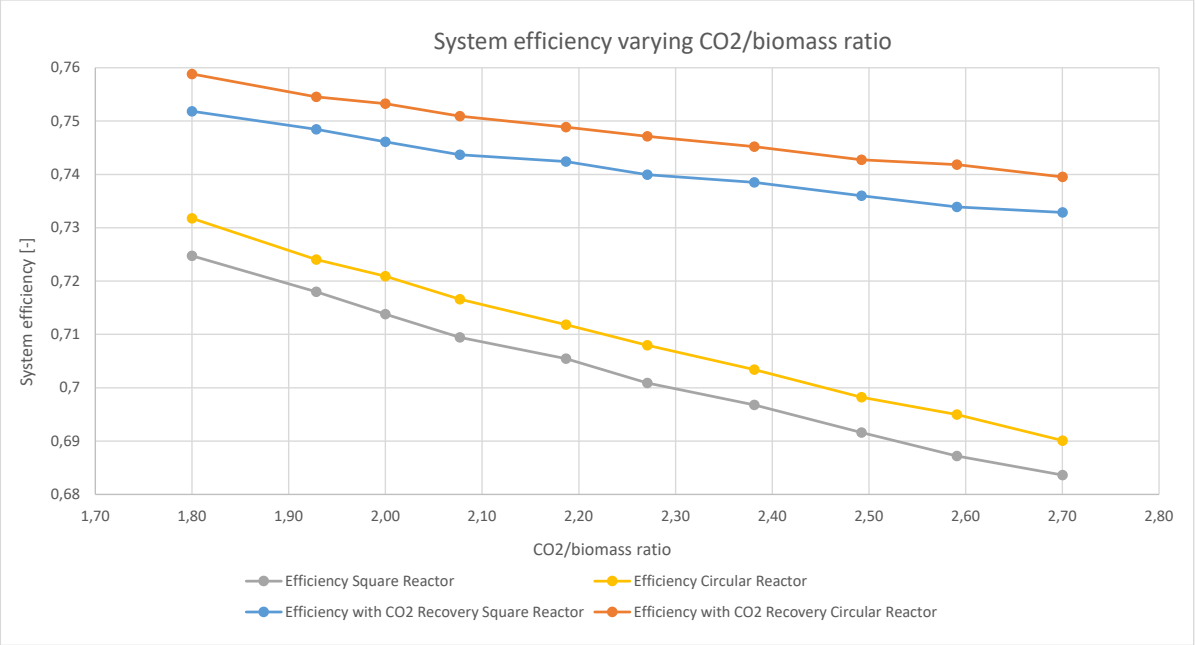

Figure 5.6: Efficiency of the complete integrated system

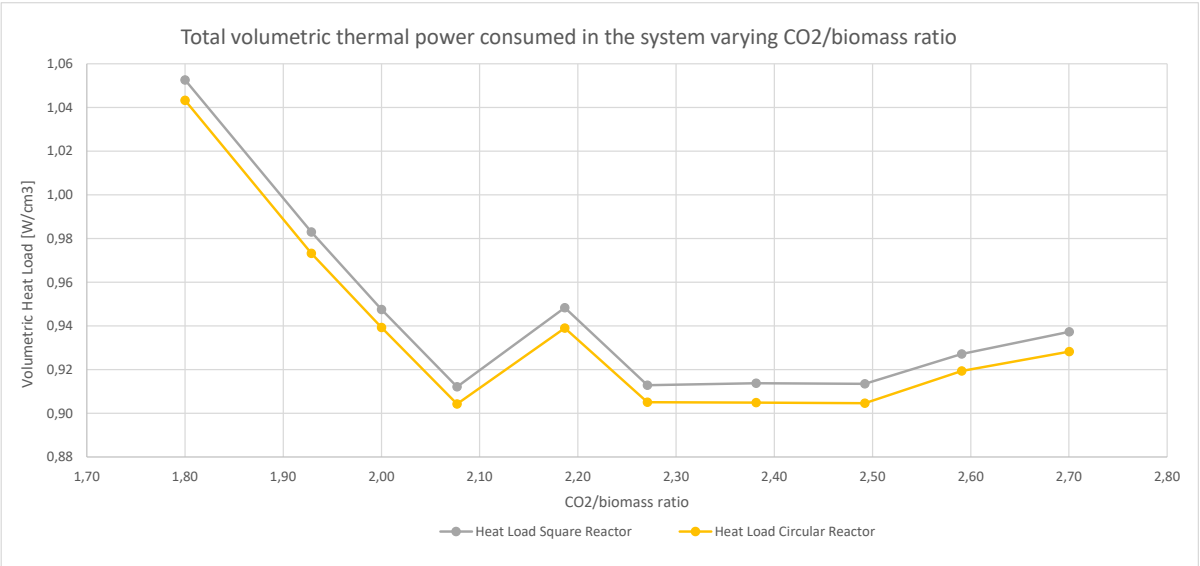

Figure 5.7: Total thermal load in the system

5.8 and 5.9, the density of the biochar locally inside the reactor has a fairly comparable value for both geometries. By local we mean that the point where the measurement was taken corresponds to a coordinate point midway between the reactor and perfectly located halfway between two SOFCs for both geometries. While by average density, we mean the average made on the whole biomass bed volume. As can be seen, the average density is much lower in the circular reactor; this is a positive behaviour because it indicates that the gasification reaction will be faster and

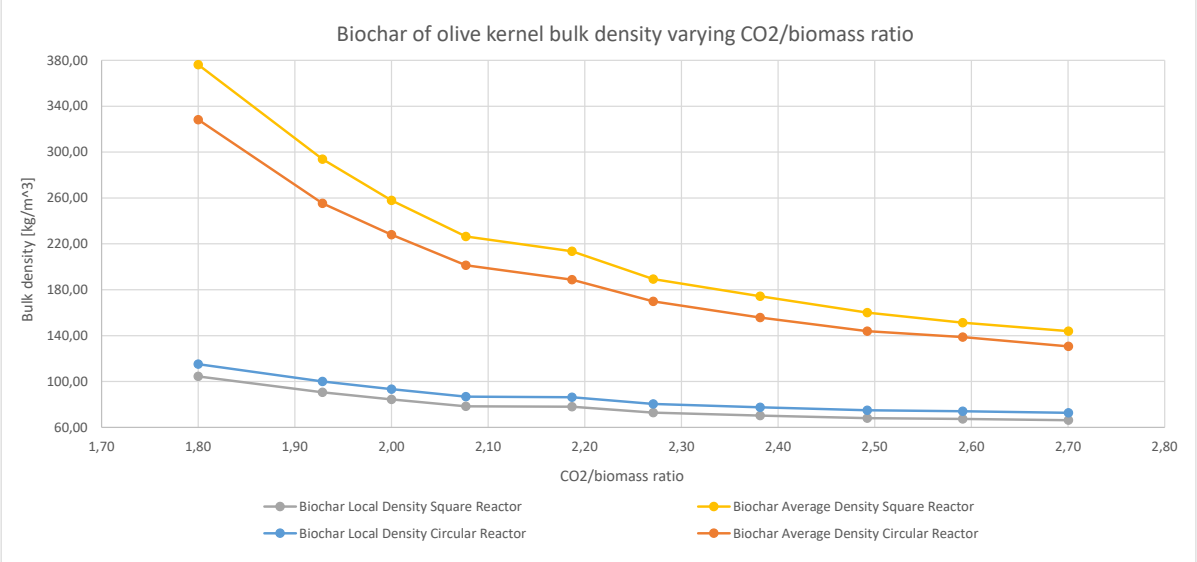

Figure 5.8: Olive kernel biochar bulk density in the system

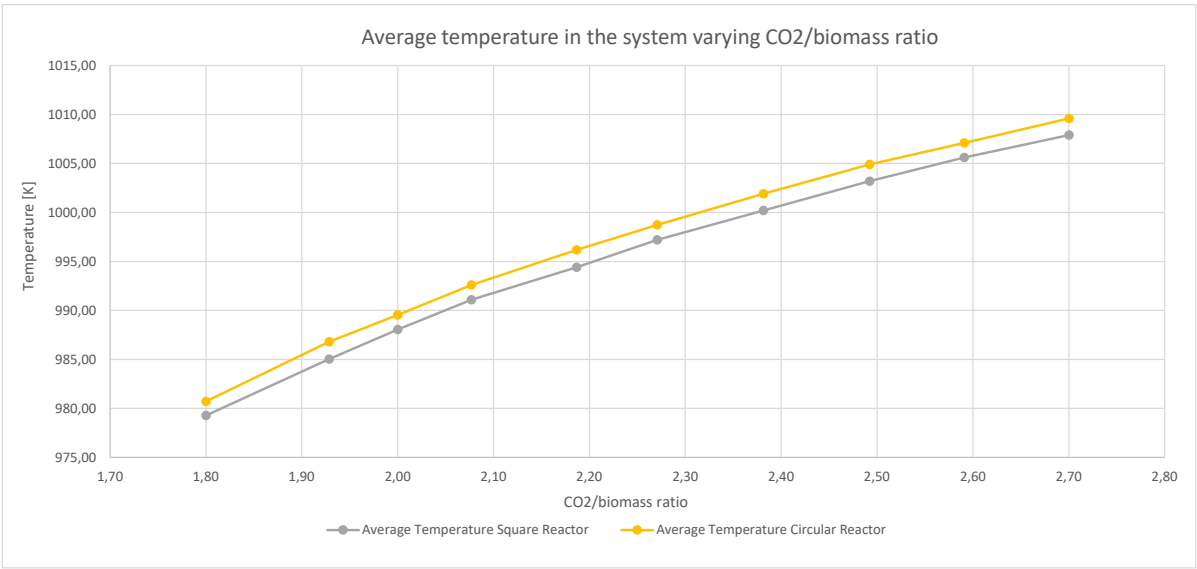

Figure 5.9: Average temperature in the porous biomass bed

less biochar will accumulate in the reactor. As far as temperature is concerned, even in this case the circular geometry has a clear superiority with respect to the other reactor geometry. Therefore, the data for the chosen ratio can be summarized. In the table 5.4 we can see the data.

5.2 COMSOL® views of the results

After importing all the most interesting general results into Excel and defining the best operating conditions as a first approximation, you can move on to analyze the main system variables in 2D

Tabel 5.4: Summarized data obtained from simulations

Variables	**Square geometry**	**Circular geometry**	**Units**
CO_2/Biomass ratio	2.08	2.08	[-]
CO_2 outlet mass fraction	43.35	43.02	[%]
CO outlet mass fraction	39.35	39.68	[%]
H_2 outlet mass fraction	0.46	0.47	[%]
H_2O outlet mass fraction	5.257	5.259	[%]
CH_4 outlet mass fraction	0.943	0.959	[%]
Tar outlet mass fraction	10.64	10.627	[%]
HHV Syngas	5.154	5.208	[MJ/kg]
Efficiency	0.709	0.717	[-]
Efficiency with CO_2 recovery	0.744	0.751	[-]
Thermal loads	0.912	0.904	$[W/cm^3]$
Local biochar density	78.41	86.75	$[kg/m^3]$
Average biochar density	226.48	201.26	$[kg/m^3]$
Average biomass bed temperature	991.08	992.59	[K]

sections. First of all, it is necessary to define reference plans on which to graph the results. First of all, it is necessary to define reference plans on which to graph the results. To meet this need, two floors have been chosen: one that cuts the z axis to 7 cm in height and the other that cuts the y axis at different points with respect to what geometry you are talking about. In the next figures we can see the plans shown. We tried to put the horizontal plane high enough to be still in the biomass bed but at the same time not to be too influenced by the CO_2 inlets, while the plane that cuts the y axis was chosen to collect details along the SOFCs and at the at the same time provide measurements near the boundaries of the device.

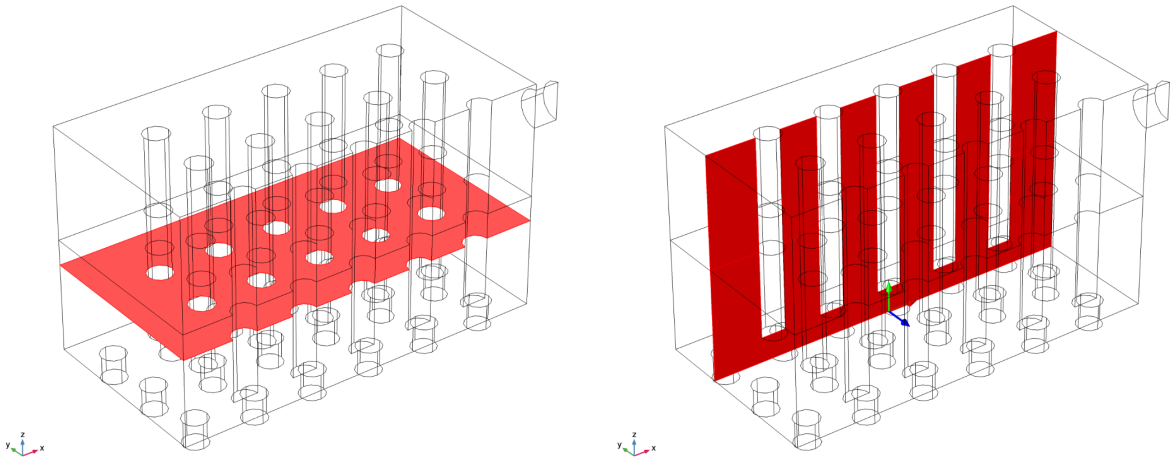

Figure 5.10: Plans in square geometry

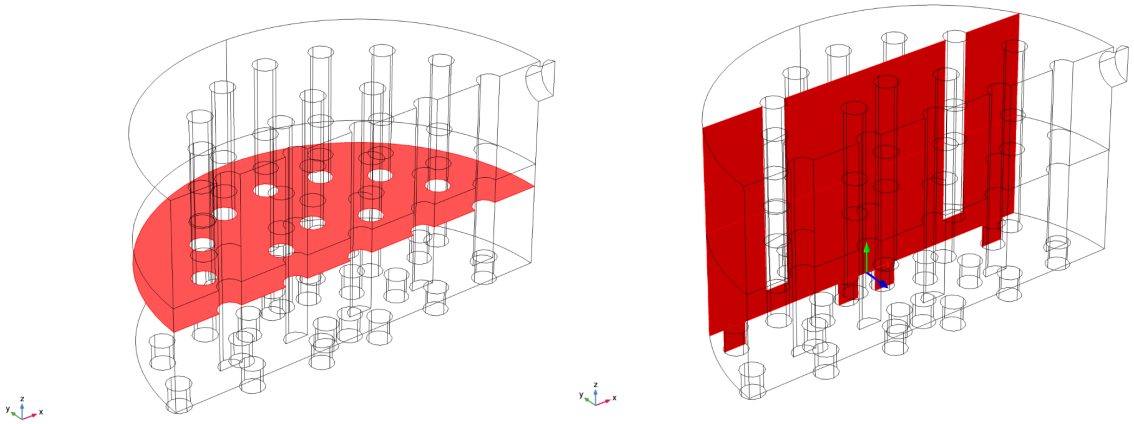

Figure 5.11: Plans in circular geometry

5.2.1 Velocity distribution

The velocity distribution within the two types of reactors is shown in the next figures. As we can

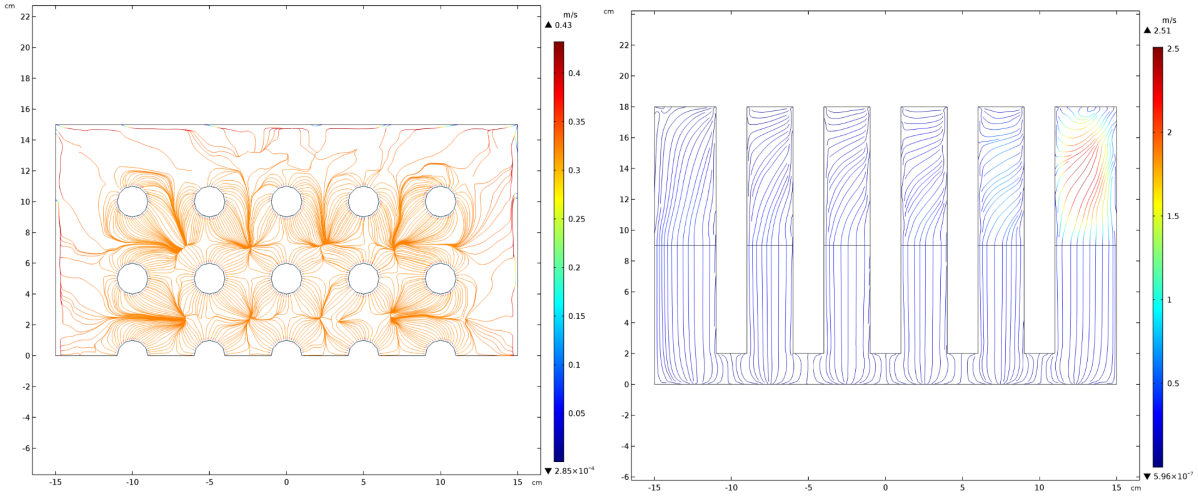

Figure 5.12: Velocity field in square geometry

see from the figures, the velocity field obtained is in any case both comparable if not almost equal. This is because in both geometries the inlet speed is almost equal and the shape of the reactor has little influence on the general velocity field, but mostly affects it in localized points.

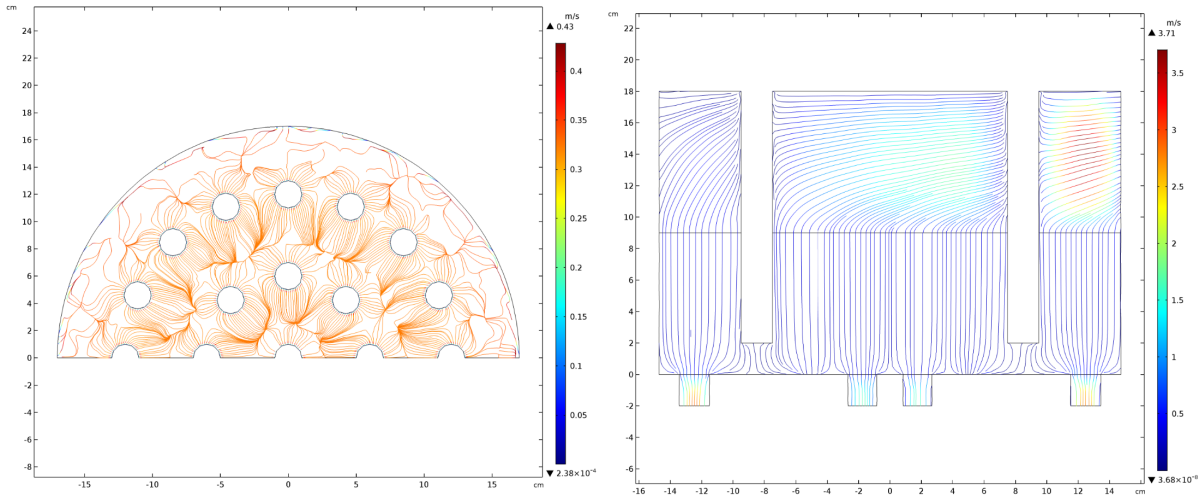

Figure 5.13: Velocity field in circular geometry

5.2.2 Temperature distribution

Much more complicated speech must be done with temperature distribution. The latter is highly dependent on the reactions taking place inside the reactor and above all mainly depends on the distribution of SOFCs. The main source of energy of the reactor are the SOFCs themselves, therefore their distribution is of fundamental importance. As we can see from the figures representing the temperature distribution, the latter is less in the boundaries of the reactor, this because the succession of gasification reactions which are for the most part endothermic, uniformly cool down the reactor, while the fuel cells are mainly more concentrated towards the center of the device. In addiction the low thermal conductivity of the biomass does not allow the temperature to be uniform over the entire reactor. The minimum temperature is very important, because where the temperature is minimum, the chemical reactions of gasification inside the reactor can slow down,therefore with the accumulation of unwanted and harmful substances for the system. The minimum temperature in both reactor geometries is shown in the next table.

Tabel 5.5: Minimum temperature depending on geometry

Parameters	**Values**	
	Square	Circular
Minimum Temperature	873.31 $[K]$	904.42 $[K]$
Minimum Biochar bulk density	38.24 $[kg/m^3]$	36.41 $[kg/m^3]$

It is obvious to consider that the minimum temperature in the square-shaped reactor is reached in the corners, while in the circular-shaped reactor there is no specific point where there is a

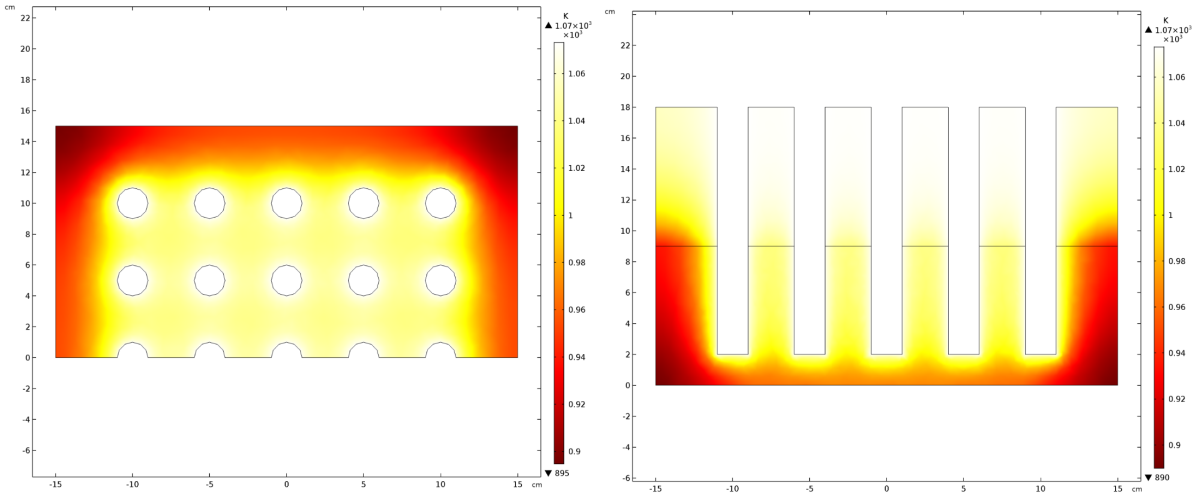

Figure 5.14: Temperature distribution in square geometry

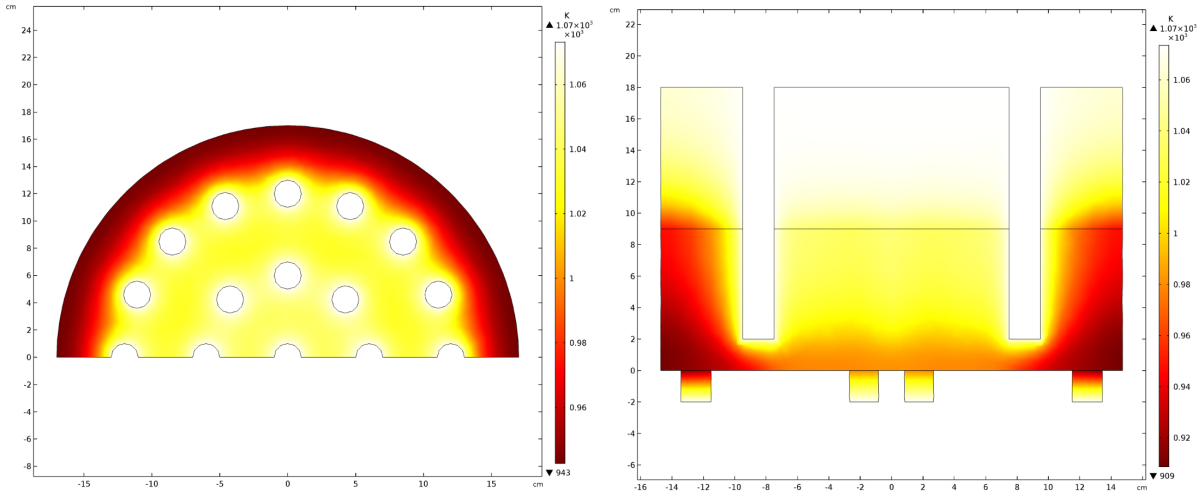

Figure 5.15: Temperature distribution in circular geometry

noticeable drop in temperature. Another consideration that can be made is that the temperature drops in the lower part of the system (biomass bed) where most of the endothermic gasification reactions take place.

5.2.3 Chemical species reaction rate and molar fraction distribution

It is also important to know how the molar fractions of the chemical species involved in the reactions within our system evolve. It is also very important to know the reaction rate of the individual chemical species to know how much and where the compounds are produced or consumed. In the next pages you will see the distributions of the molar fractions and the reaction rate in the various sections of the system.

- CO_2:

  As we can see from the figure, in both geometries, the CO_2 entering the system is almost instantly consumed in the gasification reactions. Around SOFC we can notice an increase in the molar fraction of CO_2, this is given by the fact that SOFCs absorb CO and H_2 and emit CO_2 and H_2O

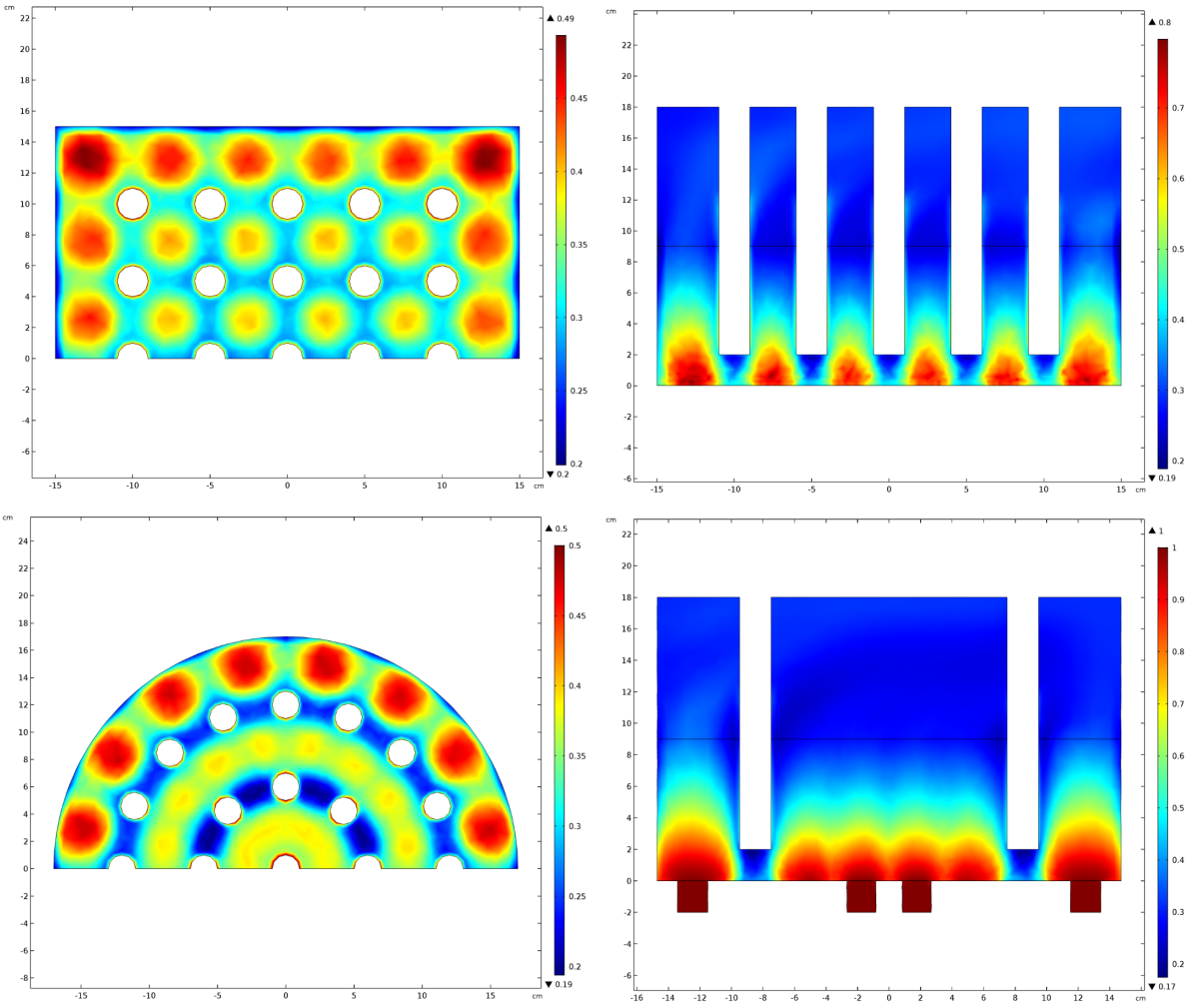

Figure 5.16: CO_2 molar fraction distribution

As we can see from the figures, near the inlets there is a significant increase in the molar fraction of CO_2. In fact, the inlets have been designed to diffuse CO_2 wherever possible in the reactor, so as not to have parts of the rector in which the char gasification reaction can trudge.

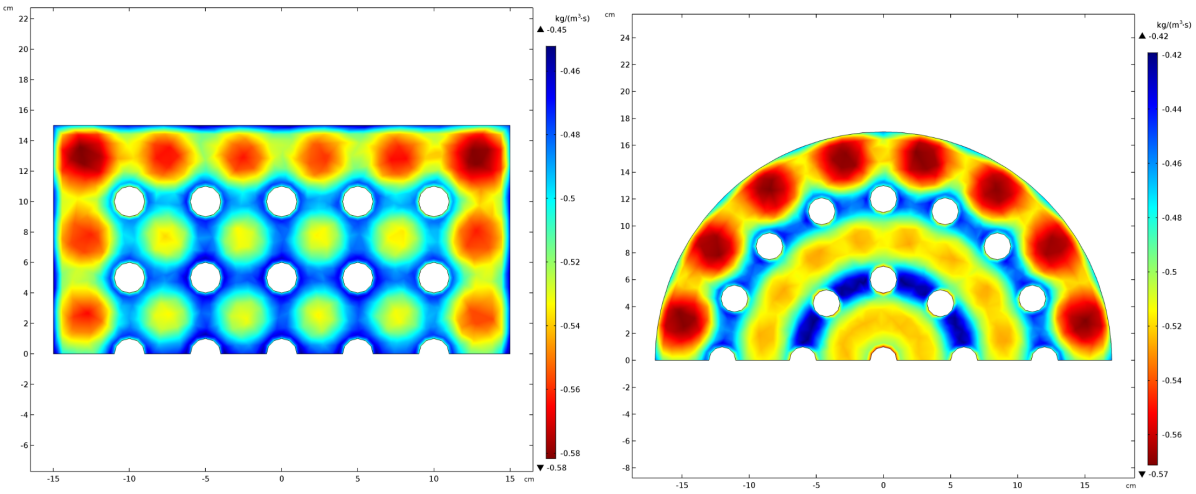

Figure 5.17: CO_2 total reaction rate

Regarding the CO_2 reaction rate, as we can see from figure 5.17, just where there is a greater concentration of CO_2, the reactions will be faster and more carbon dioxide will be consumed. The negative sign indicates the consumption of CO_2 as a reagent to create other compounds. Regarding the difference between the two geometries, with the same cutting plane of the z axis, both geometries consume almost the same quantities of CO_2, with a small difference with the circular geometry, with a maximum value slightly lower than the square geometry.

- CO:

  Around the SOFCs we can notice a strong decrease in the molar fraction of CO due to its absorption as fuel by the SOFCs. Instead, in the whole reactor there is a large concentration of CO because it is the main product in the Boudouard reaction which is very reactive in the reactor, and also because CO is also one of the most abundant products from biomass pyrolysis.

  As regards the production of CO in the system, as we can see in the figures representing the reaction rate, CO is almost uniformly produced in the reactor. Mainly there is an increase in the reaction rate in the immediate vicinity of the SOFCs, a symptom of the fact that the higher temperature and the higher concentration of CO_2 increase the reaction rate of the

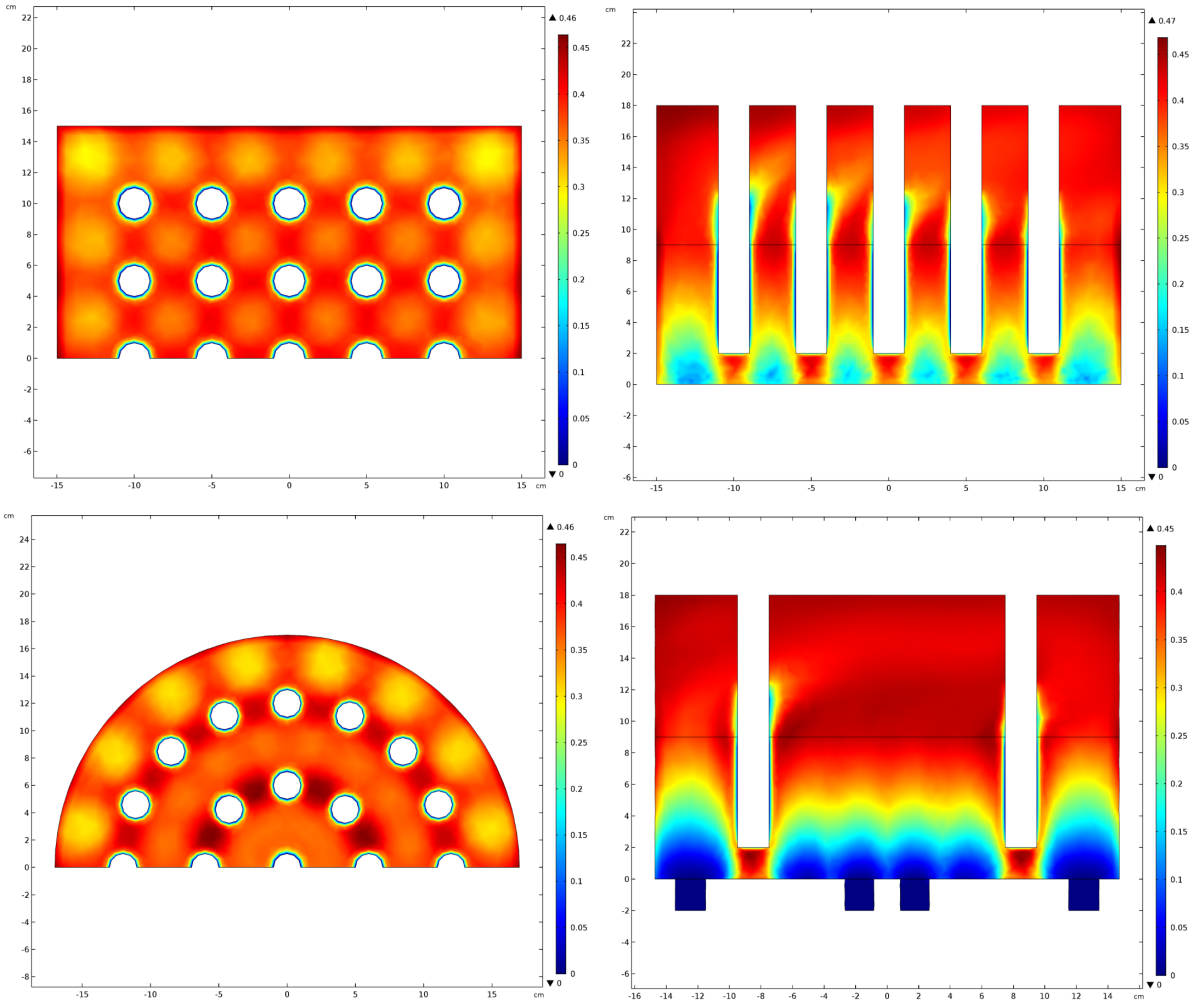

Figure 5.18: CO molar fraction distribution

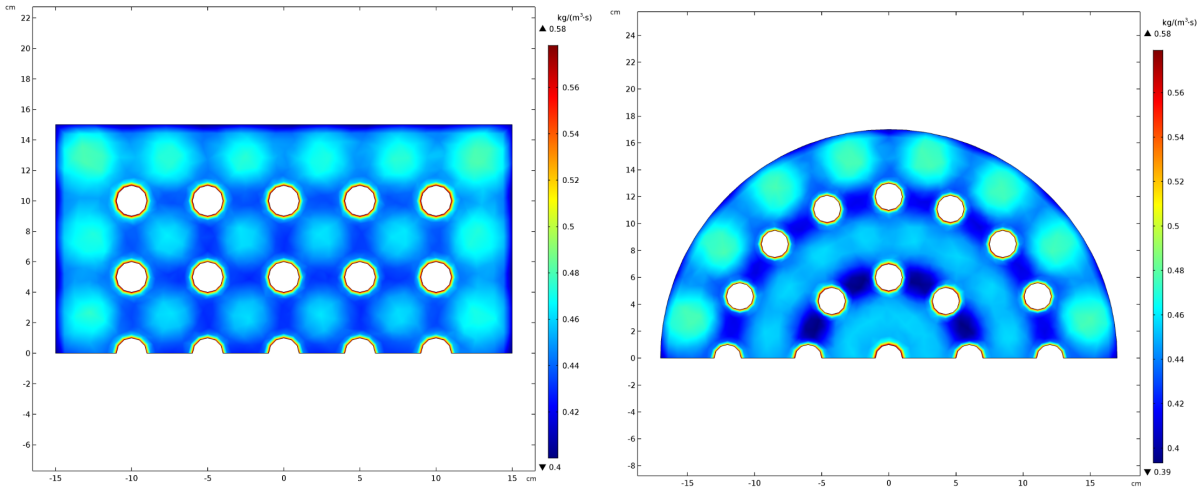

Figure 5.19: CO total reaction rate

pyrolysis and the Boudouard reaction. On the other hand, there are little changes between the two geometries both for the molar concentration of CO and for its reaction rate.

- H_2:

  As with the CO, around the SOFCs we can notice a strong decrease in the molar fraction of H_2 due to its absorption as fuel by the SOFCs. In the other parts of the reactor the H_2 is not so abundant also because of the WGS that it is not inclined to the production of H_2 due to the already presence of CO_2

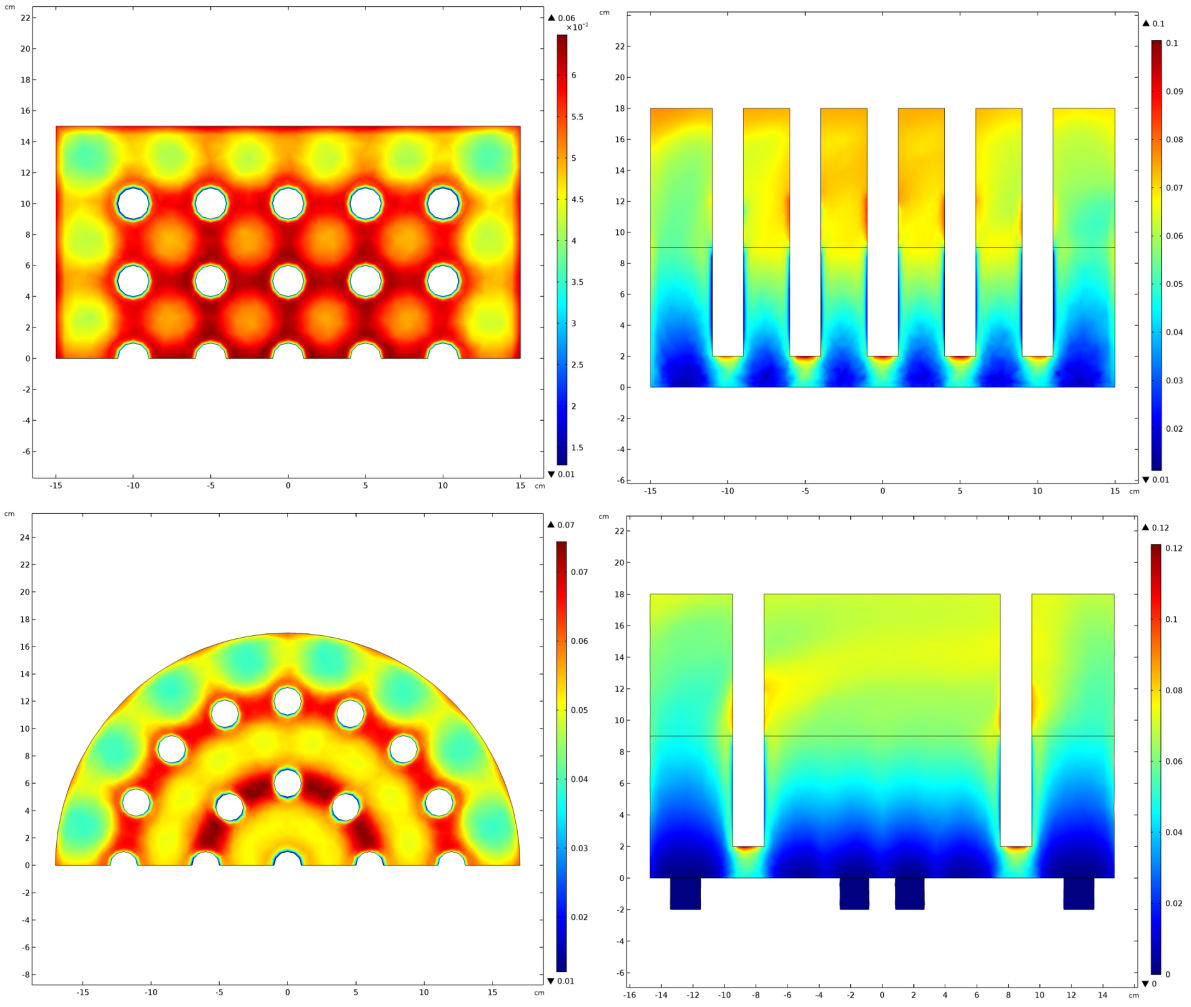

Figure 5.20: H_2 molar fraction distribution

As regards the H_2 reaction rate, both geometries have comparable values, and it can be seen that in the immediate vicinity of the SOFCs there is greater production of H_2, given above all by the higher temperature.

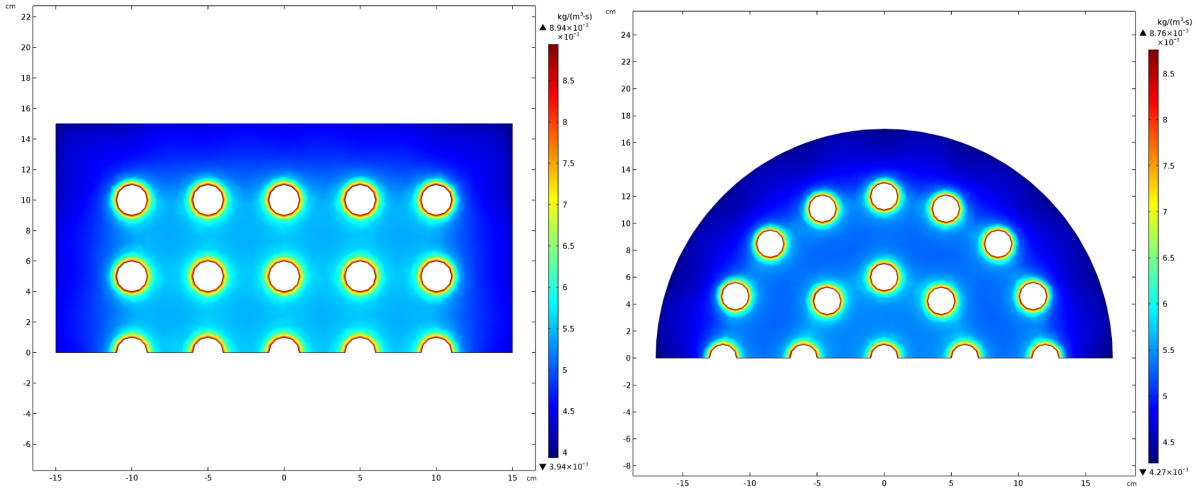

Figure 5.21: H_2 total reaction rate

- H_2O:

  The water vapour produced within our system derives mainly from the drying and primary pyrolysis of biomass. A part also derives from SOFCs which emit it as a waste from the oxidation of H_2. Inside the reactor the water vapour is also consumed in the gas gasification reaction in the Water-gas reaction, but its limited concentration makes its reactions very disadvantaged.

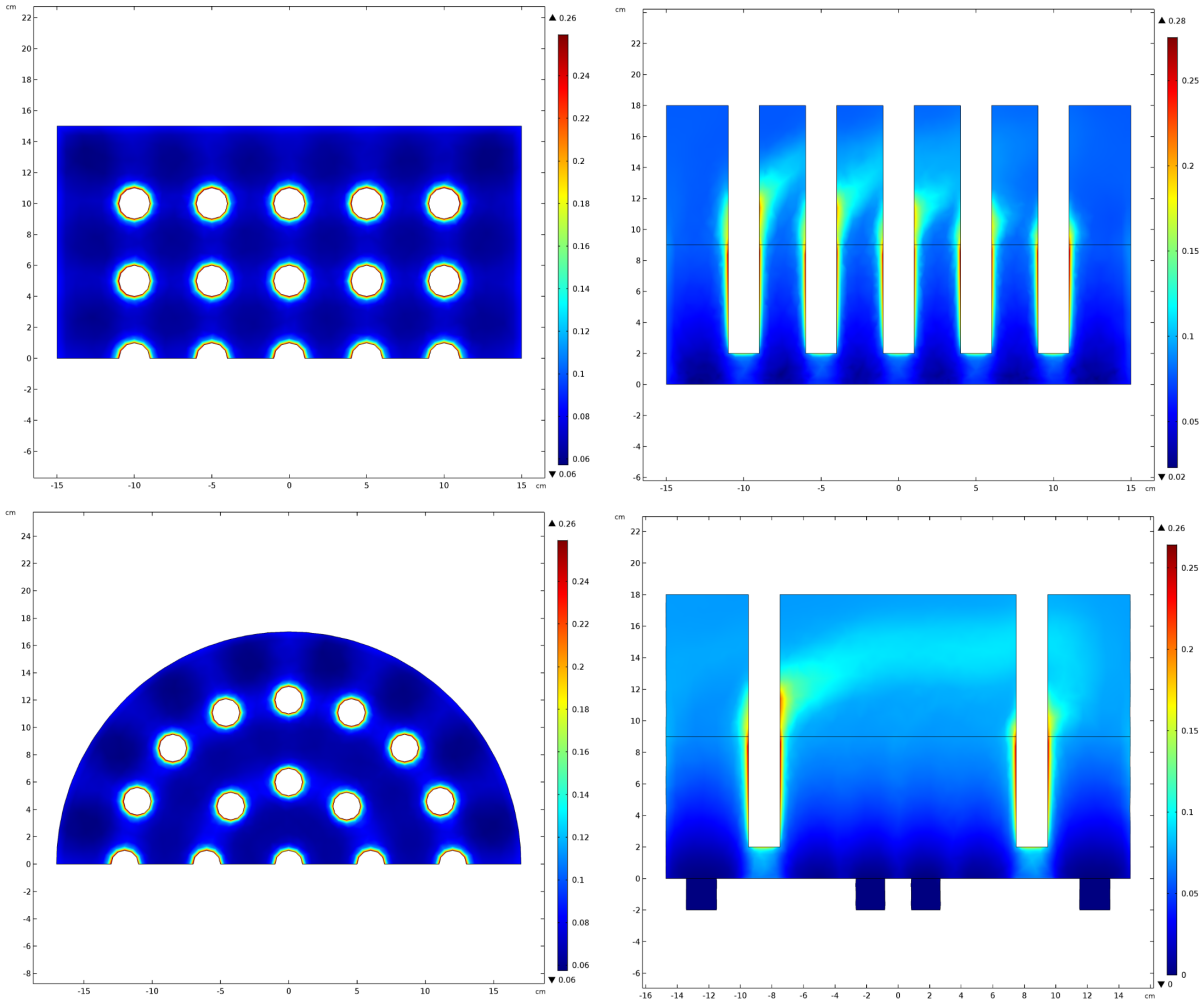

Figure 5.22: H_2O molar fraction distribution

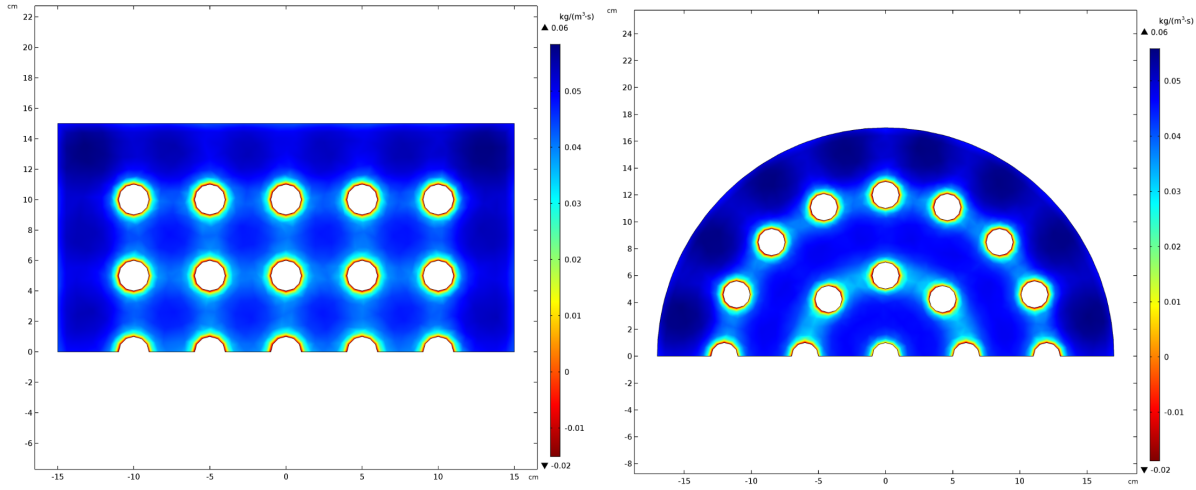

Figure 5.23: H_2O total reaction rate

- CH_4:

  The methane contained in our system is very little in relation to other fuels such as H_2 and above all CO. The little methane that is created is generated by primary and secondary pyrolysis, and is used as fuel in SOFCs only after being reformed by the nickel catalyst in the anode and therefore being transformed into CO and H_2. The highest concentrations occur in the vicinity of the cells and in the free flow.

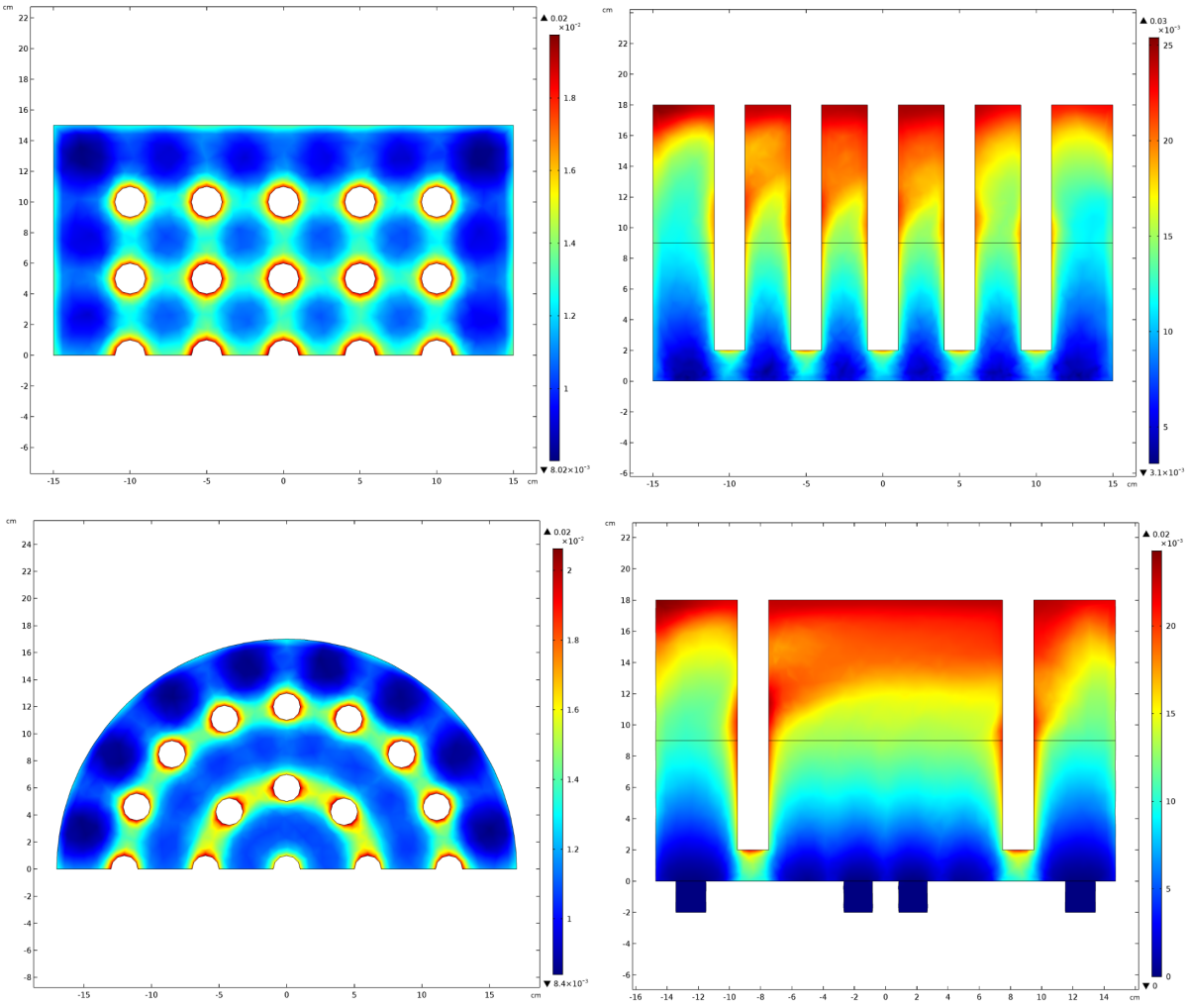

Figure 5.24: CH_4 molar fraction distribution

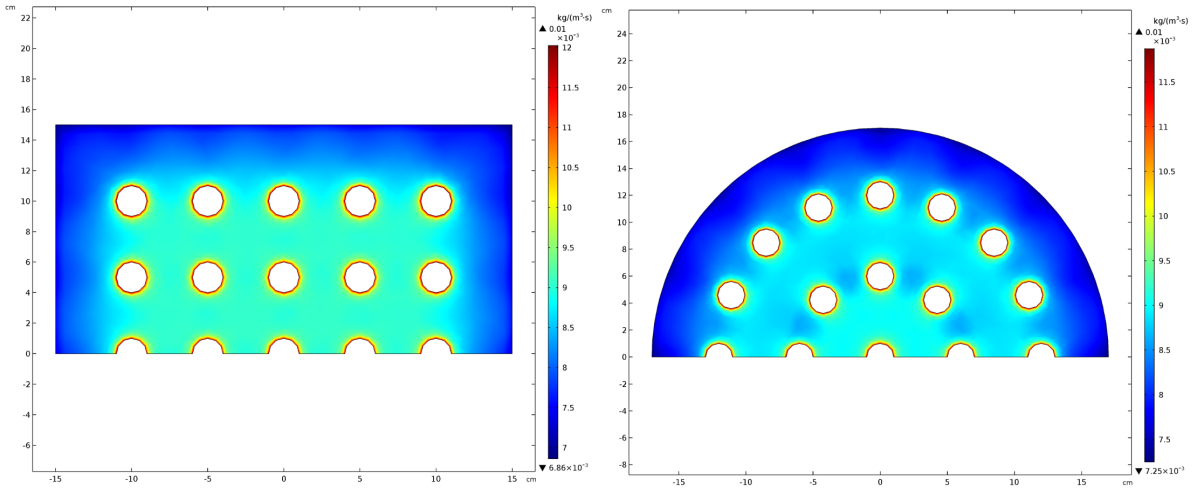

Figure 5.25: CH_4 total reaction rate

- Tar and inert Tar:

  The tars are a problem inside the gasification reactors and especially in the reactors in which SOFCs cells are integrated. The tars are the main product by weight of the primary pyrolysis, and the only way to eliminate them from the system is to make a secondary pyrolysis occur by raising the temperature, or to make them reform through a catalyst. From the reaction rate figures, we can see that near the cells where the temperature is higher, less tars are produced, or rather they are pyrolized more and therefore they accumulate much less in concentrations where the temperature is higher.

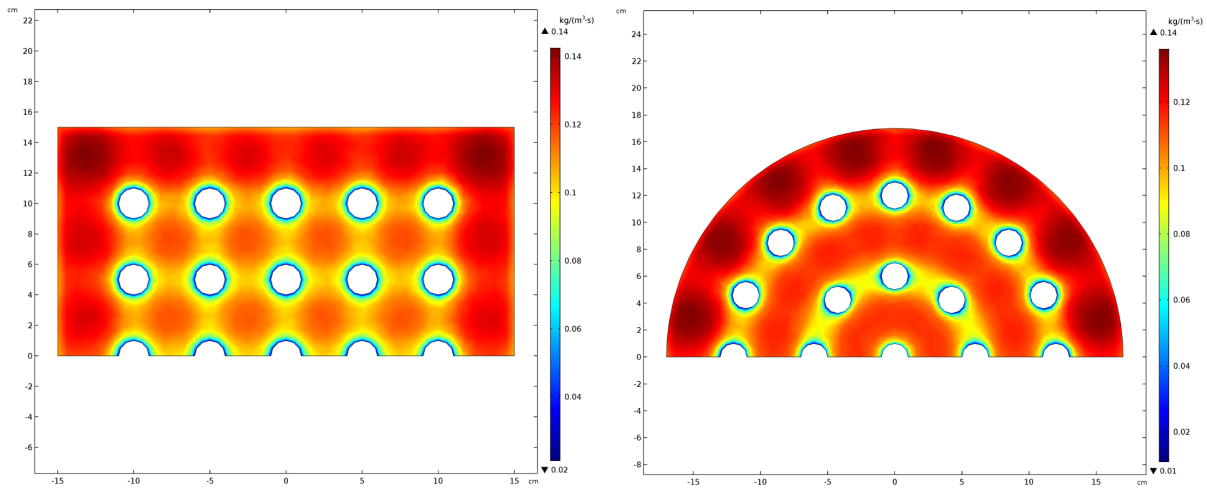

Figure 5.26: Tar total reaction rate

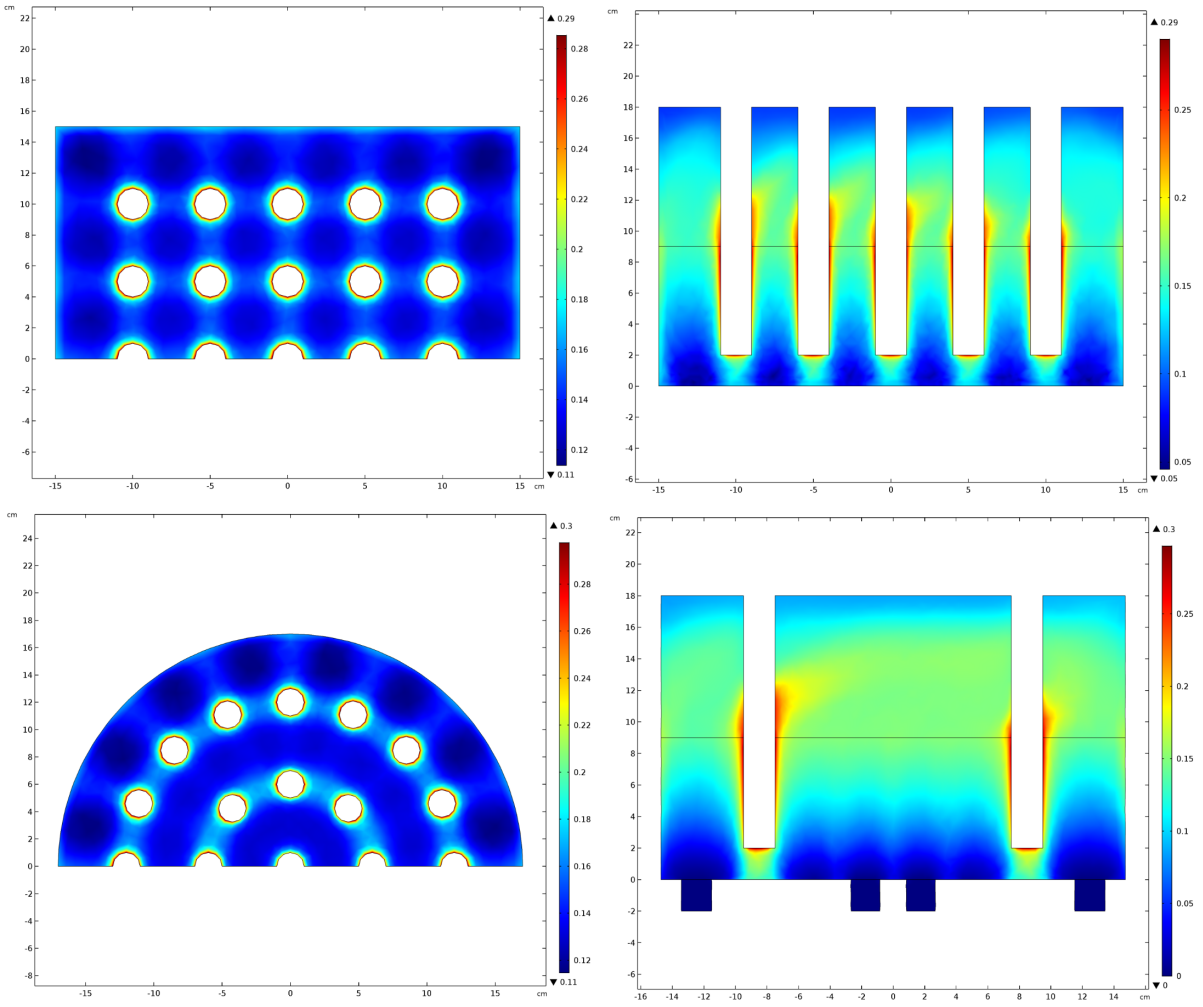

Figure 5.27: Tar molar fraction distribution

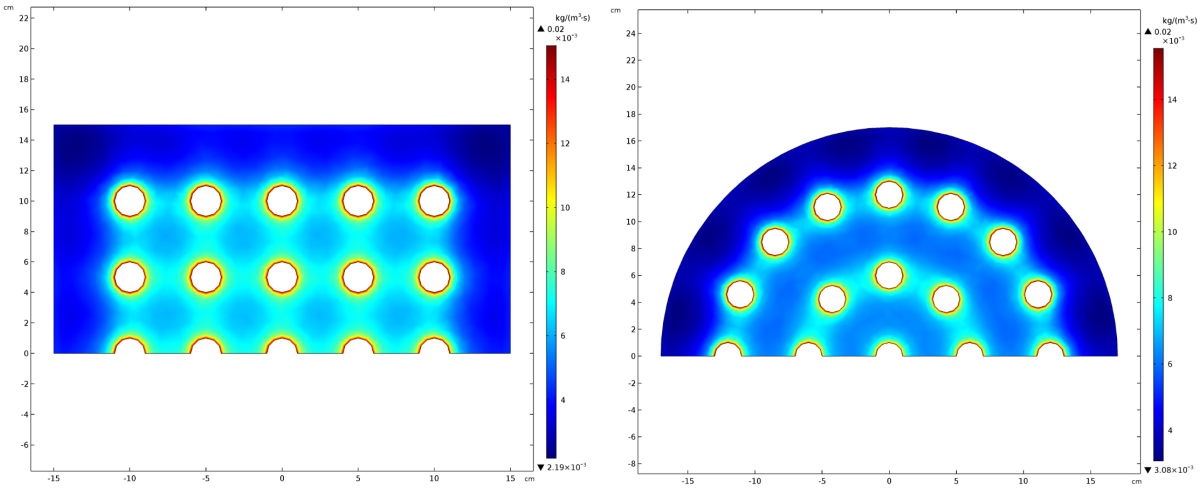

Figure 5.28: Inert Tar total reaction rate

5.2.4 Heat of reactions

One of the last aspects to be analyzed is the heat, that is the thermal power that the individual chemical reactions require. From figure 5.7 and table 5.5 we know that the total heat used in the reactor is for the square and circular reactor: 0.912 and 0.904 $[W/cm^3]$ respectively. But now it is better to know specifically which are the reactions that require more thermal power.

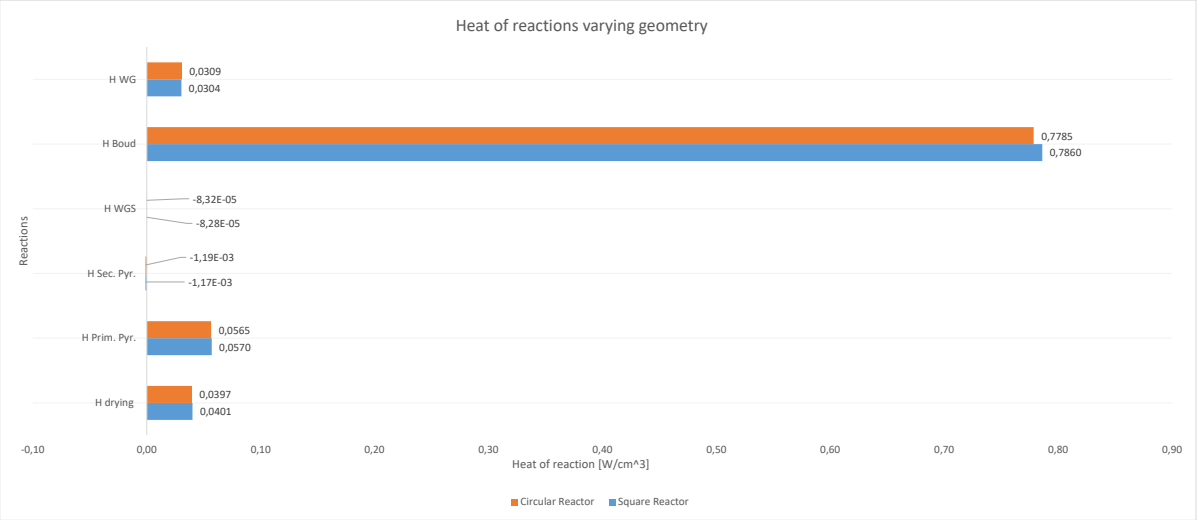

Figure 5.29: Heat of reactions

As we can see from the previous figure, most of the power required comes from the gas gasification reaction of the char with CO_2, in a reaction that we know well as Boudouard reaction. On the other hand, this reaction is also the most endothermic in the system and, given the large presence of carbon dioxide and char, it is also the most kinetically favoured. In the figures, the values with a positive sign correspond to endothermic reactions, while the negative values correspond to exothermic reactions. Regarding the differences between circular and square geometry, we can observe almost the same behaviours. The thing that stands out most is that in the circular-shaped reactor the Boudouard reaction uses less thermal energy. Always remaining in the theme of thermal energy, it is very important to know the thermal flow that is subtracted from the system to fulfil the reactions that take place in the immediate vicinity of the SOFCs anode. In fact, the reactions that take place at the anode are widely endothermic because they are reforming reactions of methane and heavy hydrocarbons. The only exothermic reaction that occurs is the catalyzed WGS. In the next figure we can see an image depicting the heat flow to SOFCs.

As we can see in the biomass bed, the thermal flux has a negative sign, therefore the reactions are endothermic, in the upper part the biomass bed has a positive sign therefore the reaction is

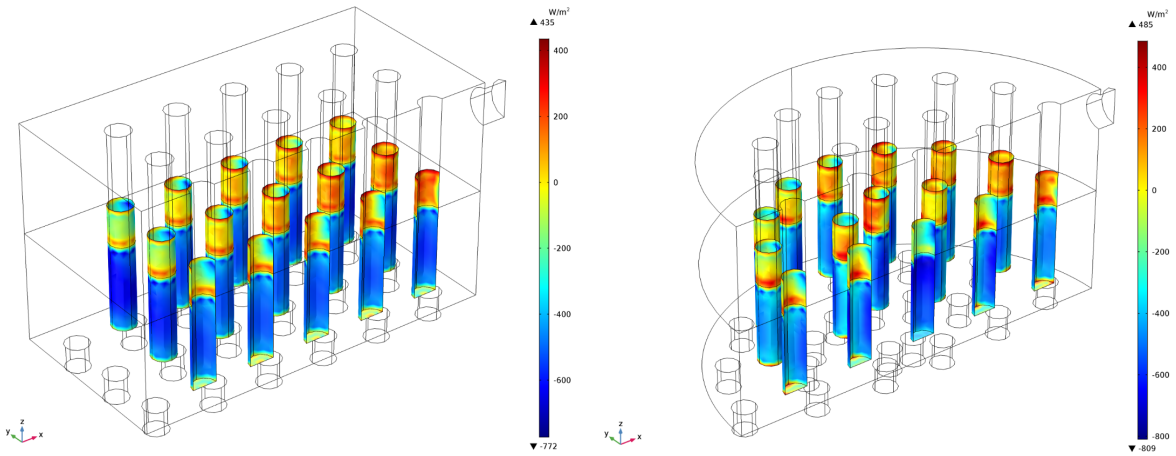

Figure 5.30: Cells heat flux

endothermic, mainly due to the contribution of the catalyzed WGS which is the only exothermic reaction. If we want to see specifically the heat removed or generated by the reactions, in the following pages you will see the sections of the system where the volumetric thermal powers will be shown.

- Heat of drying plus primary pyrolysis:

  The volumetric power given by pyrolysis and drying is constant throughout the volume because it is considered instantaneous and independent of any concentration of chemical species.

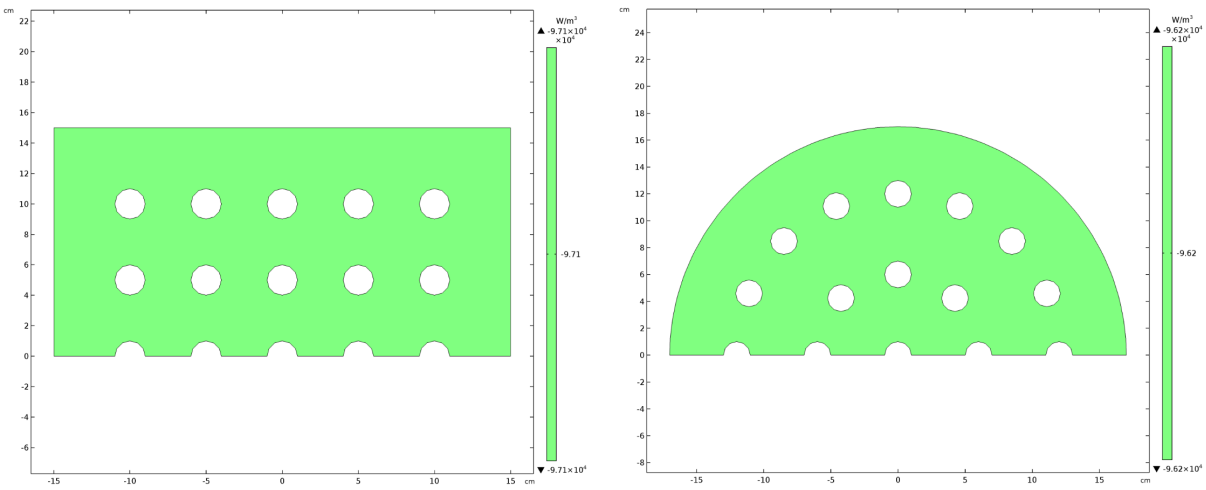

Figure 5.31: Thermal power of drying plus primary pyrolysis

- Heat of secondary pyrolysis (Tar thermal cracking):

  The tar thermal cracking reaction is considered slightly exothermic, and as you can clearly see, the heat produced from the tar cracking is proportional to the reaction rate of the tar cracking: the reaction occurs faster where the temperature is higher, and more heat is generated.

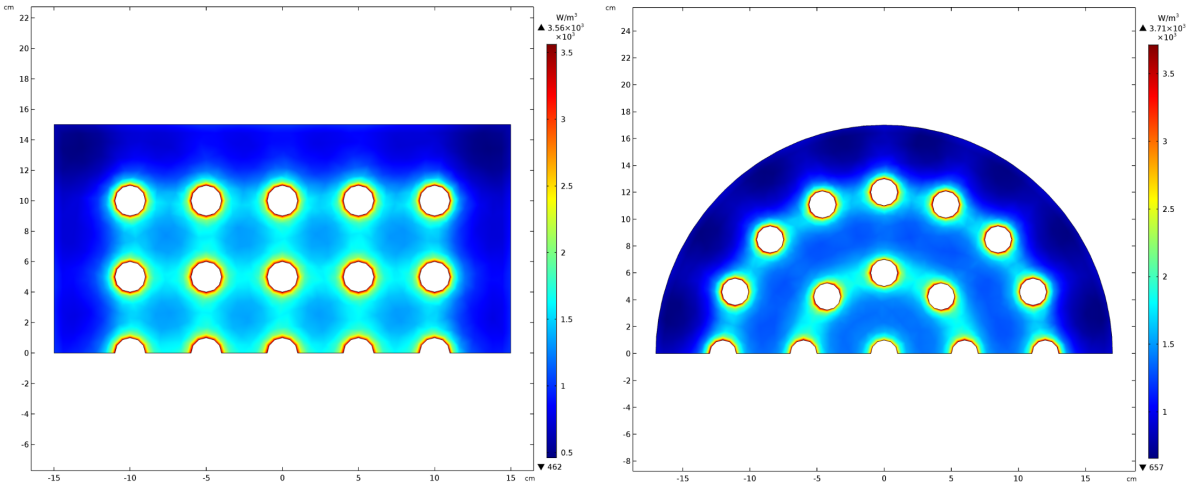

Figure 5.32: Thermal power of secondary pyrolysis

- Heat of WGS:

  The WGS reaction is exothermic. It produces energy where more CO is present, while increasing the concentration of CO_2 slows down the reaction.

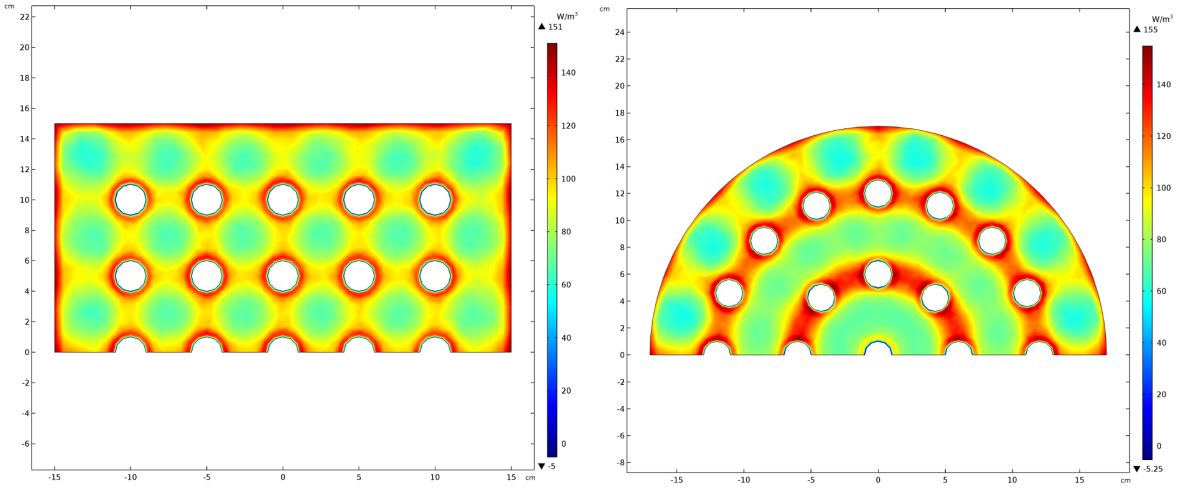

Figure 5.33: Thermal power of WGS

- Heat of Boudouard reaction:

  This is the most impressive reaction within our system that react with char. Obviously the more heat the reaction requires, the more CO_2 is consumed and CO is produced. So the reaction removes more heat where the CO_2 concentration is greater.

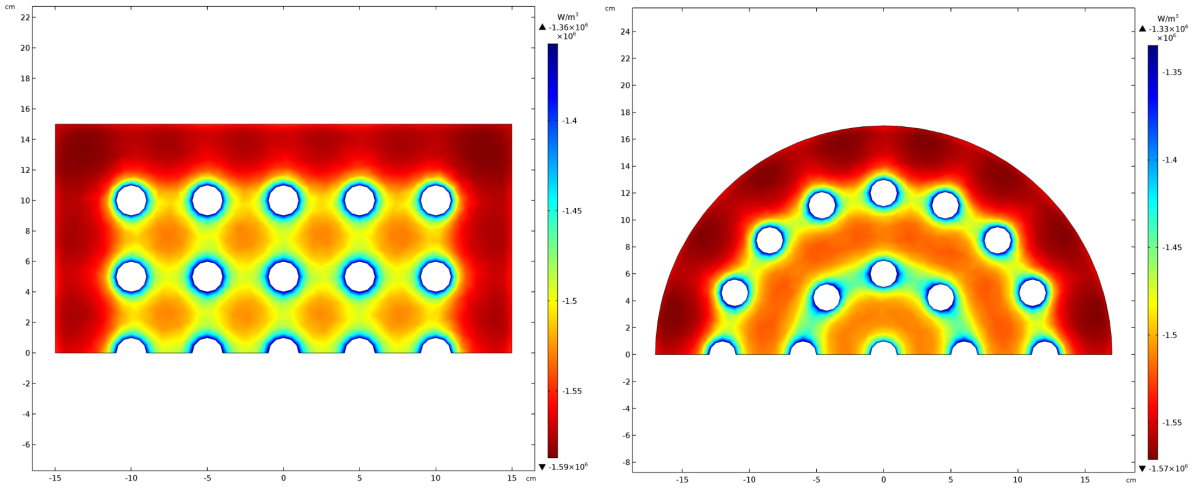

Figure 5.34: Thermal power of Boudouard reaction

- Heat of Water-gas reaction:

  It is also a char gasification reaction, which uses H_2O as the gasifying agent. So its reaction rate is proportional to the concentration of H_2O. Compared to the Boudouard reaction, this reaction is disadvantaged.

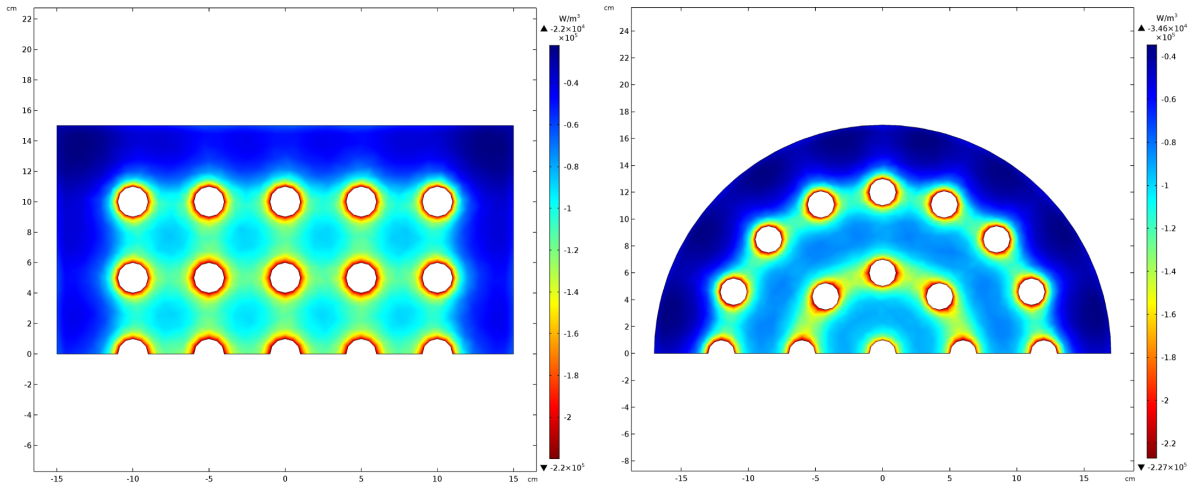

Figure 5.35: Thermal power of Water-gas reaction

5.2.5 Pressure distribution

Finally, to conclude analyzing all the most relevant parameters inside the gasifier, we talk about pressure. It is an established constant and set at 1 atm and does not have large variations, except for the changes caused by inlets and outlets. In the next figure we can see the pressure changes in the two geometry reactors.

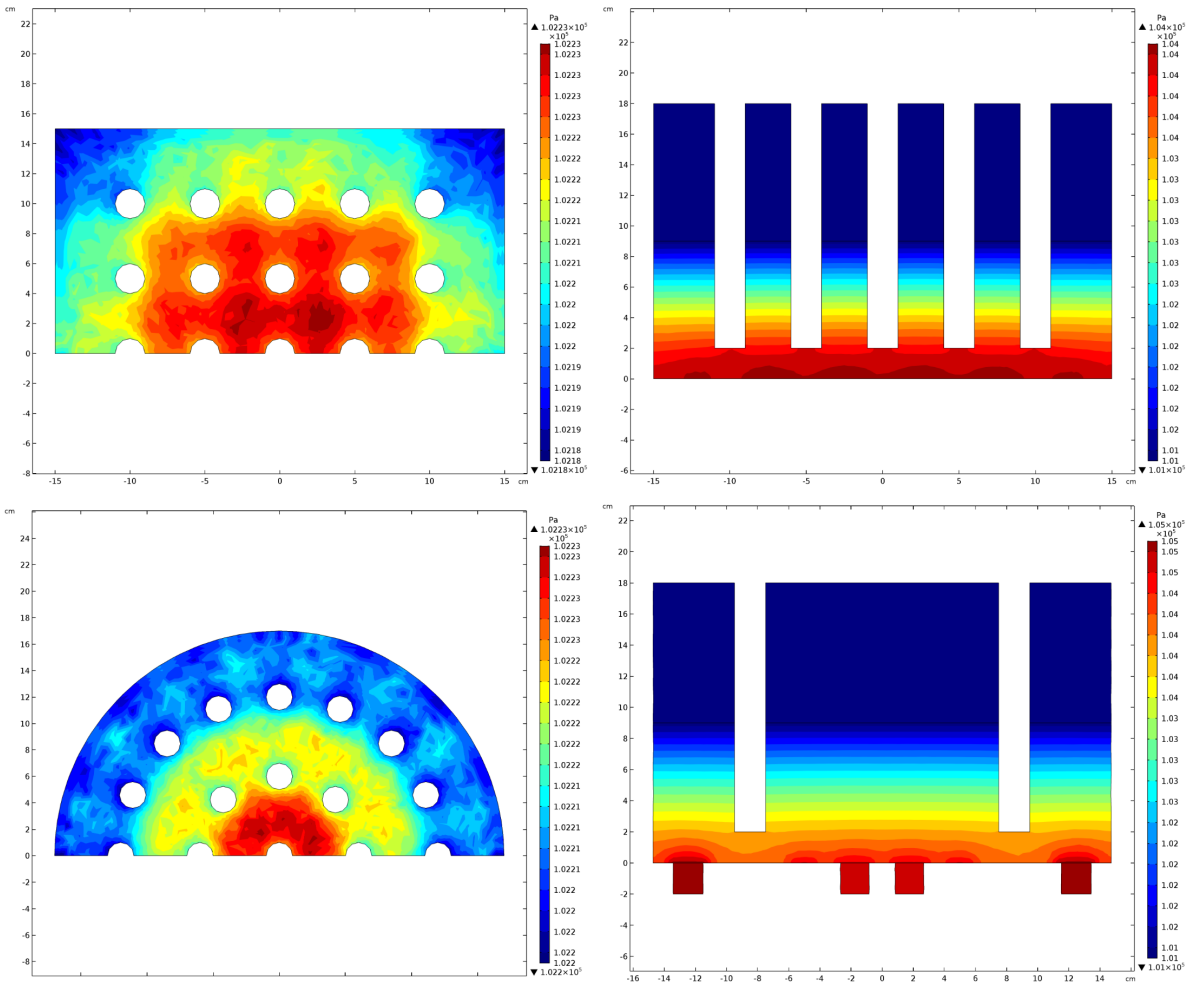

Figure 5.36: Pressure in the different geometries

Chapter 6

Final Observations and Conclusion

In this chapter we will make the final considerations regarding the study carried out so far. First we will analyze the mesh used in the model and calculate the uncertainty and therefore the relative error on the quantities obtained. After I will carry out a bibliographic research regarding the degradation of fuel cells due to carbon deposition. Finally, appropriate conclusions will be drawn on the overall work.

6.1 Model validation

As with any CFD simulation, the results depend heavily on the mesh used. The quality of the mesh is essential for reliable results. Fortunately, the COMSOL multiphysics® software is able, starting from the physics of the problem, to build a very reliable automatic mesh. The only control that must be given to the software to check the mesh is on the qualitative indication of the number of cells to be created. So, a methodological path has been taken to carry out a quantitative analysis of the error that is committed in choosing one mesh over another. First, 5 different meshes have been chosen with an increasing number of cells. Then for each mesh, two types of values have been analyzed: a local value, that is, a quantity that depends exclusively on the point where the latter is measured, and a global value that therefore does not depend on the measurement point. In the next figures we can see both, for the square geometry and for the circular geometry, the value of the minimum temperature and the average temperature as a function of the number of cells of the

simulation.

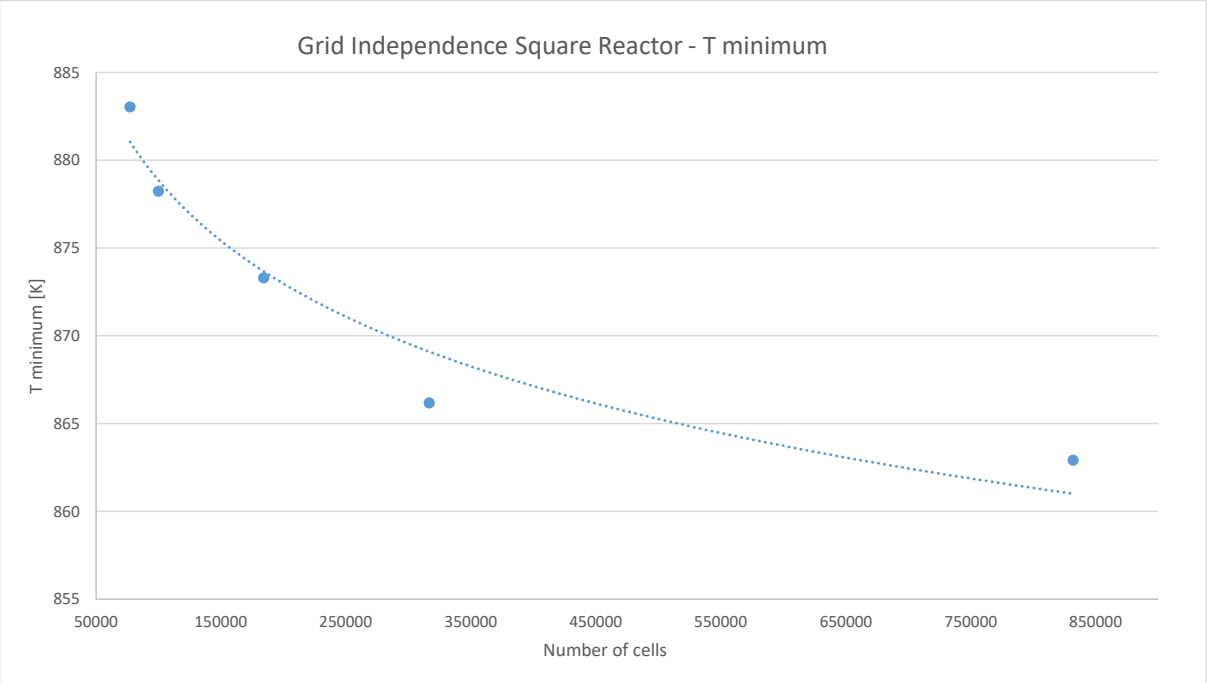

Figure 6.1: Minimum temperature in square geometry

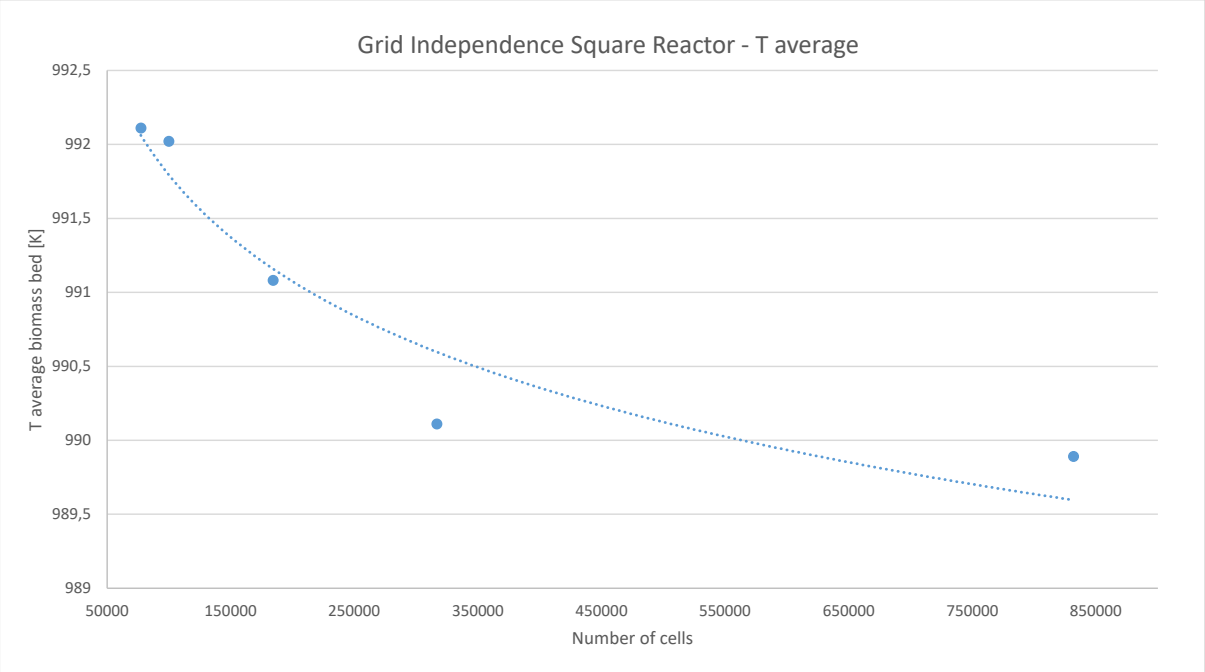

Figure 6.2: Average temperature in square geometry

But from these graphs it is difficult to extrapolate absolute information of how much the calculation error is on a well-defined quantity. For this it will be necessary to calculate the error

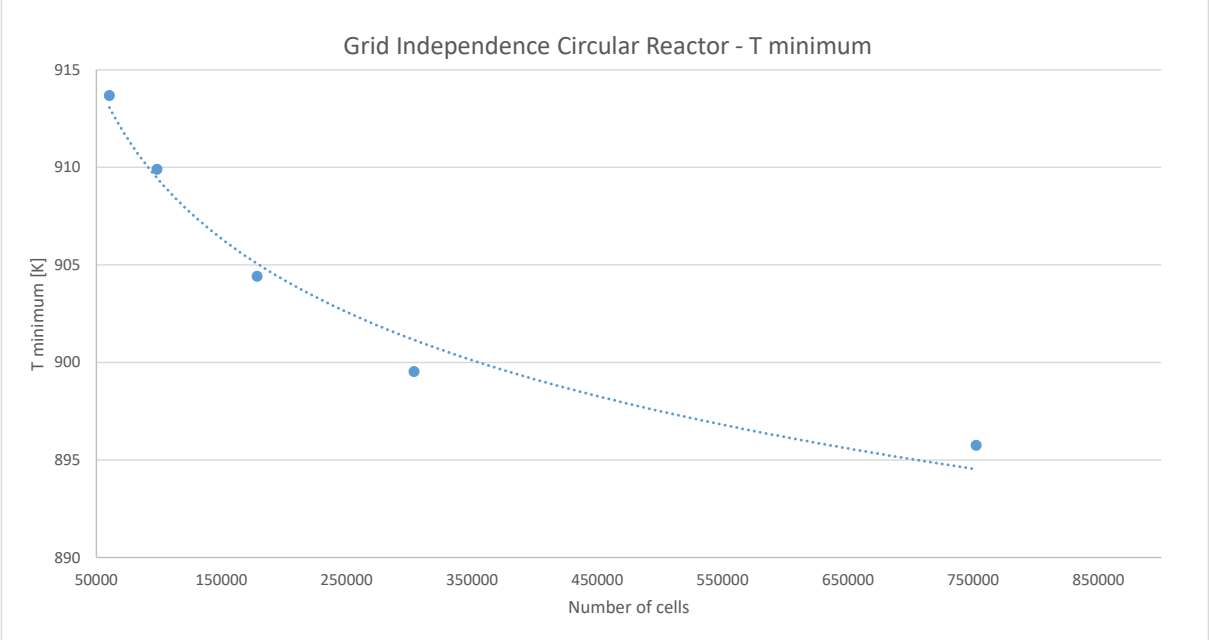

Figure 6.3: Minimum temperature in circular geometry

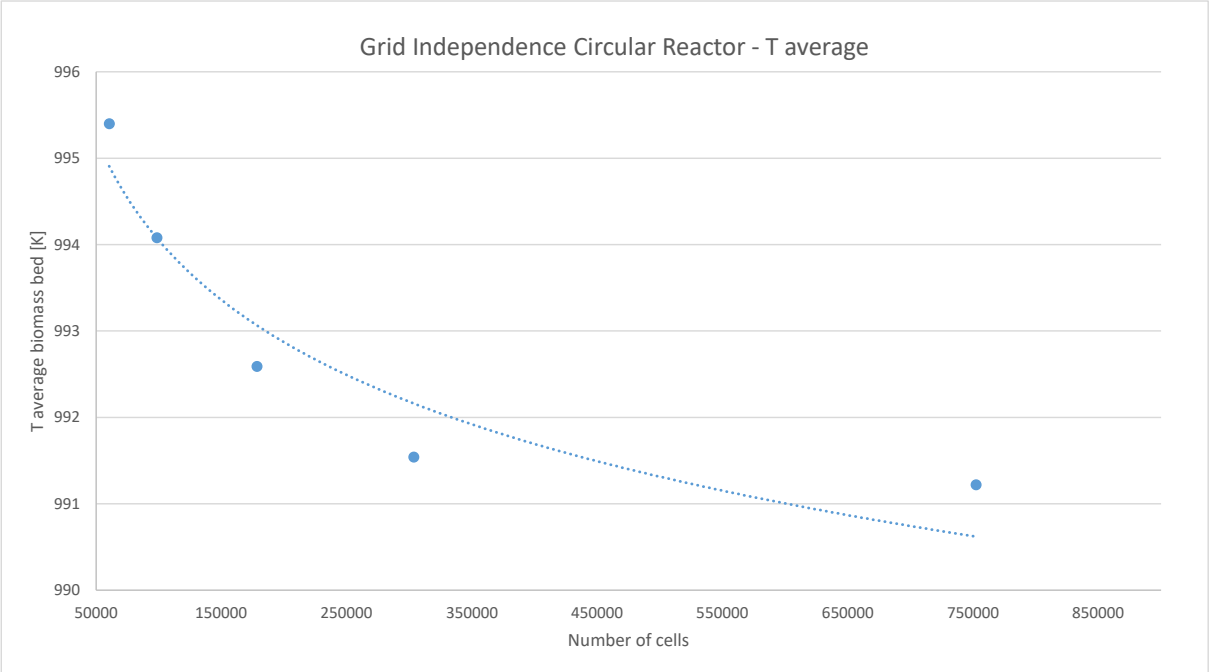

Figure 6.4: Average temperature in circular geometry

relative to the exact quantity. In our case, being computational calculations, we do not know what the exact solution is, so we will use the value obtained from the simulation with the highest number of cells as the most accurate value. The formula for calculating the relative error is:

$$\varepsilon_{rel} = \left| \frac{(X_{appr} - X_0) - (X_{exact} - X_0)}{(X_{exact} - X_0)} \right| \cdot 100 \quad [\%] \tag{6.1}$$

Where:

- ε_{rel} [%] is the percentage relative error of the generic quantity
- X_{appr} is the quantity whose error is to be calculated
- X_0 is a reference value
- X_{exact} is the exact value of the quantity

It is very important to have reported the error with respect to a reference value in order to disconnect the error from the dependence of the unit of measurement. In the case of the temperature the value X_0 is 273 [K]. So for the values first obtained the relative errors will be:

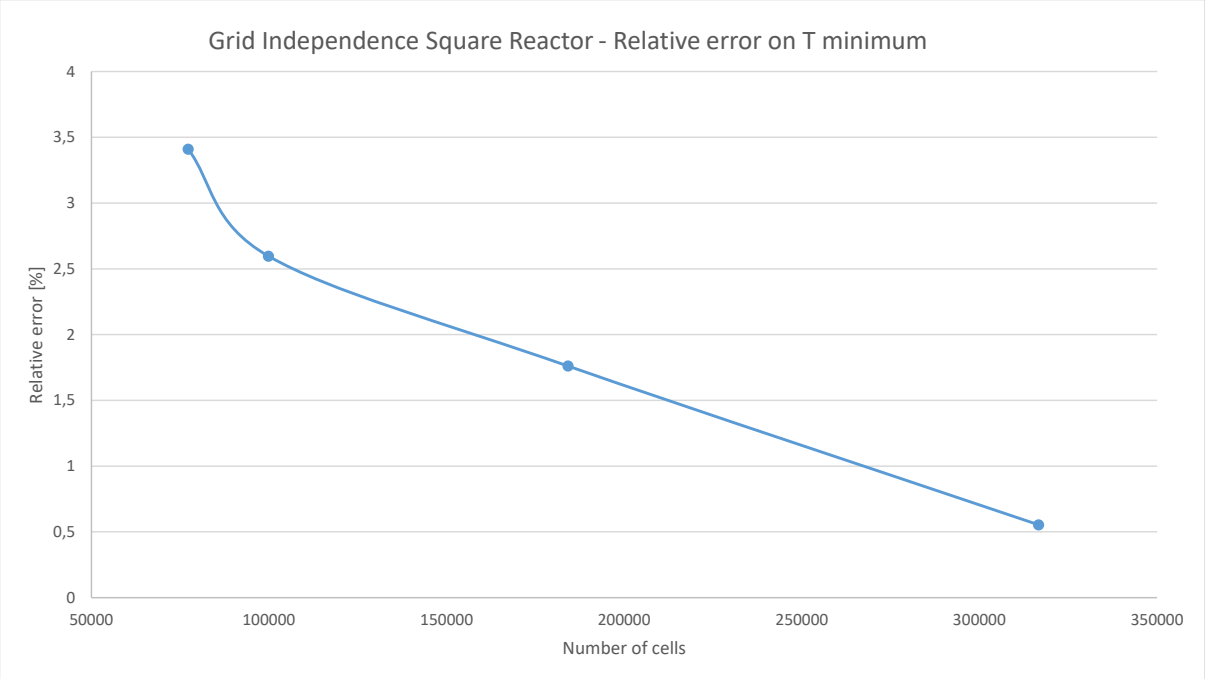

Figure 6.5: Minimum temperature relative error in square geometry

As we can see, the error trend is absolutely in line with expectations. More specifically, the average temperature error has a lower impact than the minimum temperature which instead depends on cells at a specific point. It is evident to think that obviously the more cells we have, the more precise and efficient our simulation will be; but this statement is not completely correct. In fact, another parameter to consider is the simulation time. Therefore the more cells the mesh will contain, the more precise the simulation will be, but at what computational cost.

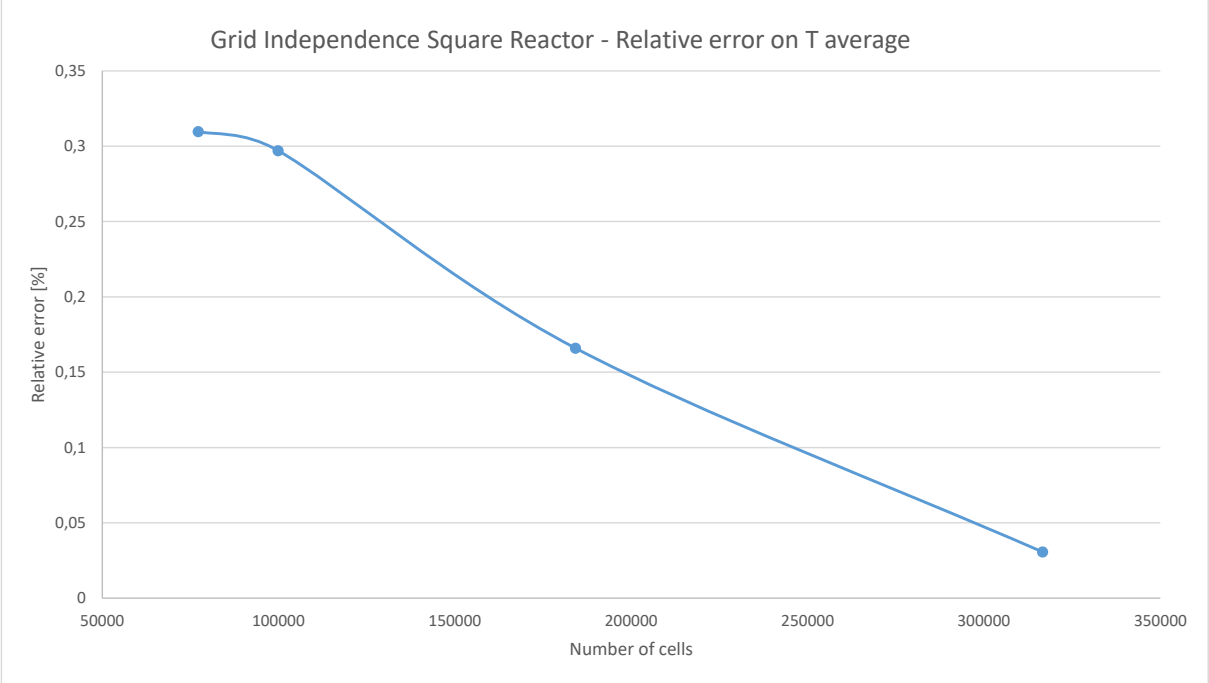

Figure 6.6: Average temperature relative error in square geometry

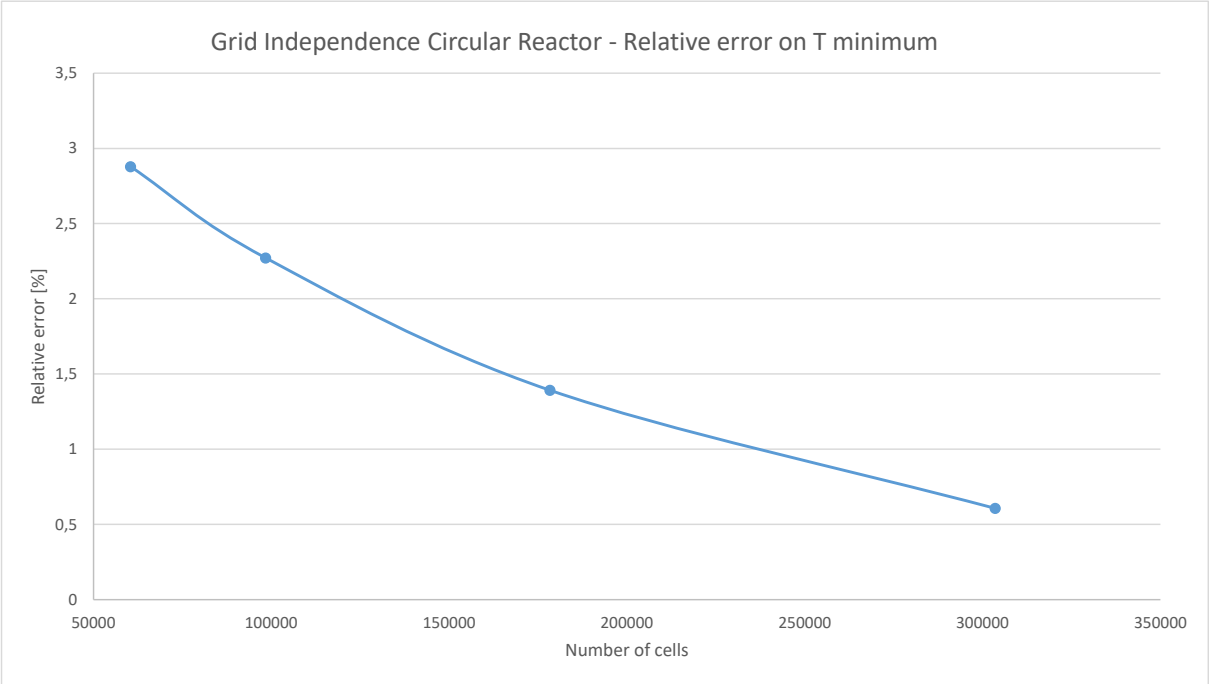

Figure 6.7: Minimum temperature relative error in circular geometry

Therefore, computational time information was also collected from previous simulations with different number of cells. Then everything was related to the faster simulation.

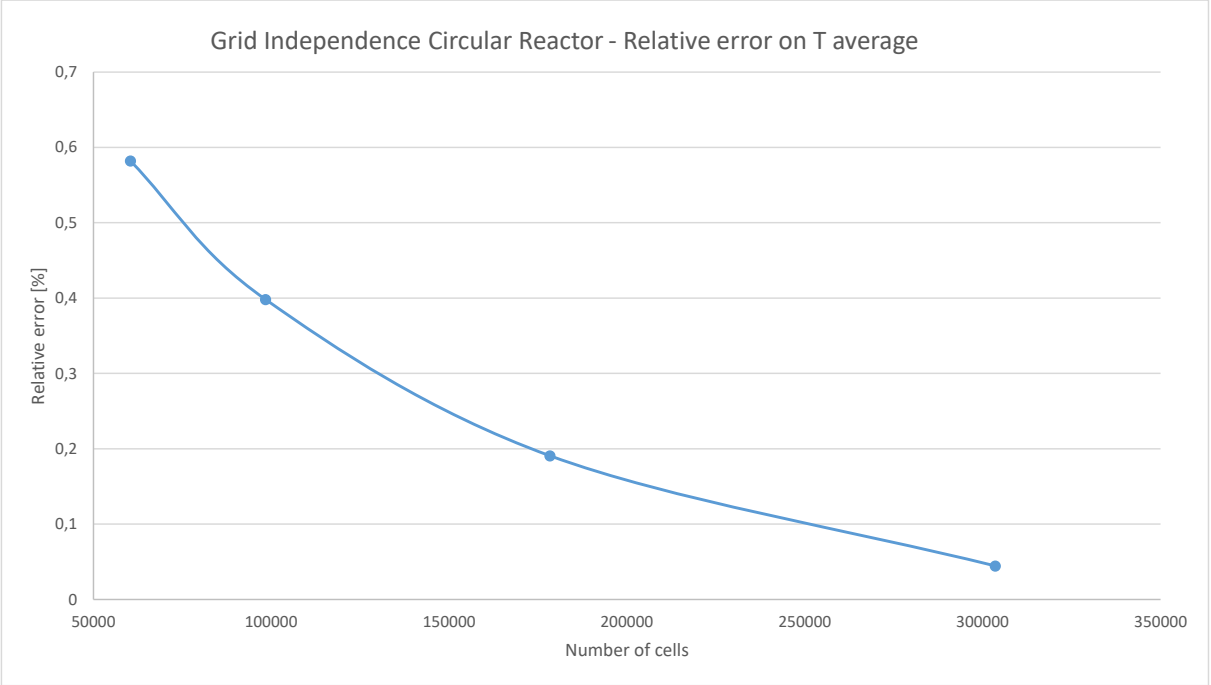

Figure 6.8: Average temperature relative error in circular geometry

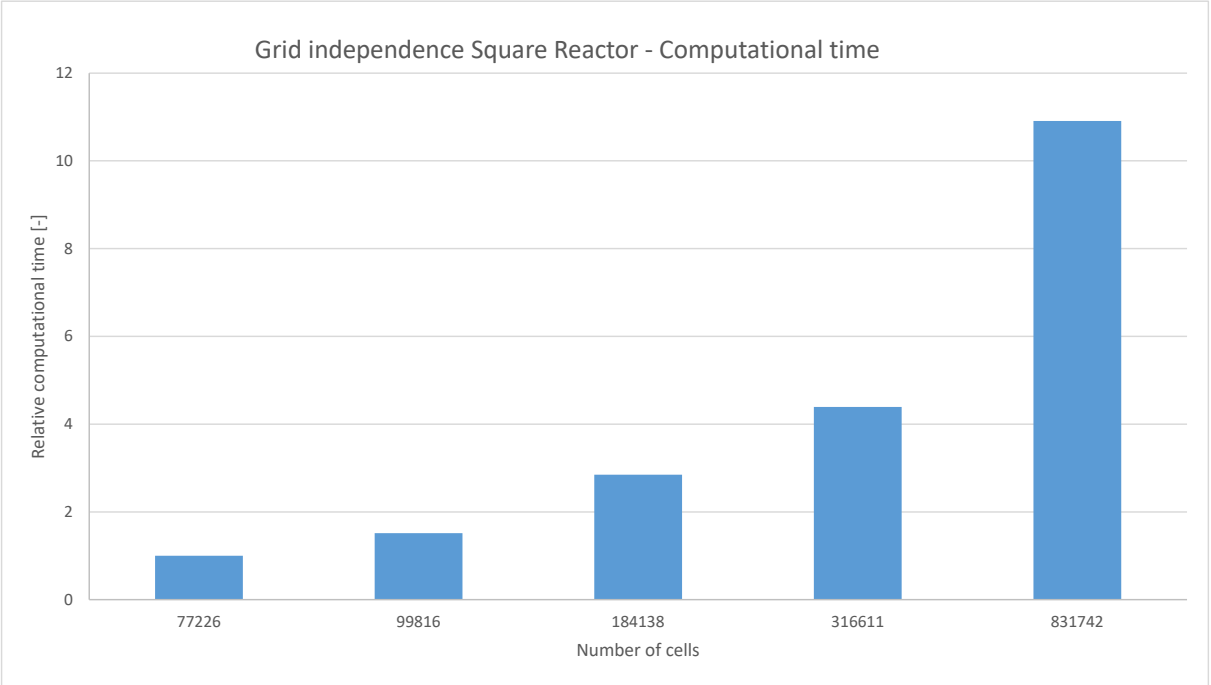

Figure 6.9: Relative computational time for square geometry

As it can be seen from the figures relating to computational time, the simulation with the largest number of cells takes more than ten times the simulation time with fewer cells. Therefore a good compromise must be found between precision of results and computational time.

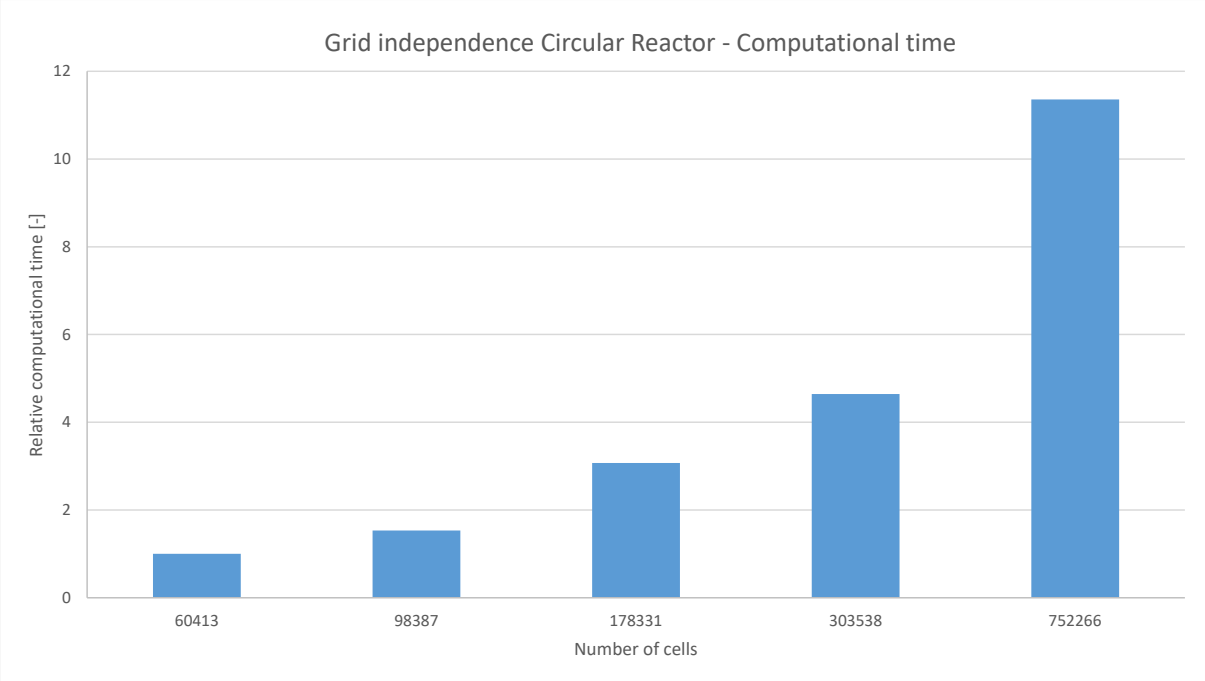

Figure 6.10: Relative computational time for circular geometry

6.2 Carbon deposition

As previously mentioned during this work, one of the most important characteristics of SOFCs is their capability to operate with different types of fuel, especially as regards carbonaceous fuels. In fact, their operation at fairly high temperatures (750 - 1000°C) and the fact that they can use various types of catalysts that do not suffer of poisoning effect by carbonaceous fuels, make them their strong point compared to other types of fuel cells. But if on the one hand we have advantages, on the other we also have disadvantages. The presence of impurities in the fuel gas of SOFCs can lead to the degradation of the anode, and the succession of reverse reactions of gasification can lead to the deposition of carbon in the electrode, thus obstructing the pores: this phenomenon is known as carbon deposition. Therefore the simultaneous presence of high temperatures, nickel catalyst and carbonaceous material, promote the degradation of the latter in pure carbon. The reactions that take place are:

- Methane cracking:

$$CH_4 \longrightarrow C + 2\,H_2 \qquad (R\,6.1)$$

- Reverse Boudouard reaction:

$$2\,CO \longrightarrow C + CO_2 \qquad (R\,6.2)$$

- Reverse water-gas reaction:

$$CO + H_2 \longrightarrow C + H_2O \tag{R 6.3}$$

The consequence of these reactions is that the carbon molecules are deposited in the porous structure of the Ni-Cermet anode. In this way the pores of the electrode are blocked and therefore the gaseous fuel cannot reach the TPB and cannot react with the O^{2-} ions. As a final consequence, after the fuel cannot reach the reaction point, oxygen oxidizes the nickel electrode, forming solid NiO, which occupies more physical space than pure Nickel, so the physical structure of the electrode can be subjected enormous structural efforts and therefore it can break. In this simulation, this phenomenon was not taken into consideration in order not to overload the numerical effort and not to make the simulated physical problem too complex. But in the reality of the facts of the project in question, this problem is more than present. In fact, given the large amount of CO, the reverse gasification reactions are possible. There are many studies in literature regarding the problem of carbon deposition on the anode surface and many of them offer more solutions to solve the problem. For example, in a study last year, the author focuses on SOFC anode material[38]. Regarding the Nickel anode, between the special feature mentioned in the report there are the formation of enhanced reaction sites and the lowering polarization resistance. Instead the drawback is that the material suffers from metal dusting, sulphur poisoning and an already mentioned several times, deposition of carbon. Instead as mentioned in the article, one of the best innovative materials to build the anode is the Ru-doped YSZ cermets which has as listed advantages the higher electrocatalytic performance for steam reforming along with negligible carbon deposition under situations of intrinsic reformation. Another article[39] states that carbon deposition basically depends on three factors: the material of the anode (as mentioned above), the amount of steam present, and the current density on which the cell is working. We have already analyzed the material issue, but other studies state that in the direct electrochemical oxidation of hydrocarbons using Ni-based anodes doped with Ceria, no presence of carbon deposition was found. Nevertheless, Ni/YSZ is widely used in SOFCs and therefore it may seem difficult and expensive to experiment with these new materials; so now let's focus on the other two characteristics analyzed: steam concentration and current density. Regarding the steam concentration, it is useful to activate the reactions such as:

$$C + H_2O \longrightarrow CO + H_2 \tag{R 6.4}$$

$$CH_4 + H_2O \longrightarrow 3\,H_2 + CO \quad (R\,6.5)$$

$$CO + H_2O \longleftrightarrow CO_2 + H_2 \quad (R\,6.6)$$

These reactions are useful to avoid carbon deposition, so it is always a good compromise to have steam near the cells. As a project, it is necessary to know how much steam is needed to avoid carbon deposition. In the article cited above it was shown that in conditions very similar to our case the limit for which the carbon deposition occurs is 10% in volume.

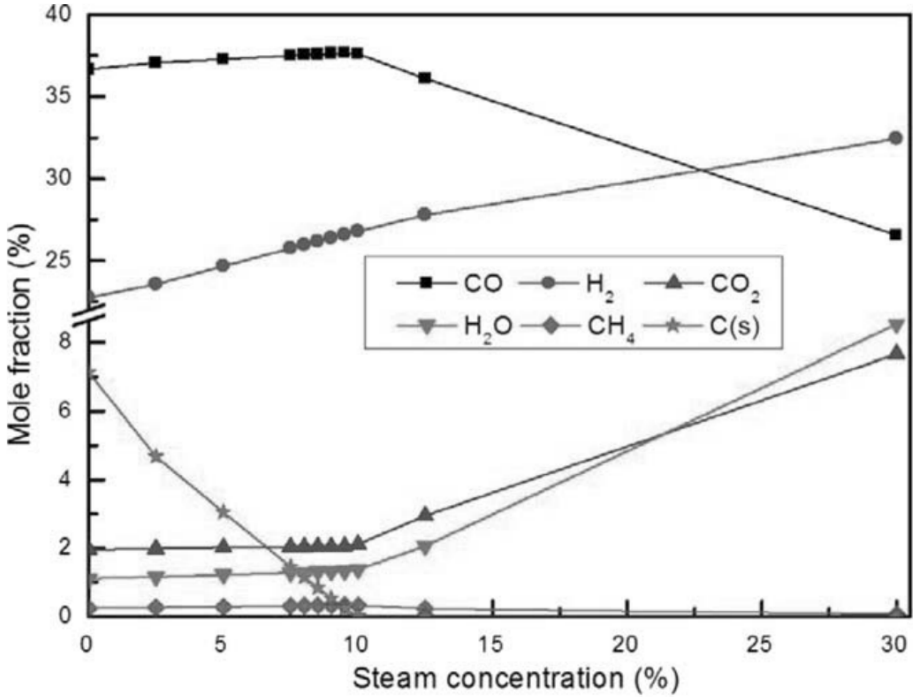

Figure 6.11: Influence of steam concentration on carbon deposition

Obviously the percentage of steam to be inserted in the reactor to avoid carbon deposition depends on the composition of the syngas. Therefore the safety threshold should be determined through an experimental campaign. Nevertheless, the results found in literature were obtained with operating conditions very similar to the project of our interest. The third and final value on which the carbon deposition depends is the current density at which SOFC operates. In an article the author analyzes precisely how carbon deposition varies according to current density[40]. The function obtained by the author also varies with the molar concentration of tar, for example in the following graph, the reference tar concentration is 2% while the reference temperature is

750°C. The article states that with the increasing molar concentration of tar, the limit threshold of current density for which carbon deposition is not favoured increases.

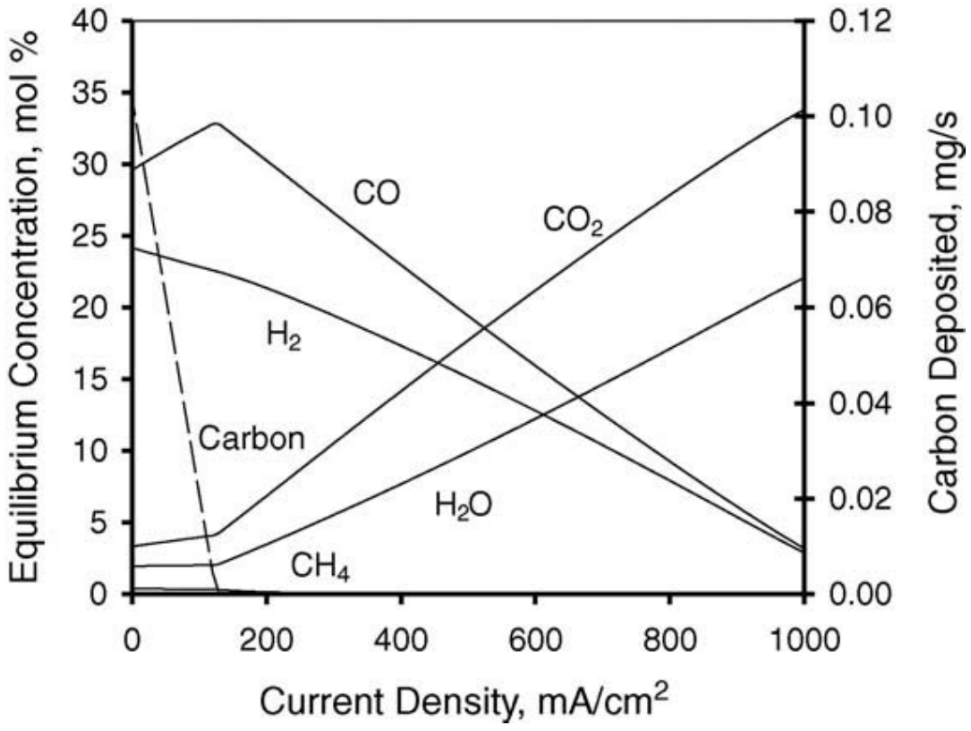

Figure 6.12: Influence of current density on carbon deposition

Finally to conclude the topic we can say that certainly in the project of interest, the problem of the carbon deposition is real, but to have more realistic data it is necessary to have done some experimental studies.

6.3 Conclusion

In conclusion, after having made all the necessary analyzes, some conjectures can be affirmed. First of all, we tried to approximate the CFD simulation as much as possible to the reality of the physics; as regards the SOFCs side, it being mostly affected by results from previous studies, there is already a certain confidence on the results, thus in this study the SOFCs were seen mainly as external components of the system. Instead, there was a more delicate situation in approximating the chain of gasification reactions as well as possible, in fact, although with kinetic values deriving from real data, we have chosen to neglect some kinetically disadvantaged chemical reactions. Therefore, when the simulation has been defined, exhaustive conclusions can be extracted from the results obtained. Among the geometries compared, it can be said that circular geometry is, albeit slightly, with an advantage respect to square geometry. As main data to confirm this theory, we can note the efficiency and also the total thermal load in the system. It should also be remembered that obviously as described in section 6.1, that all the numbers obtained are affected by uncertainty, based on the mesh used. Therefore, in future works, it will be necessary, again through CFD analysis, to integrate all the chemical and fluid dynamics aspects relating to the functioning of SOFCs and the gasification process. It will also be necessary to proceed with experimental analyzes in the laboratory of an initial prototype, to validate the results obtained in the CFD analysis.

Bibliography

[1] U.S. Energy Information Administration EIA Independent Statistics and Analysis. International energy outlook 2019. https://www.eia.gov/outlooksieo/, SEPT 2019.

[2] Gestore dei servizi energetici (GSE). Fonti rinnovabili in italia e in europa verso gli obiettivi al 2020 e al 2030. https://www.gse.it/dati-e-scenari/statistiche, JUL 2019.

[3] Sophie A. Archer and Robert Steinberger-Wilckens. Systematic analysis of biomass derived fuels for fuel cells. *International Journal of Hydrogen Energy*, 43(52):23178–23192, 2018.

[4] Cornelia Parisius. Eranetmed2-72-246, 2016. pp. 1 - 45.

[5] Prabir Basu. *Biomass gasification and pyrolysis: practical design and theory*. Academic press, 2010.

[6] Jayne H Windeatt, Andrew B Ross, Paul T Williams, Piers M Forster, Mohamad A Nahil, and Surjit Singh. Characteristics of biochars from crop residues: potential for carbon sequestration and soil amendment. *Journal of environmental management*, 146:189–197, 2014.

[7] Peter McKendry. Energy production from biomass (part 1): overview of biomass. *Bioresource technology*, 83(1):37–46, 2002.

[8] David Oakley Hall and Ralph P Overend. Biomass: regenerable energy. 1987.

[9] SA Channiwala and PP Parikh. A unified correlation for estimating hhv of solid, liquid and gaseous fuels. *Fuel*, 81(8):1051–1063, 2002.

[10] Jones Alami and Mounir El Achaby. Report on availability of biomass sources in morocco: Olive groves and vineyards. Technical report, Materials science and Nanoengineering Department, Mohamed 6 Polytechnuc University, 2018.

[11] Daniel Neves, Henrik Thunman, Arlindo Matos, Luís Tarelho, and Alberto Gómez-Barea. Characterization and prediction of biomass pyrolysis products. *Progress in Energy and Combustion Science*, 37(5):611–630, 2011.

[12] Thomas B Reed and Agua Das. *Handbook of biomass downdraft gasifier engine systems*.

Biomass Energy Foundation, 1988.

[13] Sudhanshu Dwivedi. Solid oxide fuel cell: Materials for anode, cathode and electrolyte. *International Journal of Hydrogen Energy*, 2020.

[14] Xinhong Huang, Zhihao Zhang, and Jin Jiang. Fuel cell technology for distributed generation: an overview. In *2006 IEEE international symposium on industrial electronics*, volume 2, pages 1613–1618. IEEE, 2006.

[15] Euro Mediterranean Cooperation Through ERANET Joint Activities and Beyond. Eranetmed2-72-246 - periodic activity report (month 1 - 6), 2018. pp. 1 - 45.

[16] Wei-Cheng Yan, Ye Shen, Siming You, Soong Huat Sim, Zheng-Hong Luo, Yen Wah Tong, and Chi-Hwa Wang. Model-based downdraft biomass gasifier operation and design for synthetic gas production. *Journal of cleaner production*, 178:476–493, 2018.

[17] Ramin Mehrabian, Selma Zahirovic, Robert Scharler, Ingwald Obernberger, Stefan Kleditzsch, Siegmar Wirtz, Viktor Scherer, Hong Lu, and Larry L Baxter. A cfd model for thermal conversion of thermally thick biomass particles. *Fuel processing technology*, 95:96–108, 2012.

[18] Hugo A Jakobsen. Chemical reactor modeling. *Multiphase Reactive Flows*, 2008.

[19] A Zabaniotou and Th Damartzis. Modelling the intra-particle transport phenomena and chemical reactions of olive kernel fast pyrolysis. *Journal of Analytical and Applied Pyrolysis*, 80(1):187–194, 2007.

[20] Wendi Guo, C Jim Lim, Xiaotao Bi, Shahab Sokhansanj, and Staffan Melin. Determination of effective thermal conductivity and specific heat capacity of wood pellets. *Fuel*, 103:347–355, 2013.

[21] AB Comsol and MA Burlington. Comsol multiphysics cfd user's guide, version 5.3a, 2017.

[22] Chamseddine Guizani, Olivier Louisnard, FJ Escudero Sanz, and Sylvain Salvador. Gasification of woody biomass under high heating rate conditions in pure co2: Experiments and modelling. *Biomass and Bioenergy*, 83:169–182, 2015.

[23] S Gerber, F Behrendt, and M Oevermann. An eulerian modeling approach of wood gasification in a bubbling fluidized bed reactor using char as bed material. *Fuel*, 89(10):2903–2917, 2010.

[24] Christoph Mandl, Ingwald Obernberger, and Friedrich Biedermann. Modelling of an updraft fixed-bed gasifier operated with softwood pellets. *Fuel*, 89(12):3795–3806, 2010.

[25] Chamseddine Guizani. *Effects of CO2 on the biomass pyro-gasification in High Heating Rate and Low Heating Rate conditions*. PhD thesis, 2014.

[26] P Ollero, A Serrera, R Arjona, and S Alcantarilla. The co2 gasification kinetics of olive

residue. *Biomass and Bioenergy*, 24(2):151–161, 2003.

[27] Colomba Di Blasi. Combustion and gasification rates of lignocellulosic chars. *Progress in energy and combustion science*, 35(2):121–140, 2009.

[28] Valentina Somano. *CFD model for tubular SOFC fed directly by biomass.* PhD thesis, Politecnico di Torino, 2019.

[29] Huayang Zhu, Robert J Kee, Vinod M Janardhanan, Olaf Deutschmann, and David G Goodwin. Modeling elementary heterogeneous chemistry and electrochemistry in solid-oxide fuel cells. *Journal of the electrochemical society*, 152(12):A2427–A2440, 2005.

[30] André Leonide, Simon Hansmann, and Ellen Ivers-Tiffée. A 0-dimensional stationary model for anode-supported solid oxide fuel cells. *ECS Transactions*, 28(11):341, 2010.

[31] Meng Ni. 2d heat and mass transfer modeling of methane steam reforming for hydrogen production in a compact reformer. *Energy conversion and management*, 65:155–163, 2013.

[32] Boreum Lee, Sunggeun Lee, and Hankwon Lim. Numerical modeling studies for a methane dry reforming in a membrane reactor. *Journal of Natural Gas Science and Engineering*, 34:1251–1261, 2016.

[33] Ammar Abdul Mutalib Yusup Inayat Ali Kan. Kinetic model for tar cracking in biomass steam gasification for hydrogen production. *Department of Chemical Engineering Universiti Teknologi PETRONAS Bandar Seri Iskandar*, 2016.

[34] AB Comsol and MA Burlington. Comsol multiphysics heat transfer user's guide, version 5.3a, 2017.

[35] Ashish Chaurasia. Modeling, simulation and optimization of downdraft gasifier: Studies on chemical kinetics and operating conditions on the performance of the biomass gasification process. *Energy*, 116:1065–1076, 2016.

[36] Patrick O Graf, Barbara L Mojet, Jan G van Ommen, and Leon Lefferts. Comparative study of steam reforming of methane, ethane and ethylene on pt, rh and pd supported on yttrium-stabilized zirconia. *Applied catalysis A: general*, 332(2):310–317, 2007.

[37] Pekka A Simell, Nina AK Hakala, Heikki E Haario, and A Outi I Krause. Catalytic decomposition of gasification gas tar with benzene as the model compound. *Industrial & engineering chemistry research*, 36(1):42–51, 1997.

[38] Sudhanshu Dwivedi. Solid oxide fuel cell: Materials for anode, cathode and electrolyte. *International Journal of Hydrogen Energy*, 2020.

[39] Ming Liu, MG Millan, PV Aravind, and N Brandon. Influence of operating conditions on

carbon deposition in sofcs fuelled by tar-containing biosyngas. *Journal of The Electrochemical Society*, 158(11):B1310, 2011.

[40] Devinder Singh, Eduardo Hernández-Pacheco, Phillip N Hutton, Nikhil Patel, and Michael D Mann. Carbon deposition in an sofc fueled by tar-laden biomass gas: a thermodynamic analysis. *Journal of power sources*, 142(1-2):194–199, 2005.